THE THERMO-ELECTRON ENGINE

by

GEORGE NICHOLAS HATSOPOULOS

B.S., Massachusetts Institute of Technology
(1950)

M.S., Massachusetts Institute of Technology
(1950)

Mech. Engr., Massachusetts Institute of Technology
(1954)

SUBMITTED IN PARTIAL FULFILLMENT OF THE

REQUIREMENTS FOR THE DEGREE OF

DOCTOR OF SCIENCE

at the

MASSACHUSETTS INSTITUTE OF TECHNOLOGY

May, 1956

Signature of Author. . . . . .
Department of Mechanical Engineering, May 14, 1956

Certified by . . . . . .
Thesis Supervisor

Accepted by. . . . . .
Chairman, Departmental Committee
on Graduate Students

Professor J. H. Keenan
Chairman
Departmental Committee on Graduate Students
Massachusetts Institute of Technology
Department of Mechanical Engineering
Cambridge 39, Massachusetts

Dear Sir:

In partial fulfillment of the requirements for the Degree of Doctor of Science in Mechanical Engineering, I hereby submit a thesis entitled, "The Thermo-Electron Engine".

Respectfully,

George N. Hatsopoulos

ABSTRACT

THE THERMO-ELECTRON ENGINE

BY

GEORGE NICHOLAS HATSOPOULOS

Submitted to the Department of Mechanical Engineering on May 14, 1956, in partial fulfillment of the requirements for the degree of Doctor of Science in Mechanical Engineering

A novel heat engine is described in detail and its operation analyzed. This heat engine, referred to subsequently as the thermo-electron engine, exchanges heat with two or more heat reservoirs maintained at different temperatures while producing useful electrical power. The working substance of this heat engine is an electron gas whose flow is controlled in space by crossed electric and magnetic fields. The conversion of thermal energy into electric energy by the thermo-electron engine is achieved without the use of any moving mechanical parts.

The electronic and thermodynamic analysis of the engine is given. A number of experimental models were built and tested. The results obtained from these models substantiate the basic theory and show the feasability of this novel scheme.

The main advantages of the thermo-electron engine are its great simplicity, relatively large power output per unit volume, the utilization of high temperatures and the resulting high thermal efficiency. On the basis of the existing analysis and the available experimental data power outputs from 0.5 to 5 kwatts per cubic foot with thermal efficiencies from 10 to 45 per cent appear possible. In its alternate development the thermo-electron engine could be adapted for most power needs of today.

Thesis Supervisor: Joseph Kaye

Title: Professor of Mechanical Engineering

ACKNOWLEDGMENTS

I wish to express my deepest gratitude to Professor Joseph Kaye for encouragement, invaluable guidance and support throughout the thesis program.

I wish to thank sincerely Dean C. R. Soderberg and Provost J. A. Stratton for their encouragement and support of the experimental program. I am also indebted to Professors S. J. Mason, W. P. Allis and J. H. Keenan for their encouragement, guidance and constructive criticisms.

I am grateful to Messrs. John Maris, Soterios Kitrilakis and John Welsh, whose efforts contributed greatly in the success of the experimental program.

I am also indebted to the help of the following people: Miss Patricia Potter who handled the difficult typing of the final form of the thesis; Miss Barbara Eckstein and Mr. Theodore Efstathiou who helped in the computation and the drawing of the figures; Miss Dorothy Johnson, Miss Gladys Magnasson, Messrs. J. B. Keefe, L. W. Ryan, T. Velouto and F. Rosebury who gave their invaluable help in the intricate construction of the thermo-electron engine.

The first part of the research program reported in this thesis was supported financially by the Mechanical Engineering Department of the Massachusetts Institute of Technology. The second part of the program was supported financially by the Matrad Corporation, New York, through the generous support of Mr. Peter M. Nomikos.

TABLE OF CONTENTS

	Page
NOMENCLATURE	
VALUES OF PHYSICAL CONSTANTS	
LIST OF TABLES	
LIST OF ILLUSTRATIONS	
INTRODUCTION	1
THE THERMO-ELECTRON ENGINE	4
Principle	4
The Diode	6
The Magnetic Triode	7
The Multiplate Thermo-Electron Engine	9
ANALYSIS	
The Diode	12
The Multiplate T.E.E. with Constant Plate Widths	16
Thermal Efficiency	20
Currents Emitted by Cold Plates	20
Heat Transferred to the Hot Plates	21
Cold Plates	24
Efficiency	28
Thermodynamic Analysis of T.E.E.	30
First Law	30
Second Law	31
ANALYSIS FOR THE ELECTRON FLOW	
General Equations	35
One Dimensional Electron Flow Under the Influence of Crossed Electric and Magnetic Fields	36
Boundary Conditions	38
Velocity Distribution	39

	Page
Electron Trajectories	43
Potential Distribution	44
Analysis for the Region y less than y_c	46
End Effects	47
CONSTANT MAGNETIC FIELD CASE	
Current Density	57
Plate Widths	60
Potential Barrier	62
Anode Potential	62
Cold Plates	63
Power Output	63
Heat Transferred to the Hot Plates	64
Efficiency	64
LOSSES	
Anode Potential	65
Magnetic Field	67
Vacuum	68
Heat Trasfer Losses	68
THE THERMO-ELECTRON ENGINE IN THE CYLINDRICAL FORM	69
DESIGN CONSIDERATIONS	71
Emissive Materials	71
Spatial Configurations	72
OVERALL EFFICIENCY AND POWER OUTPUT	73
EXPERIMENTAL MODELS	76
Model 1	77
Model 2	79
Model 3	79
Model 4	79
Model 5	80

Page

EXPERIMENTAL PROCEDURE 80

EXPERIMENTAL RESULTS 80

OUTLOOK IN THE FUTURE 85

BIBLIOGRAPHY 87

APPENDIX 1 . . . . . Steady-State Distribution of Potentials 88

APPENDIX 2 . . . . . Energy Distribution of Emitted Electrons 93

APPENDIX 3 . . . . . The Vacuum Systems 95

APPENDIX 4 . . . . . The Magnet 96

APPENDIX 5 . . . . . Calculation Procedure 98

BIOGRAPHICAL SKETCH 100

NOMENCLATURE

A	Richardson's constant, amp/cm^2 $^oK^2$
A_k	k^{th} anode
B	Magnetic field strength, Gauss = 10^8 weber/cm^2
E	Electric field, strength volts/cm
h	Plate length, cm
i	Interger, signifying plate number
I_a	Anode current per unit area, amps/cm^2
I_b	Current in the Helmholtz coil, amps
I_c	Output current or collected current per unit area, amps/cm^2
I_d	Current density, amps/cm^2
I_e	Emitted current per unit area, amps/cm^2
I_m	Current emitted by hot plates per unit area after m reflections, amps/cm^2
I_m'	Current$_2$emitted by cold plates, per unit area after m reflections amps/cm^2
I_s	Saturation current, amps/cm^2
k	Boltzmann's constant, volts/^oK
k	Interger, signifying plate number
l	Plate width, cm
L	Dimensionless plate width $L = l/l_1$, where l_1 is the width of the first plate
m_e	Electronic mass, grams
m	Plate width divided by chord length of trajectory, dimensionless

N	Number of molecules per cm^3, dimensionless
n	Number of hot plates
P_o	Power output, watts/cm^2
P	Hot plate
P'	Cold plate
p	pressure, mm Hg
Q	Heat transfer Btu
Q_e	Electronic charge, coulombs
q	Heat transfer per unit area and unit time, watts/cm^2
q_e	Heat losses, watts/cm^2
R_L	Load Resistance, ohms
R	Fraction of rejected electrons, dimensionless
r	Reflection coefficient, dimensionless
s	Mode number; interger
S	Rate of Entropy change, watts/^oK
T	High temperature ^oK
T'	Low temperature ^oK
t	Time, seconds
U	Energy flux, watts/cm^2
u_x, u_y, u_z	Velocity components of electrons due to thermal energy
V	Potential difference, volts
v_x,v_y,v_z	Electron velocity components, cm/sec
W	Work, watt sec

X	Dimensionless barrier, $X = e^{-S/kT}$
x	Coordinate axis
Y	Dimensionless work function Y =
y	Coordinate axis
y_a	The y coordinate of the anodes, cm
y_{ac}	Anode cathode distance, cm
y_c	The y coordinate of the emitting surface, cm
y_m	The height of the electron trajectory, cm

GREEK

α	Ratio of emitted current to current density, I_e/I_d, dimensionless
γ	Constant of the magnetic coil, gauss/amps
δ	Potential barrier, volts
ϵ_o	The permittivity of free space
ϵ	Thermal emissivity, dimensionless
ζ	Trajectory path length, cm
η	Thermal Efficiency, dimensionless
η_a	Thermal Efficiency, with radiation losses, dimensionless
λ	Trajectory chord length, cm
μ	Carnot efficiency, $\mu = 1 - T'/T$, dimensionless
μ_o	Magnetic susceptibility of air, webers/amp - meter
ξ	Parameter,
π	3.1415
ρ	Density, grams/cm^2
σ	Stephan Boltzmann's radiation constant, watts/cm^2 ($^\circ$K)^4
φ	Work function, volts
ψ	Potential, volts
ψ_a	Anode potential, volts
Ω	Collision cross section, cm^2

TABLE OF PHYSICAL CONSTANTS

Boltzmann's constant,	$k = 0.861 \times 10^{-4}$ volts/^{o}K
Electronic mass,	$m_e = 9.1055 \times 10^{-28}$ grams
Electronic charge,	$Q_e = 0.1591 \times 10^{-18}$ coulombs
Specific electronic charge,	$Q_e/m_e = 1.7462 \times 10^{-15}$ cm^2/volt sec^2
The permittivity of free space,	$\epsilon_o = 8.85 \times 10^{-14}$ amps sec/ volt cm
The magnetic susceptibility of air,	$\mu_o = 4\pi \times 10^{-7}$ webers/amp meter

LIST OF TABLES

Table Number	
I	Plate Widths and Values of Potential Barrier Dimensionless Potential Barrier for First Plate $X_1 = 1$
II	Plate Widths and Values of Potential Barrier Dimensionless Potential Barrier for First Plate, $X_1 = 3$
III	Properties of electron emissive materials
IV	Computed Quantities Thermo-Electron Engine, Oxide Coating, $n = 1$
V	Computed Quantities Thermo-Electron Engine, Impregnated Tungsten, $n = 3$
VI	Computed Quantities Thermo-Electron Engine, Impregnated Tungsten, $n = 10$
VII	Computed Quantities Thermo-Electron Engine, Impregnated Tungsten, $n = 30$
VIII	Computed Quantities Thermo-Electron Engine, Thoriated Tungsten, $n = 3$
IX	Computed Quantities Thermo-Electron Engine, Thoriated Tungsten, $n = 10$
X	Computed Quantities Thermo-Electron Engine, Thoriated Tungsten, $n = 10$
XI	Experimental Results from Model 3, Run No. 10
XII	Experimental Results from Model 3, Run No. 17
XIII	Experimental Results from Model 3, Run No. 18
XIV	Experimental Results from Model 4, Run No. 28

Table Number	
XV	Experimental Results from Model 4, Run No. 29
XVI	Experimental Results from Model 4, Run No. 30
XVII	Experimental Results from Model 4, Run No. 31
XVIII	Experimental Results from Model 4, Run No. 33
XIX	Experimental Results from Model 4, Run No. 34
XX	Calculated Results for Model 4, Run No. 28
XXI	Calculated Results for Model 4, Run No. 29
XXII	Calculated Results for Model 4, Run No. 30
XXIII	Calculated Results for Model 4, Run No. 31
XXIV	Calculated Results for Model 4, Run No. 33
XXV	Calculated Results for Model 4, Run No. 34
XXVI	Total Emitted Current and Anode Current for Circular Model 5

LIST OF ILLUSTRATIONS

Figure Number	
1	Simple Diode
2	Magnetic Triode
3	Schematic Operation of Thermal-Electron Engine
4	Diode Potential Versus Space Charge Potential Barrier, δ, for $0.01 < \delta < 1.0$ Volts
5	Diode Potential Versus Space Charge Potential Barrier, δ, for $0.1 < \delta < 1.0$ Volts
6	Diode Characteristic, Diode Current Versus Potential Difference, V, Anode-Cathode Distance, y = 0.1 cm for $-5 < V < 20$ Volts
7	Diode Characteristic, Diode Current Versus Potential Difference, V, Anode-Cathode Distance, y = 0.1 cm for $-3 < V < 0$ Volts
8	Diode Characteristic, Diode Current Versus Potential Difference, V, Anode-Cathode Distance, y = 0.01 cm for $-1.5 < V < 0$ Volts
9	Diode Characteristic, Diode Current Versus Potential Difference, V, Anode-Cathode Distance, y = 0.001 cm for $-1.5 < V < 0$ Volts
10	Power Output of Simple Diode, Versus Potential Difference
11	Efficiency of Simple Diode Without Radiation Losses Versus Potential Difference
12	Efficiency of Simple Diode with Radiation Losses Versus Potential Difference
13	Schematic Representation of T.E.E. with n Hot and n Cold Plates

Figure Number

14 Potential Distribution Above Emitting Plates Thermo-Electron Engine

15 One Dimensional Electron Flow

16 Potential Distribution Versus Distance, y, Normal to the Emitting Plate

17 Electron Trajectories, One Dimensional Electron Flow

18 Electron Flow and Potential Barrier for Plates of Width Smaller than the Trajectory Chord

19 Electron Flow and Potential Barrier for Plates of Width Larger than the Trajectory Chord

20 Circular Configuration, Thermo-Electron Engine

21 Schematic Representation, Thermo-Electron Engine Plane Configuration

22 Schematic Representation, Thermo-Electron Engine Circular Configuration

23 Thermal Efficiency with Zero Radiation Loss Versus the Carnot Efficiency, Temperature of Heat Source, $T = 1363^{o}K$

24 Thermal Efficiency with Zero Radiation Loss Versus the Carnot Efficiency, Temperature of Heat Source, $T = 3000^{o}K$

25 Thermal Efficiency with Finite Radiation Loss Versus the Carnot Efficiency, Temperature of Heat Source, $T = 2500^{o}K$

26 Thermal Efficiency with Finite Radiation Loss Versus the Carnot Efficiency, Temperature of Heat Source, $T = 3000^{o}K$

27 Thermal Efficiency and Power Output Versus Temperature of Heat Source, Constant Magnetic Field, Impregnated Tungsten, Ten Plates, Dimensionless Potential Barrier, $X_1 = 1$

Figure Number

28 Thermal Efficiency and Power Output Versus Temperature of Heat Source, Constant Magnetic Field, Impregnated Tungsten, Ten Plates, Dimensionless Potential Barrier, $X_1 = 3$

29 Thermal Efficiency and Power Output Versus Temperature of Heat Source, Constant Magnetic Field, Impregnated Tungsten, Thirty Plates, Dimensionless Potential Barrier, $X = 3$

30 Thermal Efficiency and Power Output Versus Temperature of Heat Source, Constant Magnetic Field, Thoriated Tungsten, Thirty Plates, Dimensionless Potential Barrier, $X = 3$

31 Thermal Efficiency of Composite Thermo-Electron Engine Versus Temperature of Heat Source

32 Model 1, Assembly

33 Model 1, Parts

34 Model 1, Assembled Tube

35 Model 2, Parts

36 Model 2, Assembly Drawing

37 Model 3, Assembly

38 Model 4, Cathodes

39 Model 4, Cathodes

40 Model 4, Parts

41 Model 4, Assembly Drawing

42 Model 4, Cathode Assembly and Mechanism

43 Model 4, Assembly

44 Model 5, Parts

Figure Number	
45	Model 5, Assembly Drawing
46	Model 5, Anode-Cathode Assembly
47	Model 5, Assembly
48	Emitted Current Versus Magnetic Field Strength, Model 3, Run 10
49	Emitted Current Versus Magnetic Field Strength, Model 3, Run 17
50	Calculated Chord of Electron Trajectories, Model 4, $0 < \lambda < 02$ cm
51	Calculated Chord of Electron Trajectories, Model 4, $0 < \lambda < 2$ cm
52	Emitted Current Versus Anode Potential, Model 4, Run 28
53	Output Current, Absorbed by Cathode 3, Versus Anode Potential, Model 4, Run 28
54	Anode Current, Versus Anode Potential, Model 4, Run 28
55	Emitted Current Versus Anode Potential, Model 4, Run 29
56	Output Current, Absorbed by Cathode 3, Versus Anode Potential, Model 4, Run 29
57	Anode Current Versus Anode Potential, Model 4, Run 29
58	Emitted Current Versus Anode Potential, Model 4, Run 30
59	Output Current, Absorbed by Cathode 3, Versus Anode Potential, Model 4, Run 30
60	Anode Current Versus Anode Potential, Model 4, Run 30

Figure Number

61 Emitted Current Versus Anode Potential, Model 4, Run 31

62 Output Current Versus Anode Potential, Model 4, Run 31

63 Anode Current Versus Anode Potential, Model 4, Run 31

64 Emitted Current Versus Anode Potential, Model 4, Run 33

65 Output Current Versus Anode Potential, Model 4, Run 33

66 Anode Current Versus Anode Potential, Model 4, Run 33

67 Emitted Current Versus Anode Potential, Model 4, Run 34

68 Output Current Versus Anode Potential, Model 4, Run 34

69 Anode Current Versus Anode Potential, Model 4, Run 34

70 Anodes, Model 5, After Shorting

71 Steady-State Distribution of Potentials in Thermo-Electron Engine

72 Steady-State Distribution of Potentials in Thermo-Electron Engine

73 Steady-State Distribution of Potentials in Thermo-Electron Engine

74 Steady-State Distribution of Potentials in Thermo-Electron Engine

75 Steady-State Distribution of Potentials in Thermo-Electron Engine

Figure Number

76	Schematic Representation of Vacuum Systems
77	Vacuum System
78	Bell Jar
79	Helmholtz Coil Assembly Drawing
80	Helmholtz Coil Assembly (Magnet)
81	Cooling Coil for Magnet

INTRODUCTION

Faraday's discovery of the electromagnetic induction principle resulted in the development of electric generators which are used today in power production. Reciprocating steam engines, internal combustion engines, and steam and gas turbines have been coupled with such generators in utilizing chemical heat sources such as oil, coal, and natural gas for the production of electric energy. Recently nuclear reactors and solar energy are being added to the list of heat sources used in modern electric power plants. These power plants have, however, a common disadvantage; the conversion of thermal energy into electric energy is accomplished by the utilization of moving mechanical parts. The massive bulk of equipment, the irreversibilities, and complexities of the operation involved in these conversion methods accentuate the desirability of some direct method for conversion of thermal energy into electric energy with no moving parts.

A large number of such conversion methods have been suggested in the past. The records of the United States Patent Office and the Patent Offices of other Countries display a long series of conversion devices dating back nearly one hundred years. One of the first inventors in this field was Thomas Edison, who proposed that the dependence of magnetic permeability of certain metals with temperature can be used to generate an alternating current.

Among the most important classes of direct conversion devices that have been studied in detail are first, the use of thermocouples, and

secondly, the use of high-speed flow of an ionized gas in a magnetic field. Due to numerous disadvantages these proposed methods have not proved to be practical on a large or commercial scale.

For example, devices using thermocouples possess the following limitations and disadvantages:

1. They are limited to relatively low temperatures.
2. The thermal efficiency is low due to conduction losses.
3. The voltages obtained are very small.

On the other hand, devices using ionized gas require large and continuously operating vacuum pumps which greatly reduce their efficiency.

Today there is an increasing effort to discover and develop a more practical means for converting thermal energy directly into electric energy. This effort is emphasized by the development of the nuclear reactor with its high available temperatures and high heat-transfer rates, and the need to harness solar energy against the day when our diminishing supply of chemical fuels will be exhausted. The thermoelectron engine is the result of such an effort. It is a new and unique application of known principles of electron emission from heated surfaces together with controlled electron flow. This engine utilizes the thermal energy of the emitted electrons and translates it continuously into electric energy by means of crossed electric and magnetic fields.

On the basis of the existing analysis and the available experimental data, it appears possible to obtain from this novel heat engine, power

outputs as high as 5 kw per ft^3 with thermal efficiencies of 45%. These figures should not be considered as upper bounds but are based on designs that seem practical at this time.

In addition to its great simplicity a major advantage of the thermo-electron engine is that it can use much higher temperatures than do conventional power plants. In conventional power plant the temperatures used are limited by the strength of the engine material but similar considerations are not valid for the thermo-electron engine.

The applications of the thermo-electron engine are practically unlimited ranging from car batteries to atomic power plants. The thermo-electron engine can be adapted for most electric power needs of today.

THE THERMO-ELECTRON ENGINE

The Thermo-Electron Engine is defined as a continuously operating thermodynamic system which receives heat from one reservoir at a given level of temperature and rejects heat to a second reservoir at a lower temperature, and which delivers useful work in the form of electric energy. The working substance of this engine is an electron gas which is formed over surfaces of low work function maintained at relatively high temperatures, and whose flow is controlled in space by crossed electric and magnetic fields.

The conversion of heat energy into electric energy by the above system is achieved without the use of any moving mechanical parts.

Principle

It is well known that the free electrons existing in a metal have a Fermi-Dirac energy distribution. This energy distribution depends primarily on the temperature of the metal. If an electron acquires an energy large enough to overcome the potential barrier (work function) existing at the surface of the metal, it can escape from the metal surface. The number of escaping electrons increases as the temperature of the metal is increased. It can be shown by either Fermi-Dirac statistics or by thermodynamic reasoning that the number of escaping electrons, measured by the current emitted by a metallic surface, is given by Richardson's equation:

$$I_s = AT^2 \exp.(-\varphi/kT)$$

where

A Constant depending on the metal (amps/cm^2 °K^2)

φ Work function of the metal (volts)

and

T The surface temperature in degrees absolute

The electron gas formed at the surface of the metal can be assumed to have a Maxwellian[1] energy distribution. It is shown in Appendix 2 that for this Maxwellian energy distribution, the average kinetic energy of the emitted electrons, in a direction normal to the emitting surface, is equal to 2 kT. Hence a large fraction of these electrons can be made to move to a region having a potential which exceeds the potential of the emitting surface by an amount of the order of 2 kT. It is understood that no matter how low or how high the potential difference of the two regions is, due to the nature of the assumed energy distribution, there is always a fraction of the emitted electrons which can penetrate the second region as well as a fraction of the electrons which can never penetrate the second region.

The thermo-electron engine is a device which utilizes the above principle to supply a continuous output current at a fixed potential difference.

[1] See Reference R6

The Diode

Consider two parallel metallic plates, P and P', separated by a gap y. Plate P is of a material of low work function and is maintained at a relatively high temperature, T. Plate P' is, in turn, maintained at a relatively low temperature, T'. Due to the difference in emission of the two surfaces, a potential difference will be established between the plates. More specifically, the cold plate P' will acquire a negative potential of such magnitude that the net flow of current between the two plates is zero.

If now the two plates are connected by an external circuit, as shown in Fig. 1, a current will flow through the load and the potential difference between the two plates will adjust itself to a value necessary to sustain this net flow of current.

The power output of such a device is calculated in detail later in this report. At this point we can estimate roughly this power output as follows. We have mentioned previously that the average kinetic energy of the emitted electrons equals 2 kT. For a temperature T equal to 1100°K, which is a normal operating temperature for the usual emitting materials, the average energy is of the order of 0.2 electron volts. Assuming an emission current of 5 amps/cm^2 we obtain an available power of 1 watt/cm^2.

Not all of this power can be utilized for the following reasons:

1. For the assumed Maxwellian energy distribution, only a fraction of the emitted electrons have energies greater than 2 kT and consequently only this fraction can reach the cold plate P'.

2. The electrons which are traveling from the hot to the cold plate, will build up a space charge above these plates, and this charge will tend to repel electrons emitted subsequently from the hot plate. This effect of space charge will result in a finite reduction of the net flow of current between the hot and cold plates.

This action of the space charge is the major limitation in the operation of an ordinary diode as a heat engine. It will be shown later that the space charge can be greatly reduced if the gap between the two plates is made very small. However, even for separations of 0.1 cm, which can be easily achieved in practice, the power output for optimum conditions is only of the order of 0.1 milliwatts/cm^2.

Another limitation in the operation of a diode as a heat engine is the relatively large loss by means of radiation between hot and cold plates. This large loss, together with the small power output of the device, results in a very small value of overall efficiency. For a separation of 0.1 cm for optimum conditions the efficiency is of the order of 0.02%.

The Magnetic Triode

In the device, which we have labelled as a magnetic triode, the effects of both space charge and radiation losses are greatly reduced.

Consider two plates P and P' maintained at temperatures T and T' respectively, where T is greater than T', as shown in Fig. 2. The two plates are made of a material of relatively low work function. Temperature T' is assumed to be so low that the emission from plate P' can be neglected. A third plate, or anode, A_1 is placed parallel to plates P

and P' at a distance y_a. Plate A_1, is maintained at a high positive potential with respect to hot plate P, by means of a suitable external battery.

A uniform magnetic field B is maintained in a direction parallel to the adjacent edges of plates P and P' by means of either a Helmholtz coil or a permanent magnet.

Let us now observe the operation of such a device as the temperature of the hot plate approaches the value T. The electrons emitted from the hot plate P are accelerated towards the positively charged anode A_1, but are also deflected from it by the magnetic field B. The path the electrons will follow in space, for appropriate values of the magnetic and electric fields, will be similar to an elongated cycloid. After the electrons reach the highest point of their trajectory they will be directed towards the cold plate P'. From this point onward the electrons are deccelerated by the existing electric fields as they approach cold plate P'; at this surface the electrons have an average kinetic energy of 2 kT equal to the average kinetic energy at the emission point of plate P.

If an external load is connected between plates P and P', current will flow through this load. The net flow of current between the plates and the potential difference between the plates will adjust according to the resistance of the load. It will be shown later that for maximum power output the potential difference between the plates should be of the order of kT volts.

In general the potential of the cold plate P' can be set at any potential -V with respect to hot plate P. In this general case the fraction of the electrons emitted from the hot plate which do not have suffi-

cient kinetic energy to overcome the potential -V will approach plate P' but will reach a zero velocity at a finite distance above plate P'. They will then be accelerated away from plate P' by the anode and continue to move to the right of plate P'. For this reason either a third collector plate, not shown in Fig. 2, should be added or the geometry should be modified so that these rejected electrons can return to the original plate P. These modifications will be discussed later in detail.

The magnetic field may be supplied by a permanent magnet which consumes no power or by an Helmholtz coil consuming a very small fraction of the net power output of the device.

The auxiliary battery used to maintain a positive potential at the anode will consume zero power if no electrons reach the anode, or if no current flows from either hot or cold plate to the anode. Theoretically it is possible to satisfy this condition. Practically, however, a small current will flow to the anode due to perturbations of electron paths caused by electron collisions with gas molecules even of the highest vacuum obtainable, and due to irregularities of the magnetic field, the electric field, and the geometry.

The Multiplate Thermo-Electron Engine (T.E.E.)

Consider a set of hot and cold plates, connected electrically as shown in the schematic diagram of Fig. 3. The hot plates P_1, P_2, and P_3 are maintained steadily at a high temperature T'.

The operation of this device is as follows:

Starting with the first hot plate 1 at a potential of zero, the electrons emitted by plate 1 are controlled by means of the crossed electric and magnetic fields, E_1 and B, respectively, so that they flow towards the adjacent hot plate 2 at a higher negative potential of $-V_1$, at a rate of I amperes. The current of I amperes approaching the second hot plate 2 from the first hot plate 1 is partly absorbed and partly rejected by the second hot plate. Rejection occurs since some electrons do not have sufficient energy to overcome the potential barrier at the surface of the hot plate 2. The fraction, RI, is rejected and moves in a controlled series of paths or trajectories to a final sink or absorber (plate 3') at the same potential of the second hot plate 2 shown in Fig. 3. The other fraction of the electron current, namely (1-R), is absorbed by the second hot plate 2.

The emission of a current of I amperes occurs also from the second hot plate 2 and this current is now directed towards the third hot plate 3 at a potential of $-(V_1 + V_2)$ volts; again this current of I amperes is split at the third hot plate 3 into a rejected fraction, RI, and an absorbed fraction, (1-R) I.

From the last hot plate 3, at a potential of $-(V_1 + V_2)$ volts, in Fig. 3, a series of cold plates begins; these cold plates are at such a low temperature that their own thermal rate of electron emission is insignificant. The electron current of I amperes from the third hot plate 3 is directed to the first cold plate 1' at a higher negative potential of $-(V_1 + V_2 + V_3)$. In addition, all the rejected electrons

from the first two hot plates, 1 and 2, approach the first cold plate 1', but are completely rejected, as a first approximation, by this first cold plate 1'. Hence, the only current absorbed by the first cold plate 1' is I amperes. The rejected currents of the first two hot plates, 1 and 2, approach the second cold plate 2' at a potential of $-(V_1 + V_2)$, but only the rejected current (RI amperes) from the second hot plate 2 at potential $-(V_1 + V_2)$ will be completely absorbed. Similarly for the remaining cold plate 3'. This process could be repeated indefinitely but for reasons of simplicity and illustration only three hot plates are shown in Fig. 3 and only one complete set of trajectories is shown there.

Note that hot and cold plates of the same potential are connected by electrical leads so as to permit all currents emitted by each of the series of hot plates, except for the first one, to be returned from the collector or cold plates to the respective hot plates.

In the optimum design the plates will be of different width in the direction of electron flow and the anodes will be maintained at different potentials due to the variation of the space charge between adjacent plates. To obtain useful electrical work or power output of this heat engine a load of proper resistance is connected between the first hot plate 1 and the first cold plate 1'. A current of I amperes will flow through the load at a potential difference of $(V_1 + V_2 + V_3)$ volts, which is of the order of magnitude of 6 kT volts.

The basic operation of the above described device is essentially the same as that of the magnetic triode. However, the T.E.E. achieves larger voltages and a significant reduction of heat losses. A detailed analysis

of the T.E.E. will be presented later.

ANALYSIS

The Diode

Referring to Fig. 1, assume for the sake of simplicity that the two plates P and P', maintained at temperatures T and T', are made of the same material, i.e. have identical work functions.

The electron emission from plate P is given by eq. 1, Richardson's equation:

$$I_s = A T^2 \exp(-\varphi/kT) \tag{1}$$

In order for the emitted electrons to reach cold plate P', and to be absorbed by it, they have to overcome:

First: The potential difference V existing between P and P'.

Second: The potential barrier δ caused by the space charge of the electrons in the gap y.

The fraction of the emitted electrons having sufficient energy to overcome the potential $-(V+\delta)$ is computed in Appendix 2 as:

$$\exp\left[-(V+\delta)/kT\right] \tag{2}$$

The net flow of current leaving plate P becomes:

$$I_e = AT^2 \exp(-\varphi/kT) \exp[-(V+\delta)/kT] \tag{3}$$

The potential barrier due to the space charge is obtained by the Child-Langmuir equation:

$$I_e = (\epsilon_o/9\pi)(2Q_e/m_e)^{1/2}(\delta^{3/2}/y^2) \tag{4}$$

From eqs. (3) and (4) we find $V = f(\delta)$

This function is plotted in Figs. 4 and 5 for impregnated tungsten plates $\varphi = 1.7$ volts, $A = 5$ (amps/cm^2°K) and for a temperature T equal to 1500°K. Each curve corresponds to a given gap, y = 0.1, 0.01, 0.001 cm.

In Figs. 6, 7, 8, and 9, the net current I_e is plotted versus the potential difference V. This graph is essentially the well-known "diode" characteristic".

The region of interest to us is only for negative values of V_1, since in this case the diode acts as a power generator.

Figure 10 shows the power output $I_e V_1$ versus V_1 for negative values of V_1. The point of maximum power can be easily noticed. The power out-

put becomes appreciable only for the very small gaps of 0.01 cm and 0.001 cm. At the present time no technique is known by which one can obtain these small gaps in practice.

The thermal efficiency of the T.E.E. can be easily computed from the standard figure of merit, $\eta \equiv w_{net}/\Sigma q_{in}$. The emission of electrons from hot plate P of a number equal to :

$$I_s = AT^2 \exp(-\varphi/kT) \exp[-(V+\delta)/kT]$$

requires a heat input to hot plate P equal to

$$q_i = (\varphi + V_1 + \delta + 2kT) I_e \qquad (5)$$

where

φ is the work function, equivalent to the latent heat of vaporization of the electrons,

$(V_1+\delta+2kT)$ is the thermal energy of the fraction of electrons having energies above $(V_1+\delta)$ as computed in Appendix 2.

Without taking into account radiation losses the thermal efficiency becomes:

$$\eta = \frac{I_e V_1}{(4 + V_1 + \delta + 2kT) I_e} \qquad (6)$$

Figure 11 shows this thermal efficiency versus V_1 for different values of the gap width. The radiation losses are computed by the Stefan-Boltzmann law.

$$q_i = \sigma \frac{1}{\frac{1}{\epsilon_1} + \frac{1}{\epsilon_2} - 1} \left[T^4 - (T')^4 \right] \tag{7}$$

where

σ is Stefan Boltzmann's constant watts/$^\circ K^4$

ϵ_1 is the emissivity of surface P

ϵ_2 is the emissivity of surface P'

For values of the cold plate temperature of T' near atmospheric temperature the contribution of the term T' can be neglected.

The actual thermal efficiency of the diode taking account of heat losses, then becomes:

$$\eta = \frac{I_e V_1}{I_e(\varphi + V_1 + \delta + 2kT) + q_e} \tag{8}$$

Figure 12 shows this actual thermal efficiency η_a for impregnated tungsten (φ equal to 1.7 volts and A equal to 5 amps/cm$^2 \cdot K^2$) for temperature T equal to 1500°K and T' equal to 300°K, and for gap widths of 0.1 cm,

and 0.001 cm.

For a gap width of 0.1 cm, which is practical, the optimum thermal efficiency is seen to be 0.0137% and the corresponding power output is 0.000196 watts/cm^2. If a gap width of 0.001 cm were possible, an efficiency of 12.26% at power output of 0.1518 watts/cm^2 would be achieved.

The Multiplate T.E.E. With Constant Plate Widths

The analysis for the magnetic triode and the multiplate T.E.E. are combined in this section since the former is a special case of the latter, in which the number of hot plates is unity.

Consider 2n electron emissive plates P_1, P_2, ...P_n and P_1', P_2', ...P_n' as shown in Fig. 13. A corresponding number of anodes A_1, A_2....A_n, A_1', A_2',....A_n' are placed parallel to the plates at a distance y_a from them. The anodes are maintained at potentials $\psi_1, \psi_2 \text{----} \psi_n$ and $\psi_1', \psi_2' \text{----} \psi_n'$ respectively, by means of suitable batteries. A magnetic field is created between the anodes and the plates at a direction normal to the plane of Fig. 13. Plates P_1, P_2,....P_n, P_1', P_2',....P_n' are all assumed to be of the same width and of unit depth.

Plates P_1, P_2....P_n are now brought to a uniform temperature T of relatively high value, while plates P_1', P_2'....P_n' are maintained at a lower temperature T'. As the temperature of plates P_1, P_2....P_n is increased, electron emission takes place from their surfaces. The existing electric field will accelerate the emitted electrons and the magnetic field will deflect them. If other effects were ignored the resulting electron

paths would be cycloids. However, a space charge results from the emitted electrons near the plate surface. This space charge affects the potential distribution normal to the plates and consequently the shape of the electron trajectories. It will be shown in a later section that the potential of the anode can be selected so as to produce a potential distribution of the form indicated in Fig. 14. This potential distribution possesses a depression near the surface of the emitting plates, which is typical of "space charge limited" emission phenomena. The emission current depends on the magnitude δ of this potential barrier. The space-charge limited emission current is given by:

$$I_e = AT^2 \exp(-\varphi/kT) \exp(-\delta/kT) = I_s \exp(-\delta/kT) \qquad (9)$$

It will be shown that the potential of the anode may be adjusted to obtain almost any value of δ. Hence, set δ equal to V_o for all hot plates (P_1, P_2,....P_n) and δ equal to 0 for all cold plates P_1', P_2'.... P_n'. Then only electrons with kinetic energies in the y direction [2], greater than V_o, will be emitted from the hot plates. The electron trajectories, when space charge is taken into account, will be shown in a later section to be similar to elongated cycloids.

Since the width of each hot plate is $m\lambda$, the electrons emitted from the left hand edge of any hot plate will approach that plate "m" times before they pass to the next one. For the entire hot plate, the

---

[2] By kinetic energy in the y direction is meant the kinetic energy corresponding to the velocity component in the y direction, normal to the plate surface.

net current emitted is:

$$I_s \lambda (1+r+r^2 \ldots +r^{m-1}) \exp(-V_o/kT) = I_s \lambda \left[\frac{r^m-1}{r-1}\right] \exp(-V_o/kT) \quad (9a)$$

or per unit area:

$$I_m = (I_s/m)\left[\frac{r^m-1}{r-1}\right] \exp(-V_o/kT) \quad (10)$$

This electron gas in the space above the hot plate is assumed to have a Maxwellian[1] energy distribution so that $\exp(-V_o/kT_1)$ is the fraction of the emitted electrons which have kinetic energies in the y direction greater than V electron volts.

At this point in order to facilitate the study of the operation of the system, assume that the potentials of the hot plates P_2, P_3....P_n are held at $-V_o$, $-2V_o$, $-3V_o$,....$-nV_o$ with respect to hot plate P_1. It will be shown in Appendix 1 that this potential distribution will occur at steady state.

Since plate P_2 has a potential $-V_o$ above plate P_1, only the fraction $\exp(-V_o/kT_1)$ of the electrons emitted by plate P_1 will reach plate P_2. The remaining fraction $1-\exp(-V_o/kT_1)$ will be rejected[3] by P_2, and since all subsequent plates have greater negative potentials than P_1, these electrons will also be rejected by all these plates. These rejected electrons are absorbed only by cold plate[4] P_n' at the same potential as hot plate P_2.

---

[3] By rejected is meant the electrons that do not have enough energy to overcome the potential barrier, $\delta = V_o$, near the surface of plate P_1.

[4] All the electrons emitted by P_1 can be absorbed by P_n' since we have set the potential barrier, $\delta = o$, for all condenser plates.

The $I_m \exp(-V_o/kT)$ electrons that can reach plate P_2 through its barrier V_o, will strike this plate "m" times. Consequently $r^m I_m \exp(-V_o/kT)$ will be reflected and $(1-r^m)I_m \exp(-V_o/kT_1)$ will be absorbed. The reflected electrons will pass on to the condenser and can be absorbed only by P_n'. (Note that even if the reflection coefficient is large, since its value must be less than unity, the value of m may be selected so that r^m is much less than 1. (e.g. for r equals 0.25 and m equals 4, r^m is less than 0.4%). Thus the reflected current can be neglected.)

The current $I_m \left[1 - \exp(-V_o/kT) \right]$ rejected by P_2 and absorbed by P_n' is returned to P_2 by a suitable electric conductor.

The above analysis holds for any corresponding set of plates since all adjacent plates have the same potential difference V_o. It follows that starting from hot plate P_1 a net current I_m passes from hot plate to hot plate to successively higher negative potentials. This current is totally absorbed by the first cold plate P_1' having a zero potential barrier. But P_1' is cold and its emitted current can be neglected as a first approximation. Consequently in order for the potential of plate P_1' to be maintained at $-(n + 1)V_o$ volts above plate P_1 a current of magnitude I_m must be conducted through the external load. The <u>power output</u> is:

$$P = n + V_o I_m = \eta V_o I_s \frac{r^m - 1}{m(r-1)} \exp(-V_o/kT) \qquad (11)$$

Thermal Efficiency

The thermal efficiency of any heat engine is defined by

$$\eta_t = P_{net} / \Sigma q_{in}$$

where P_{net}, and Σq_{in} denote the net power output and rate of heat input to the hot plates, respectively.

In the next section, the heat transferred to the hot plates, the heat transferred from the cold plates and the thermal efficiency are computed.

Currents Emitted By Cold Plates

The currents emitted by the cold plates have been neglected in the previous calculations. However, in order to compute the thermal efficiency, these currents must be considered, especially if T_2 approaches T_1.

Let I_m' be the emitted current per unit area of a cold plate at a temperature of T'. Then, from the previous analysis:

$$I_m' = A(T')^2 \exp(-\varphi/kT) \left[(1-r^m)/m(1-r)\right] \qquad (13)$$

This current, emitted by any cold plate, P_k', is deflected by the crossed electric and magnetic field to the adjacent cold plate on the right, or to P_{k+1}' as shown in Fig. 13, and is totally absorbed by plate P_{k+1}'. However,

the current emitted from the last cold plate, P_n', will be "lost" if no provision is made to collect it. (For the cold plate at room temperature this "lost" current is infinitessimal.) Hence, the net current produced by the engine is:

$$I_{net} = I_m - I_m' \tag{14}$$

For the purposes of making a complete energy balance, it is assumed that the "lost" current is collected at the first hot plate, P_1.

Heat Transferred To The Hot Plates

Consider any hot plate, P_k, except the first plate, P_1. A control volume is drawn around the surface of this plate. An external observer "sees" a heat flux q_k supplied to this control volume, a stream of electrons approaching from P_{k-1}, and a second stream of electrons leaving this control volume.

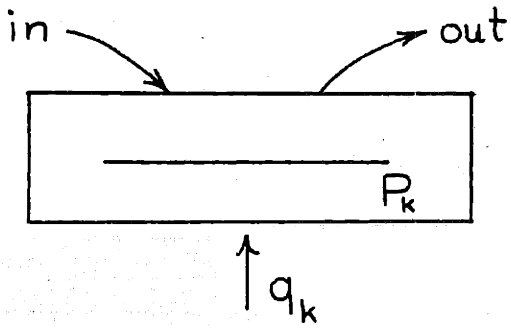

For steady state, the First Law applied to this control volume yields:

$$q_k = U_{in} - U_{out}$$

where U_{in} and U_{out} denote the energy fluxes of electrons entering and leaving this control volume, respectively. The energy balance then yields:

a) Energy Flux of Outgoing Electrons

Average kinetic energy per electron[5]	$V_o + 2kT$
Heat of vaporization per electron	φ
Total average energy per electron	$V_o + 2kT + \varphi$
Current emitted	I_m
Energy flux of outgoing electrons	$(V_o + 2kT + \varphi) I_m$

b) Energy Flux of Approaching Electrons

The electrons approaching plate P_k have been emitted from plate P_{k-1}, but since plate P_k has a potential $-V_o$ with respect to plate P_{k-1}, the average kinetic energy of the electrons with respect to plate P_{k-1}, i.e. $(2V_o + 2kT)$, is increased by $-V_o$ with respect to the control volume around plate P_k. Hence:

Average kinetic energy per electron at P_{k-1}	$2V_o + 2kT$
Heat of condensation per electron	φ
Increase of potential energy with respect P_k	$-V_o$
Total average energy per electron	$(2V_o + 2kT + \varphi - V_o)$
Current absorbed by plate P_k	$I_m \exp(-V_o/kT)$
Energy flux of incoming electrons:	$(V_o + 2kT + \varphi) I_m$

---

[5] See Appendix 2

c) Heat Flux Input to Hot Plate, P_k

$$q = -(V_o + 2kT_1 + \varphi) I_m \exp(-V_o/kT) + (V_o + 2kT + \varphi) I_m$$

$$= (V_o + 2kT_1 + \varphi) I_m [1 - \exp(-V_o/kT)] \qquad (15)$$

For the first hot plate P_1, the results of a similar analysis are as follows:

a) Energy Flux of Outgoing Electrons

Average kinetic energy per electron	$V_o + 2kT$
Heat of vaporization	φ
Total average energy per electron	$V_o + 2kT + \varphi$
Number of electrons emitted	I_m
Energy flux of outgoing electrons	$(V_o + 2kT + \varphi) I_m$

b) Energy Flux of Incoming Electrons

The incoming electrons are assumed to arrive at the first hot plate P_1 from the last cold plate P_n'.

Average kinetic energy per electron	$2kT'$
Heat of condensation per electron	φ
Decrease of potential energy with respect to plate P_1 per electron	V_o
Total average energy per electron	$(V_o + 2kT' + \varphi)$
Number of electrons absorbed by plate P_1	I_m'
Energy flux of incoming electrons	$(V_o + 2kT' + \varphi) I_m$

c) Heat Input to Hot Plate P_1

$$q = (V_o + 2kT + \varphi) I_m - (V_o + 2kT' + \varphi) I_m' \tag{16}$$

According to the above analysis the total heat flux to all hot plates is:

$$\sum_{k=1}^{n} q_k = \sum_{k=2}^{n} q_k + q_1$$

$$= (n-1)(V_o + 2kT + \varphi) I_m \left[1 - \exp(-V_o/kT) \right]$$

$$+ (V_o + 2kT + \varphi) I_m - (V_o + 2kT' + \varphi) I_m' \tag{17}$$

Cold Plates

Consider any cold plate, P_k', except the first plate, P_1'. A control volume is drawn around the surface of this plate. An external observer "sees" a heat flux q_k' rejected from this control volume, a stream of electrons leaving this control volume.

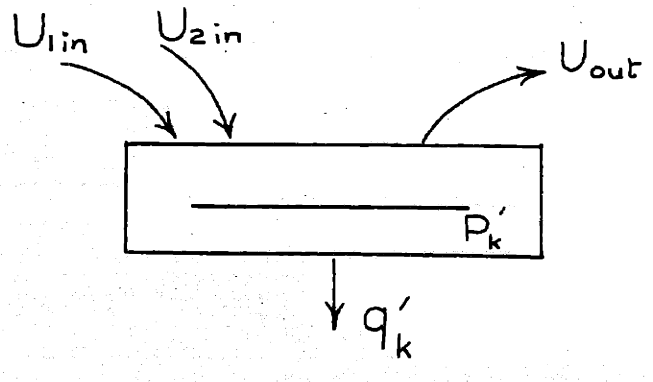

For steady state, the First Law applied to this control volume yields:

$$q_k' = U_{1\ in} + U_{2\ in} - U_{out}$$

where $U_{1\ in}$, $U_{2\ in}$ are the incoming energy fluxes of electrons and U_{out} is the outgoing energy flux of those electrons, respectively.

a) Energy Flux of Outgoing Electrons

Average kinetic energy per electron	$2kT'$
Heat of vaporization per electron	φ
Total average energy per electron	$2kT' + \varphi$
Number of electrons emitted	I_m'
Energy flux of outgoing electrons	$(2kT' + \varphi) I_m$

b) Energy Flux of Approaching Electrons from Plate P_{n-k}

Average kinetic energy per electron at P_{n-k} [6]	$V_o \left[\frac{1-2\exp(-V_o/kT)}{1-\exp(-V_o/kT)}\right] + 2kT$
Heat of condensation per electron	φ
Increase of potential energy with respect to plate P_k'	$-V_o$
Total average energy per electron	$V_o \left[\frac{1-2\exp(-V_o/kT)}{1-\exp(-V_o/kT)}\right] + 2kT + \varphi - V_o$
Number of electrons	$I_m [1 - \exp(-V_o/kT)]$

---

[6] See Appendix 2

Energy flux of incoming electrons from boiler plate P_{n-k}

$$\left[V_o\left\{\frac{1-2\exp(-V_o/kT)}{1-\exp(-V_o/kT)}\right\}+2kT+\varphi-V_o\right] I_m\left[1-\exp(-V_o/kT)\right]$$

$$= (2kT+\varphi) I_m\left[1-\exp(-V_o/kT)\right] - V_o I_m \exp(-V_o/kT)$$

c) Energy of approaching electrons from plate P'_{k-1}

Average kinetic energy	$2kT'$
Heat of condensation per electron	φ
Decrease of potential energy	V_o
Total average energy per electron	$(V_o+2kT+\varphi)$
Number of electrons absorbed	I'_m
Energy flux of incoming electrons	$(V_o+2kT+\varphi) I'_m$

d) Heat Rejected from Cold Plate, P_k'

$$q_k = (2kT+\varphi) I_m \left[1-\exp(-V_o/kT)\right] - V_o I_m \exp(-V_o/kT)$$

$$+ (V_o+2kT'+\varphi) I'_m - (2kT'+\varphi) I'_m$$

$$= (2kT+\varphi) I_m\left[1-\exp(-V_o/kT)\right] - V_o I_m \exp(-V_o/kT) V_o I_m$$

(18)

For the first cold plate P', the results of a similar analysis are as follows:

a) Energy Flux of Outgoing Electrons

Average kinetic energy per electron	$2kT'$
Heat of vaporization	φ
Total average energy per electron	$2kT' + \varphi$
Number of electrons emitted	I_m'
Energy flux of outgoing electrons	$(2kT' + \varphi) I_m'$

b) Energy Flux of Incoming Electrons from Hot Plate P_n

Average kinetic energy per electron	$V_o + 2kT$
Heat of condensation	φ
Increase of potential energy	$-V_o$
Total average energy per electron	$2kT + \varphi$
Number of electrons absorbed by plate P_1'	$I_m \exp(-V_o/kT)$
Energy flux of outgoing electrons	$(2kT + \varphi) I_m \exp(-V_o/kT)$

c) Heat Rejected from Cold Plate P_1'

$$q_1' = (2kT + \varphi) I_m = (2kT' + \varphi) I_m'$$

According to the above analysis the total heat rejected from all cold plates is:

$$\sum_{k=1}^{n} q_k' = \sum_{k=2}^{n} q_k' + q_1' = (n-1)(\varphi + 2kT) I_m \left[1 - \exp(-V_o/kT)\right]$$

$$+ (\varphi + 2kT) I_m - (n-1) V_o I_m \exp(-V_o/kT) + (n-1) V_o I_m' - (\varphi + 2kT') I_m' \quad (19)$$

Thermal Efficiency

From the previously calculated heat input and power output the thermal efficiency, neglecting radiation losses, can be easily calculated.

$$\eta = \frac{P_{net}}{\sum_{k=1}^{n} q_k} = \frac{n V_o \left[1 - I_m'/I_m\right]}{(V_o + \varphi + 2kT)\left[n - n\exp(-V_o/kT) - I_m'/I_m\right]} \tag{20}$$

substituting values for I_m and I_m' from eqs. (10) and (13) we get:

$$\eta = \frac{n V_o \exp(-V_o/kT) - (T'/T)^2 \exp\left[-\varphi(T/T'-1)/kT\right]}{(V_o + 2kT + \varphi)\left[n\exp(-V_o/kT) - n\exp(-2V_o/kT) - (T'/T)^2\exp\left[-\varphi(T/T'-1)/kT\right]\right]} \tag{21}$$

For the case of the magnetic triode where n equals 1.

Assuming T much greater than T' we obtain:

$$\eta = \frac{V_o}{(V_o + 2kT + \varphi)\left[1 - \exp(-V_o/kT)\right]} \tag{22}$$

For large values of n the efficiency becomes substantially independent of n

$$\eta = \frac{X\left\{\exp(-X) - (1-\mu)^2 \exp\left[-Y\mu/(1-\mu)\right]\right\}}{(X+Y+2)\left[1-\exp(-X)\right]\exp(-X)} \tag{23}$$

where

$$\mu = 1 - T'/T \qquad X = V_0/kT \qquad Y = \varphi/kT$$

For thoriated tungsten ($\varphi \cong 2.4$ volts $A \cong 3$ amps/cm^2 °K^2)

the efficiency given by eq. (23) is plotted versus μ in Figs. 23 and 24, for values of X = 1, 2, 3, 5, and 7.

Figures 23 and 24 show that the efficiency increases with increasing values of X, but the power output per unit area of the device decreases with increasing X. This power decrease follows from the fact that the output power is proportional to X exp(-X)[7]. The maximum power output occurs at X equals 1.

For values of μ greater than 0.5, the efficiency remains substantially constant, or no appreciable increase of efficiency can be achieved by

---

[7] See eq. (11)

lowering the absolute cold plate temperature below half the absolute temperature of the hot plates. (For $\mu = 0.5$, $T'/T = 0.5$).

Thermodynamic Analysis of T.E.E.

The First and Second Laws of Thermodynamics provide a check of the results obtained in the previous analysis. In addition, the Second Law of Thermodynamics provides means for locating possible irreversibilities, which might be reduced to increase the efficiency.

First Law

In the multiplate configuration the heat flux supplied to the hot plates, the heat flux rejected by the cold plates, and the output power flux have been derived independently. Hence, substitution of these three quantities into the First Law expression provides a check on the consistency of the analysis.

From the First Law we have:

$$\sum_{k=1}^{n} q_k - \sum_{k=1}^{n} q'_k - P_{net} \equiv 0$$

Substituting from eqs. (11), (17), and (19), we get:

$$\sum_{k=1}^{n} q_k - \sum_{k=1}^{n} q'_k - P_{net} = I_m (n-1)(V_o + 2kT + \varphi)\left[1 - \exp(-V_o/kT)\right]$$
$$+ I_m (V_o + 2kT + \varphi) - (V_o + 2kT + \varphi) I'_m$$
$$- I_m (n-1)(\varphi + 2kT)\left[1 - \exp(-V_o/kT)\right] - I_m (\varphi + 2kT)$$
$$+ I_m (n-1) V_o \exp(-V_o/kT) - I'_m (n-1) V_o + (\varphi + 2kT') I'_m$$
$$- I_m (n+1) V_o + V_o I'_m \equiv 0 \qquad (24)$$

Second Law

An expression for the thermal efficiency of the T.E. engine is given by eq. (23). One of the parameters in this equation is μ which equals the efficiency of a reversible engine operating between the temperature levels T and T'.

From the Second Law we should have:

$$\eta \leq \mu$$

Let us first consider some limiting cases. We notice that for very small values of X, eq. (23) reduces to:

$$\eta = \frac{1 - X^2 - [1+X](1-\mu)^2 \exp\left[-Y\mu/(1-\mu)\right]}{X + Y + 2} \qquad (25)$$

where we have approximated e^{-X} by $1 - X$ and $(1 - X)^{-1}$ by $1 + X$

In expression (25) η increases for decreasing X. Consequently, it will reach its maximum for $X = 0$.

$$\eta_{X=0} = \frac{1-(1-\mu)^2 \exp[-Y\mu/(1-\mu)]}{Y+2} \tag{26}$$

A decrease of parameter Y in expression (26) will result in an increase of the efficiency η . This means that a decrease of the work-function or an increase of the temperature will result in an increase of efficiency.

The effect of the temperature on the efficiency is self evident. The effect of the work function is due to a heat of transport associated with an electron flow between two surfaces. This heat of transport equals

$$I\varphi$$

where I is the current flow. If the two surfaces have temperatures T and T' respectively, the increase of entropy due to an electron flow I from the surface at T to the surface at T' is

$$\Delta S = \frac{I\varphi}{T'} - \frac{I\varphi}{T} = kI\frac{\varphi}{kT}\left[\frac{T}{T'} - 1\right] = kIY\frac{\mu}{1-\mu} \tag{27}$$

Since a material with zero work function does not exist and since there is a practical limitation on the temperature the lowest value of Y is limited. However, let us assume Y equals 0. The efficiency will be:

$$\eta = \mu - \frac{\mu^2}{2} \tag{28}$$

which is less than the reversible efficiency. The irreversibility here is due to the energy distribution of the electrons. This irreversibility is minimized as $\mu \to 0$, for which case $\eta \to \mu$

From the previous discussion we conclude that the efficiency given in eq. (26) is always smaller than the reversible efficiency.

Let us now consider the case of finite Y , in eq. (26). If we let μ approach zero we get:

$$\eta_{\mu \to 0} = \frac{1-(1-2\mu)(1-Y\mu)}{Y+2} = \frac{1-1+Y\mu+2\mu-2Y\mu^2}{Y+2}$$

$$= \frac{(Y+2)\mu}{(Y+2)} = \mu \tag{29}$$

This means that for any fixed value of work function and temperature T, if the voltage step (proportional to X), and the temperature step (proportional to μ) are made very small, the engine will approach the reversible efficiency. This fact is of great importance for an actual design since it is possible to have a number of engines operating in series approximately in this fashion between a fixed temperature drop.

Let us now consider the other limiting case of large values of X, in eq. (23). If X is large, exp(-X) is very small. Since we are only

interested in positive values of efficiency, the value of the term $(1-\mu)^2 \exp[-Y\mu/(\mu-1)]$ should be comparatively small. In other words, for a fixed value of Y, μ must approach unity. Assuming a value of μ of 1 we obtain the expression:

$$\eta = \frac{X}{(X+Y+2)\left[1-\exp(-X)\right]} \tag{30}$$

Equation (30) approaches unity for large values of X, or for values of μ approaching one, and very large values of X the efficiency of the engine approaches the reversible efficiency. This trend is very easily seen in Figs. 23 and 24.

However, this second limiting case appears to have no practical importance. In an actual case, the radiation losses are finite and should be included in the efficiency. On the other hand, an increase of X will result in a decrease of the output power. Consequently, the value of the actual efficiency will tend to zero regardless of the value of the lossless efficiency given by eq. (23).

THE ANALYSIS OF THE ELECTRON FLOW

In the previous sections we have assumed the shape of the electron trajectories as well as the shape of the potential distribution in the region between the anodes and the cathodes. In this section an analysis is presented which relates the election paths, the potential distribution, and the current densities involved to the critical parameters of the configuration such as anode-cathode distance, magnetic field, anode potential, etc.

General Equations

Consider an electron gas flowing in free space under the influence of an electric field $\vec{E}$ (x,y,z,t) and a magnetic field $\vec{B}$ (x,y,z,t), where x, y, and z are the Cartesian coordinates and t the time.

Let:

$\vec{V}$ (x,y,z,t)	the velocity vector of the electron gas at a point (x,y,z) and time t.
ρ (x,y,z,t)	the mass density of the gas
m_e	the electronic mass
Q_e	the electronic charge

The flow of the electron gas will be governed by the following general equations.

1. Equation of Motion

$$\frac{Q_e}{m_e}\left[\vec{E} + \vec{V} \times \vec{B}\right] = \frac{D\vec{V}}{dt} \tag{31}$$

2. The Continuity Equation

$$\frac{\partial \rho}{\partial t} + \text{div}\,(\rho \vec{V}) = 0 \tag{32}$$

3. Poisson's Equation

$$\text{div}\,\vec{E} = \frac{Q_e}{m_e}\,\frac{\rho}{E_o} \tag{33}$$

One Dimensional Electron Flow Under The Influence Of Crossed Electric And Magnetic Fields

Consider two parallel plates, P and A_1, separated by a distance y_a small compared to the dimensions of the plates, as shown in Fig. 15. Plates P and A_1 are maintained at a potential difference Ψ_a while a uniform magnetic field B_z is established in the space between the plates. Let a uniform electron current be emitted from plate P. At steady state all time derivatives will equal zero. Due to symmetry, we can assume also for points near the center of plates P and A, all gradients along the x and z directions, shown in Fig. 15, as well as the electric field components E_x and E_z to equal zero. In addition, since no forces act on the electron on the z direction or the direction of the magnetic field, the electron velocity in the z direction, V_z, also equals zero. The above assumptions are equivalent to assuming one dimensional electron flow.

If now we expand eqs. 31, 32, and 33, and set

$$\frac{\partial}{\partial x}=0\,,\frac{\partial}{\partial z}=0\,,\ \frac{\partial}{\partial t}=0\,,E_x=0\,,E_z=0\,,B_x=0\,,B_y=0\,,V_z=0$$

we obtain the following set of ordinary differential equations:

$$\frac{Q_e}{m_e}B_z=\frac{dV_x}{dy} \tag{34}$$

$$\frac{Q_e}{m_e}\left[E_y-V_xB_z\right]=V_y\frac{dV_y}{dy} \tag{35}$$

$$\frac{Q_e}{m_e}\frac{\rho}{\epsilon_o}=\frac{dE_y}{dy} \tag{36}$$

$$\frac{d(\rho V_y)}{dy}=0 \tag{37}$$

Integrating eq. 37 we obtain

$$\frac{Q_e}{m_e}\rho V_y=2I_d \tag{38}$$

where $2I_d$ is a constant equal to the total current crossing a unit area parallel to the plates. If current flows in both positive and negative y directions in the same amount, I_d, the current density will denote the current flowing in each direction.

Boundary Conditions

The electrons emitted from an actual cathode have a Maxwellian energy distribution. It is evident that whereas the average velocity components in the x and z directions at the emitting surface are zero the y component of velocity will have a finite value. The emitted electrons will tend consequently to move away from the emitting surface. However, the electrons that are already in the space neighboring to the emitting surface will create a field which tends to oppose any motion of electrons from the surface. Resulting from the above interactions is a potential distribution possessing a minimum very close to the emitting surface. This well-known phenomenon is discussed in a later section.

Let:

y_c the distance of the potential minimum from the emitting surface.

$-\delta$ the potential at the potential minimum with respect to the emitting surface.

We fix our coordinate system so that the emitting surface is the plane $y = -y_c$ and the potential minimum lies at $y = 0$. (Fig. 16)

Neglecting the thermal velocities of the electron as compared to the electron velocities caused by the accelerating field we have:

for

$$y=0 \quad V_y=0 \quad V_x=0 \qquad \text{and} \qquad \frac{d\psi}{dy} = E_y = 0 \tag{39}$$

Velocity Distribution

Substituting eq. 38 into eq. 36

$$\frac{2 I_d}{E_o V_y} = \frac{dE_y}{dy} \tag{40}$$

Differentiating eq. 35

$$\frac{Q_e}{m_e}\left[\frac{dE_y}{dy} - B_z \frac{dV_x}{dy}\right] = 1 \tag{41}$$

Let

$$C_1 = \frac{2 Q_e I_d}{m_e \epsilon_o} \qquad C_2 = \left(\frac{Q_e}{m_e} B_z\right)^2 \tag{42}$$

We get from eq. 42

$$\frac{C_1}{V_y} - C_2 = \left(\frac{dV_y}{dy}\right)^2 + V_y \frac{d^2 V_y}{dy^2} \tag{43}$$

We make the transformation of variables

$$\frac{dV_y}{dy} = \left[\frac{dy}{dV_y}\right]^{-1} \tag{44}$$

and

$$\frac{d^2V_y}{dy^2} = \frac{d}{dy}\left[\left(\frac{dy}{dV_y}\right)^{-1}\right] = -\left(\frac{dy}{dV_y}\right)^{-3}\frac{d^2y}{dV_y^2} \tag{45}$$

Substituting eqs. 44 and 45 into eq. 43:

$$\frac{C_1}{V_y} - C_2 = \left[\frac{dy}{dV_y}\right]^{-2} - V_y\left[\frac{dy}{dV_y}\right]^{-3}\frac{d^2y}{dV_y^2} \tag{46}$$

Let

$$\frac{dy}{dV_y} = \xi^{-1/2} \qquad \text{and} \qquad V_y = j \tag{47}$$

Substituting into eq. 46

$$\frac{C_1}{j} - C_2 = \xi + j\,\frac{1}{2\xi^{-3/2}}\,\xi^{-3/2}\frac{d\xi}{dj} \quad \text{OR} \quad \frac{C_1}{j} - C_2 = \xi + \frac{j}{2}\frac{d\xi}{dj} \tag{48}$$

The solution of differential eq. 48 is:

$$\xi = e^{-\int \frac{2}{j} dj} \int e^{\int \frac{2}{j} dj} \left[\frac{2C_1}{j^2} - \frac{2C_2}{j} \right] dj + C_3' \, e^{-\int \frac{2}{j} dj}$$

or

$$\xi = \frac{C_3}{j^2} + \frac{2C_1}{j} - C_2 \tag{49}$$

Substituting the original variables

$$\frac{dy}{dV_y} = \left[\frac{C_3}{V_y^2} + \frac{2C_1}{V_y} - C_2 \right]^{-1/2} \tag{50}$$

Substituting eq. 50 into eq. 35

$$\frac{Q_e}{m_e} \left[E_y - V_x B_z \right] = \left[C_3 + 2C_1 V_y - C_2 V_y^2 \right]^{1/2} \tag{51}$$

From boundary conditions eq. 39

$$\text{For } V_y = 0 \,, \; V_x = 0 \quad \text{and} \quad E_y = 0$$

or

$$C_3 = 0 \tag{52}$$

Integrating eq. 50 with $C_3 = 0$

$$y = \int \left[\frac{2C_1}{V_y} - C_2\right]^{-1/2} dV_y$$

$$= -\frac{\sqrt{V_y(2C_1 - V_y)}}{C_2} - \frac{2C_1}{C_2\sqrt{C_2}} \sin^{-1}\left[\pm\sqrt{1 - \frac{C_2}{2C_1}V_y}\right] + C_4 \qquad (53)$$

but for $y = 0 \quad V_y = 0$

so

$$C_4 = \mp \frac{2C_1}{C_2\sqrt{C_2}} \frac{\pi}{2} \qquad (54)$$

Let y_m be the maximum height of the electron trajectories where

$$V_y = 0$$

We find that from eqs. 53 and 54

$$y_m = \mp \frac{2C_1}{C_2\sqrt{C_2}} \frac{\pi}{2} \pm \left(s\pi + \frac{\pi}{2}\right) \frac{2C_1}{C_2\sqrt{C_2}} = \pm s\pi \frac{2C_1}{C_2\sqrt{C_2}} \qquad (55)$$

where s a positive integer.

Substituting the values of C_1 and C_2 in eq. 55 we get:

$$y_m = s \frac{4\pi}{\epsilon_o} \frac{I_d}{B_z^3} \left(\frac{m_e}{Q_e}\right)^2 \tag{56}$$

Electron Trajectories

Integrating eq. 34 and setting $V_x = 0$ for $y = 0$ we get:

$$V_x = \frac{Q_e}{m_e} B_z y \tag{57}$$

Equations 53 and 57 give us the velocity component V_x and V_y as a function of y. However, eq. 53, being a transcendental equation, can not be solved explicitly in the form $V_y = (y)$, and a graphical procedure must be used in order to map the velocity fields, and to trace the electron trajectories.

It is seen in eq. 56 that the maximum height of the electron trajectory y_m depends on the value of the integer s and consequently is indetermined. This indeterminary is discussed in detail by Stater in reference R7. The meaning of eq. 56 is that a discrete number of modes for the electron trajectories are possible, each mode being characterized by the corresponding value of s.

Experimentally, the first two modes for s = 1 and s = 2 have been observed in the present program[7].

Figure 17 shows the electron trajectories for the first three modes, S = 1, S = 2, and S = 3. It can be shown from the foregoing analysis that the chord of the electron trajectories is:

$$\lambda = 2 S n y_m \tag{58}$$

Potential Distribution

Let ψ be the potential of any point y above the emitting surface. From energy considerations the potential energy of the electron at any point y must equal the kinetic energy of these electrons.

$$Q_e \psi(y) = \frac{1}{2} m_e V^2 = \frac{1}{2} m_e (V_y^2 + V_x^2) \tag{59}$$

Substituting eq. 57 into eq. 59

$$\psi(y) = \frac{1}{2} \frac{m_e}{Q_e} V_y^2 + \frac{1}{2} \frac{Q_e}{m_e} B_z^2 y^2 \tag{60}$$

By combining eqs. 53 and 60 the potential distribution can be readily found.

---

[7] See experimental results

Equation 60 gives the potential distribution for any point y less than y_m. At points y greater than y_m no electrons exist and consequently the potential distribution must be linear

for

$$y > y_m \quad \psi' = C_7 y + C_8 \tag{61}$$

The two curves defined by eqs. 60 and 61 must join smoothly at the point $y = y_m$ or

at

$$y = y_m \quad \psi = \psi' \text{ and } \frac{d\psi}{dy} = \frac{d\psi'}{dy} \tag{62}$$

By imposing conditions eq. 62 on eq. 61 we can solve for the constants C_7 and C_8. The potential ψ' becomes accordingly:

$$\psi' = \frac{1}{2} \frac{Q_e}{m_e} B^2 y_m \left[2y - y_m\right] \tag{63}$$

Let y_a be the distance of the anode from the center of the coordinate axis. If y_a is greater than y_m the anode potential will be given by:

$$\psi_a = \frac{1}{2} \frac{Q_e}{m_e} B^2 y_m \left[2y_a - y_m\right] \tag{64}$$

From our definition of the coordinate axis the anode cathode distance is

$$y_{ac} = y_a + y_c \tag{65}$$

However, since in most cases

$$y_c \simeq 0 \qquad y_{ac} \simeq y_a \tag{66}$$

Analysis For The Region, y less than y_c

In this region adjacent to the emitting surface the electron velocities will be of the order of the thermal velocities and the energy distribution will be Maxwellian. A detailed analysis of this region is given by Slater in reference R7. Slater obtains the following result for the distance between the point of the potential minimum and the emitting surface:

$$y_c = \left(\frac{2E_o}{I_e Q_e}\right)^{1/2} \frac{(kT)^{3/4}}{(2\pi m_e)^{1/4}} \cos^{-1} e^{-\delta/2kT} \tag{67}$$

and in the present units

$$y_c = 1.54\times10^{-6} \frac{T^{3/4}}{I_e^{1/2}} \cos^{-1} e^{-\delta/kT}$$

$$= 1.54\times10^{-6} \frac{T^{3/4}}{I_e^{1/2}} \cos^{-1} \left(I_e/I_s\right)^{1/2} \tag{68}$$

where δ the potential of the cathode with respect to the point of potential minimum.

End Effects

In the preceding analysis we have considered the emitting surface and anode to be infinite plates so that end effects can be neglected. In that case the current emitted by each element of the emitting surface equals the current absorbed by it. If I_e is the current emitted per unit area of the emitter, the current per unit area crossing in either direction an element of surface parallel to the emitting surface will be $2I_e$. In eq. 38 we called this total current $2I_d$. Consequently:

$$I_e = I_d \tag{69 a}$$

or the emitted current equals the current density.

Let us now consider a finite emitting surface in which the flow is directed from left to right. We distinguish two cases:

a. The trajectory chord λ is smaller than the plate width ℓ, (Fig. 18)

b. The trajectory chord λ is larger than the plate width ℓ, (Fig. 19)

In the first case it is clear that no current is absorbed by any parts of the emitting plate. Consequently the current crossing any surface element parallel to the emitter must equal the emitting

current. This emitting current is not uniform. This is due to the fact that the total charge lying directly above any element of the plate varies from a zero value at the left side of the plate to a maximum value at the right side of the plate (Fig. 18). A consequence of the above is the continuous variation of the potential barrier δ from a zero to a maximum value, δ_{max}, as shown in Fig. 18. An exact solution of this problem can be obtained from eqs. 31 to 33 with the aid of digital computers. This solution is not available at present. However, we can compute approximately the average value of the emitted current from

$$\bar{I}_e = 2I_d \tag{69b}$$

where I_d is given from eq. 56.

In an actual case the independent variables will be the anode potential ψ_a, the magnetic field B and the anode cathode distance $y_a + y_c$. Assuming $y_c \simeq 0$ the height of the electron trajectories, y_m, can be computed from eq. 64. Equation 56 can now be used to compute the current density, I_d. The emitted current per unit area will be given by eq. 69b.

The second case, where $\lambda > \ell$ is more complex. Here the emitting plate contains more than one complete trajectory, (Fig. 19).

Let:

λ be the chord length of the first trajectory

λ' the chord length of the second trajectory

I_s the saturation emission current of the emitter

δ the average potential barrier over the span of the first trajectory

$\bar{I}_e$ the average emitted current per unit area over the span of the second trajectory

δ' the average potential barrier over the span of the second trajectory

$\bar{I}_e'$ the average emitted current per unit area over the span of the second trajectory

The emitted current, $\bar{I}_e$, will be related to the current density, I_d, defined in eq. (38) by:

$$I_e = \alpha I_d \tag{70}$$

where $1 < \alpha < 2$

The limiting cases are:

$$\alpha = 1 \quad \text{for} \quad \lambda \ll \ell \tag{71}$$

$$\alpha = 2 \quad \text{for} \quad \lambda > \ell \tag{72}$$

as discussed previously.

The current density I_d', for the second trajectory, can be found by dividing the total current crossing a surface parallel to the emitting surface and of area λ' by twice the area . (The depth of the emitting plate in a direction normal to the plane of Fig. 19 is assumed unity)

$$I_d' = \frac{\lambda \bar{I}_e + \lambda \bar{I}_e \left\{1 - \exp\left[-(\delta' - \delta)/kT\right]\right\} + \lambda' I_e'}{2\lambda'} \tag{73}$$

but

$$\bar{I}_e = \bar{I}_s \exp\left[-\delta/kT\right]$$
$$\text{and}$$
$$\bar{I}_e' = I_s \exp\left[-\delta'/kT\right] \tag{74}$$

substituting eq. (74) into eq. (73) and rearranging

$$I_d' = I_s \left\{ \frac{\lambda}{\lambda'} + \tfrac{1}{2}\left(1 - \frac{\lambda}{\lambda'}\right) \exp\left[-(\delta' - \delta)/kT\right] \right. \tag{75}$$

Combining eqs. (70), (74), and (75)

$$\frac{I_d'}{I_d} = \alpha \left\{ \frac{\lambda}{\lambda'} + \frac{1}{2}\left(1 - \frac{\lambda}{\lambda'}\right) \exp\left[-(\delta' - \delta)/kT\right] \right. \tag{76}$$

We now can compute the ratio λ/λ' the following way. From eq. (58)

$$\frac{\lambda}{\lambda'} = \frac{y_m}{y_m'} \tag{77}$$

and from eq. (56), for the first mode s equals 1 and constant magnetic field B

$$y_m / y_m' = I_d / I_d' \tag{78}$$

or from eqs. (77) and (78)

$$\lambda / \lambda' = I_d / I_d' \tag{79}$$

Let us substitute

$$I_d / I_d' = \lambda / \lambda' = 1 - \beta \tag{80}$$

into eq. (76) and determine whether β is positive or negative.

$$\begin{aligned} I_d' / I_d &= \alpha \left\{ 1 - \beta \pm \tfrac{1}{2} \beta \exp\left[-(\delta' - \delta)/kT \right] \right\} \\ &= \alpha \left\{ 1 - \beta \left(1 - \tfrac{1}{2} \exp\left[-(\delta' - \delta)/kT \right] \right) \right\} \end{aligned} \tag{81}$$

If

$\beta < 0$ from eq. 80

$$I_d / I_d' > 1 \quad \text{or} \quad I_d' / I_d < 1 \tag{82}$$

but since $1 - \frac{1}{2} \exp\left[-(\delta' - \delta)/kT\right] > 0$

and $\alpha > 1$

from eq. (81) $I_d'/I_d > 1$

which contradicts eq. (82).

Consequently

$$\beta > 0 \ , \ y_m'/y_m = \lambda'/\lambda \text{ and } I_d'/I_d > 1 \tag{83}$$

We can get an estimate of the magnitude of β the following way.

Since the minimum value of $\exp\left[-(\delta' - \delta)/kT\right]$ is zero, we get from eq. (81)

$$I_d'/I_d > \alpha(1-\beta) \tag{84}$$

Substituting eq. (80) into eq. (84)

$$\alpha(1-\beta)(1+\beta) < 1 \tag{85}$$

or

$$\beta > \sqrt{1 - 1/\alpha} \tag{86}$$

and

$$y_m/y_m' < 1 - \sqrt{1 - 1/\alpha} \tag{87}$$

The quantities y_m and y_m' must also satisfy eq. (64). Noting that ψ_a and B are the same for the two cases we obtain from eq. (64)

$$\frac{y_m' (2y_a' - y_m')}{y_m (2y_a - y_m)} = 1 \tag{88}$$

or

$$\frac{2y_a'/y_m' - 1}{2y_a/y_m - 1} = \left(\frac{y_m}{y_m'}\right)^2 = (1-\beta)^2 \tag{89}$$

since $1 > \beta > 0$

from eq. (89)

$$\frac{2y_a'/y_m'}{2y_a/y_m} < (1-\beta)^2 \tag{90}$$

or

$$y_a'/y_a < 1-\beta \tag{91}$$

and using a relation (65), for constant anode to cathode distance y_{ac}

$$\frac{y_{ac} - y_c'}{y_{ac} - y_c} < 1-\beta \tag{92}$$

and

$$\frac{1 - y_c'/y_{ac}}{1 - y_c/y_{ac}} < 1 - \beta \tag{93}$$

Let us now get an idea of the order of magnitude of the ratio y_c/y_{ac} for an actual case. The anode cathode distance y_{ac} is usually of the order of 0.5 cm. The boundary layer thickness y_c can be computed from eq. (68). For

$$I_e = 1 \text{ amp/cm}^2 = 10^4 \text{ amps/m}^2$$
$$I_s = 10 \text{ amp/cm}^2$$
$$T = 1800^\circ K \quad , y_c = 5.25 \times 10^{-4} \text{ cm}$$

For these values of y_c and y_{ac} the ratio y_c/y_{ac} is approximately 10^{-3}, and can be neglected in eq. (93). Thus

$$1 - y_c'/y_{ac} < 1 - \beta$$

or

$$y_c'/y_{ac} > \beta > \sqrt{1 - 1/\alpha} \tag{94}$$

In estimating the value of α a certain value may be assumed leading to a number of conclusions which may or may not justify the original choice.

Let us make the educated guess α equals 3/2. Equation (94) yields

$$y_c' > \sqrt{1/3}\, y_{ac} \tag{95}$$

and for y_{ac} approximately equal to 0.5 cm

$$y_c' > 0.288 \text{ cm}$$

In order to have y_c' greater than 0.288 cm. we see from eq. (68) that

$$I_e' < \frac{(1.54)^2}{0.288}\ 10^{-12}\ T^{-6/4} \text{ amp/cm}^2$$

and for T equals 1800°K

$$I_e' < 10^{-8} \text{ amps/cm}^2 \tag{96}$$

This emission current for the span of the second trajectory is negligible compared to the emission current I_e for the span of the first trajectory. We conclude that the emission from a plate of length $\ell > \lambda$ is confined to the portion of the plate under the first trajectory.

Let us divide the chord of the first trajectory into two regions. Region ab, which is the first half and region bc the second half (Fig. 19)

For these two regions we can say approximately:

(a) for region ab, $I_e = 2I_d$ since no returning current flows in this region

(b) for point b, $I_e = 2I_d$

(c) for point c, $I_e = 0$ since no emission occurs beyond point c.

Assuming the electron boundary layer to be continuous in the region bc in a rough approximation we will have for region bc

$$I_e = \frac{2I_d + 0}{2} = I_d$$

and the average for the first cycloid

$$\bar{I}_e = \frac{(I_e)_{ab} + (I_e)_{cd}}{2} = \frac{2I_d + I_d}{2} = \frac{3}{2} I_d \tag{97}$$

or

$$\alpha = \frac{3}{2} \tag{98}$$

Even though the above analysis is approximate, experimental results seem to justify it not only qualitatively but also quantitatively.

THE CONSTANT MAGNETIC FIELD CASE

In the previously presented analysis of the multiplate thermoelectron engine the plate widths were assumed constant. This configuration is, however, impractical for the following reason. The current density over each plate becomes successively larger since the successive plates are subjected to current emitted from all previous plates, except for their own emission. This relation is clearly seen in Fig. 3. An inspection of eq. (56) shows that two possible quantities can be varied in order to accomodate the variation in I_d; the magnetic field or the trajectory size, determined by y_m. Since it is extremely difficult, in practice, to have predetermined local variations of the magnetic field, the remaining choice is the variation of the height of the trajectory, y_m, and consequently its length, .

Current Density

Consider a series of n hot and n cold plates having widths l_1, $l_2 \ldots l_n$ and l'_1, $l'_2 \ldots l'_n$ respectively. The current flowing in the neighborhood of the k^{th} plate can be divided into the following categories:

1. The current emitted by the k^{th} plate
2. The current emitted by plate (k-1)
3. The portion of the current emitted by plate (k-1) and rejected by plate k
4. The current emitted by plates 1, 2....k-2, and rejected by plates 2, 3....k-1 respectively.

According to definition (38) the current density in the neighborhood of plate k will equal the total current over plate k divided by twice the area of this k^{th} plate.

As an illustration, the current density for the first three plates is computed below.

Plate 1.

Approaching current	0
Current emitted by 1	$h \ell_1 I_S \exp(-\delta_1/kT)$
Plate area	$h \ell_1$
Current density	$I_{d_1} I_S \exp(-\delta_1/kT)$ (99)

where ℓ_1 the width of plate 1

h the length of plate 1

δ_1 the potential barrier at the surface of plate 1

Plate 2.

Approaching current	$h \ell_1 I_S \exp(-\delta_1/kT)$
Current emitted by 2	$h \ell_2 I_S \exp(-\delta_2/kT)$
Current rejected	$h \ell_1 I_S [\exp(-\delta_1/kT) - \exp(-\delta_2/kT)$
Current density	

$$I_{d_2} = I_S / 2\ell_2 \left\{ \ell_1 \left[2 \exp(-\delta_1/kT) - \exp -(\delta_1+\delta_2)/kT \right] \ell_2 \exp(-\delta_2/kT) \right\} \quad (100)$$

Plate 3.

Approaching current (emitted by plate 2)

$$h \ell_2 I_s \exp(-\delta_2/kT)$$

Approaching current (emitted by plate 1)

$$h \ell_1 I_s \left[\exp(-\delta_1/kT) - \exp\{-(\delta_1+\delta_2)/kT\}\right]$$

Current emitted by 3

$$h \ell_3 I_s \exp(-\delta_3/kT)$$

Current emitted by 2 and rejected by 3

$$h \ell_2 I_s \left\{\exp(-\delta_2/kT) - \exp[-(\delta_2+\delta_3)/kT]\right\}$$

Current emitted by 1 and rejected by 2 and 3

$$h \ell_1 I_s \exp$$

Current density

$$I_{d3} = \frac{I_s}{2\ell_3}\left\{2\ell_1\left(\exp(-\delta_1/kT) - \exp\left[-(\delta_1+\delta_2)/kT\right]\right)\right\}$$
$$+ \ell_2 \exp(-\delta_2/kT) + \ell_3 \exp(-\delta_3/kT)$$
$$+ \ell_2\left\{\exp(-\delta_2/kT) - \exp\left[-(\delta_2+\delta_3)/kT\right]\right\} \qquad (101)$$

The general expression for the current density in the neighborhood of the k^{th} plate is:

$$I_{dk} = \frac{I_s}{2\ell_k}\left\{2\left[\sum_{i=1}^{k-1}\ell_i \exp(-\delta_i/kT)\left[1-\exp(-\delta_{i+1}/kT)\right]\right]\right.$$
$$\left.+\ell_k \exp(-\delta_k/kT)+\ell_{k-1}\exp\left[-(\delta_{k-1}+\delta_k)/kT\right]\right\} \tag{102}$$

From eqs. (56) and (58) we can evaluate the value of the ratio I_{dk}/ℓ_k assuming the first mode s equals 1.

$$\frac{I_{dk}}{\lambda_k} = \frac{\epsilon_o B_z^3}{8\pi^2}\left(\frac{Qe}{m_e}\right)^2 \tag{103}$$

and since B_z is assumed constant

$$\frac{I_{d1}}{\lambda_1} = \frac{I_{d2}}{\lambda_2} = \cdots = \frac{I_{dk}}{\lambda_k} \tag{104}$$

Plate Widths

At steady state the current emitted by each plate of the series must be constant. In the event that it is not, a continuous accumulation of electric charge on each plate would take place, but this is contrary to the assumption of steady state. Consequently:

$$h\ell_1 I_s \exp(-\delta_1/kT) = h\ell_2 I_s \exp(-\delta_2/kT) = \cdots$$
$$= h\ell_k I_s \exp(-\delta_k/kT) \tag{105}$$

or

$$\ell_k \exp(\delta_k/kT) = \ell_1 \exp(-\delta_1/kT) \tag{106}$$

We define the dimensionless ratio

$$L_k = \frac{\ell_k}{\ell_1} \quad \text{where} \quad L_1 = 1 \tag{107}$$

Equations 104 and 106 can be written:

$$L_k = \frac{I_{dk}}{I_{d_1}} = \frac{\exp(-\delta_1/kT)}{\exp(-\delta_k/kT)} \tag{108}$$

Eliminating I_{d_k}, I_d, and $\exp(-\delta_k/kT)$ from eqs. (99),(102), and (108), and rearranging, we obtain an expression for the dimensionless width of the k^{th} plate.

$$L_k^3 - (2k+1)L_k + 2L_k \sum_{j=2}^{k} \frac{\exp(-\delta_1/kT)}{L_j} \exp(-X_1) = 0 \tag{109}$$

where

$$X_1 = \delta_1/kT \tag{110}$$

In eq. (109), X_1 is an independent parameter. Once the value of X_1 is fixed, the dimensionless widths of all plates can be found from eq. (109). It will be seen in a later section that an increase of X_1 will result in an increase of the thermal efficiency and a

decrease of the power output of the thermo-electron engine. The optimum value of X_1 will then depend on the actual requirements. Tables I and II show the values of the plate widths L_k, for the first 30 plates, and for X_1 equals one and three.

Potential Barrier δ_k

The potential barrier, δ_k, at any plate k and consequently the current emitted by plate k, $I_s \exp(-\delta_k/kT)$ can be readily determined from eq. (108) once the plate width L_k for a given X_1 $(X_1 = \exp(-\delta_1/kT))$ is known.

Values of $X_k = \exp(-\delta_k/kT)$ are given in Tables I and II for the first 30 plates and for X_1 equals 1 and X_1 equals 3.

Anode Potential ψ_{ak}

In the foregoing analysis we have assumed the chord of the electron trajectories equal to the corresponding plate width. In other words $$m = \frac{\ell_k}{\lambda_k} = 1$$

The height of the electron trajectories can thus be determined from eq. (58),

$$y_{mk} = \frac{\lambda_k}{2n} = \frac{\ell_k}{2n} \qquad (111)$$

as a function of ℓ_k.

The anode potential of the k^{th} anode can be found from eq. 64.

$$\psi_{ak} = \frac{1}{2} \frac{Qe}{me} B^2 y_{mk} \left[2y_{ac} - y_{mk} \right] \tag{112}$$

for a given anode-cathode distance, y_{ac}.

Cold Plates

It can be easily shown that the current density in the vicinity of the k^{th} cold plate equals the current density at the vicinity of the hot plate $(n - k + 1)$. It follows that:

$$L_k' = L_{(n-k+1)} \text{ and } \psi_{ak} = \psi_{a(n-k-1)} \tag{113}$$

Power Output

The power output of the engine will equal the product of the output voltage times the current output[8]

$$\ell_1 h I_s = \ell_1 h I_s \exp(-\delta/kT) = \ell_1 h I_s \exp(-X)$$

The voltage output is the potential difference between the first hot plate, P_1, and the first cold plate, P_1'. With a technique similar to the one presented in Appendix 1, it can be shown that the potential difference between plates P_1 and P_1' equals the sum of the

---

[8] This is the current output obtained if emission from cold plates is neglected.

potential barriers of all hot plates.

$$V = \delta_1 + \delta_2 + ----+\delta_n \tag{114}$$

The power output then becomes

$$P_o = I_s \exp(-X) \sum_{i=1}^{n} \delta_i = kT I_s \exp(-X_1) \sum_{i=1}^{n} X_i \tag{115}$$

Heat Transferred to the Hot Plates

The heat transferred to the hot plates can be easily computed by means of an energy balance for each of the emitting plates, as was done previously for the constant plate width case.

The total heat input to all hot plates is found to be

$$\sum_{i=1}^{n} q_i = \ell_1 h I_s \exp(-X_1) \left\{ (\varphi + \delta_1 + 2kT) + \sum_{i=2}^{n} [\varphi + \delta_i + 2kT] [1 - \exp(-\delta_i/kT)] \right\} \tag{116}$$

Thermal Efficiency

The thermal efficiency can be readily calculated.

$$\eta = \frac{\sum_{i=1}^{n} \delta_i}{(\varphi + \delta_1 + 2kT) + \sum_{i=2}^{n} (\varphi + \delta_i + 2kT) [1 - \exp(-\delta_i/kT)]} = \frac{\sum_{i=1}^{n} X_i}{(Y + X_1 + 2) + \sum_{i=2}^{n} (Y + X_i + 2) [1 - \exp(-X_i)]} \tag{117}$$

LOSSES

In formulating and computing the efficiency and the power output of the thermo-electron engine two important factors have been neglected up to now.

1. The power consumed by the auxiliary equipment.
2. Heat transferred from the hot to the cold reservoir by means other than electron flow, i.e. heat losses.

These two factors are of great importance in computing the expected overall efficiency and power output of an actual engine. They are evaluated below.

The auxiliary equipment necessary for the operation of the device are:

a. Equipment necessary to maintain the anode potential
b. Equipment necessary to maintain the magnetic field
c. Equipment necessary to maintain the vacuum

Anode Potential

The anode can be maintained at the prescribed potential with respect to the cathode by means of suitable batteries or electric generators. If generators are used the power necessary for their operation can be supplied from the power output of the engine. It is expected that the anode power loss will be a small fraction of the power output.

The anode power is given by

$$P_a = I_a \psi_a \tag{118}$$

where

ψ_a the anode potential

and

I_a the anode current

Theoretically the anode current will be zero for proper values of the electric and magnetic fields. In practice, however, a small current will flow to the anodes. This current can be attributed to the following causes:

1. Collisions of electrons with gas molecules, which are inevitably present in the space between anodes and cathodes even at the highest vacua.
2. Non-uniformities of the electric and magnetic fields.
3. Electrons reflected from the last cold plate. These reflected electrons can only move in a direction towards the last anode.

The anode current due to collisions of electrons with gas molecules can be easily computed from the following expression.

$$I_a = I_e \left[1 - \exp\left(-N\Omega\zeta\right)\right] \tag{119}$$

where

I_e the emitted current per unit area, amps/cm^2

N the number of gas molecules per cm^3

Ω collision cross section in cm^2

ζ the total path of the emitted electrons

The number of molecules per cm^3 depends on the gas pressure.

$$N = 2.7 \times 10^{19} \, p / 760 \qquad (120)$$

where

p in mm Hg

The effect of the nonuniformities of the electric and magnetic fields could not be evaluated quantitatively. However, these effects are taken into consideration in the qualitative discussion of the experimental results.

In addition to the anode current due to the above effects, a relatively larger current is expected to flow to the last anode. This large end-anode current is due to the inevitable reflections of electrons from the last cold plate, since they can only move in a direction towards the last anode.

The end-anode current can be reduced to a small fraction of the power output of the device by utilizing a large number of hot and cold plates. In a design presented later, this end-anode loss is almost totally eliminated.

Magnetic Field

In the experiment presented in this report, a Helmholtz coil was used in order to produce a magnetic field easily adjusted and measured.

By proper design of the coils, the power necessary to maintain the magnetic field can be reduced to any desired fraction of the power

output of the device. It has been calculated that a copper coil occupying half the volume of the overall engine would require a power consumption equal to about 10% of the evaluated power output of the engine.

Permanent magnets can also be used requiring no power.

Vacuum

Thermo-electron engines of relatively small size are expected to be evacuated at the time of construction and then permanently sealed. In the case of a larger size, a continually operating vacuum pump would probably have to be used.

Heat Transfer Losses

The heat transfer losses can be divided into two categories:

a. Heat transfer from hot plates to environment

b. Heat transfer from hot to cold plates

The heat transfer from the hot plates to the environment can be reduced to any desirable degree by proper use of insulation material and radiation shields.

The heat transfer from the hot to the cold plates, however, can be reduced only to a certain degree. The limitation in this case is the radiation between the hot and the cold plates through the opening allowed for the electron flow. In the compact designs shown in a later section this radiation loss constitutes the major part of all heat losses.

Since the height of the electron passage, namely the anode to cathode distance y_{ac}, is small compared to dimensions of the enclosures formed by the hot plates and the anodes or the cold plates and the anodes, the two enclosures can be assumed black bodies. The net heat transfer by radiation will then be given by

$$q_e = \sigma\, y_{ac}\, h \left[T^4 - (T')^4\right] \tag{121}$$

where

h the common length of the plates in the direction of the magnetic field.

Assuming an average separation of anode to cathode

$$y_{ac} = 1/3\, l_n \tag{122}$$

where

l_n the width of the last hot plate,

the radiation losses per unit hot plate area become

$$q_e = \frac{\sigma}{3} \frac{L_n}{\sum_{i=1}^{n} L_i} \left[T^4 - (T')^4\right] \tag{123}$$

THE THERMO-ELECTRON ENGINE IN THE CYLINDRICAL FORM

In the previous section the power losses associated with the operation of the thermo-electron engine were discussed. The most important of these losses is the one caused by the anode current. This fact can be readily seen by observing that the output voltage of the device is a small fraction of the imposed anode potential. Consequently, in order for the

device to produce a positive net power the anode current must be an even smaller fraction of the current output.

From the analysis and from experimental data described later, it is shown that the ratio of the current output to the current collected by the first 2 n-1 anodes is of the order of ten thousand to one. With such a ratio the power consumed by the first 2 n-1 anodes as compared with the power output of the device can be neglected.

However, this is not the case for the last anode, namely, anode A_n'. The current absorbed by anode A_n' is the current reflected by the last cold plate, P_n' and has a magnitude of the order of the output current. It is clear that the elimination of this current is of major importance.

Figure 20 shows a configuration of the thermo-electron engine in which the end-anode current is eliminated. In this configuration the n hot and the n cold plates are arranged as to form a cylindrical surface which closes on itself. As a result of this configuration the current reflected by the last cold plate recirculates in the annular space formed by the anodes and cathodes, following the prescribed trajectories and is eventually absorbed.

In Fig. 20 only seven hot and seven cold plates are shown. The electric connections are essentially the same as for the plane configuration.

DESIGN CONSIDERATIONS

The design criteria applicable to any heat engine are:

1. Maximum thermal efficiency
2. Maximum power output per unit volume and/or weight
3. A reasonable life of the equipment

In the case of the thermo-electron engine, these criteria will affect the choice of the emitting material, the operating temperature, and the special layout of the different components. The other important parameters, such as insulation material, material for the supports, actual dimensions, etc., which are determined by a detailed heat-transfer and structural study are beyond the scope of this report.

Emissive Materials

In choosing the emissive material the following factors must be considered:

1. The material must have a low work function in order to obtain high thermal efficiencies and high values of power output.
2. The material must have a reasonable life at the highest temperature used.
3. The material must be reasonably machinable.
4. The material must be non-magnetic, or operated above its Curie point.
5. The material must be chemically stable even when exposed to atmospheric temperature.

In Table III the most important properties of three commercially available emissive materials are shown. It can be seen from the table that even though impregnated tungsten has a higher work function than the oxide coated nickel, it is the most desirable from an overall point of view.

Spacial Configurations

The requirements of maximum power output per unit volume and minimum heat losses can be satisfied by means of a number of compact configurations in which large emissive areas are contained in a minimum volume.

Figures 21 and 22 show two possible compact designs of the thermo-electron engine. Figure 21 is a plane configuration whereas Figure 22 is a cylindrical configuration. In both these figures the hot and cold plates are arranged in consecutive layers. Each layer consists of an equal number of hot and cold cathodes together with the appropriate anodes, and consequently each layer constitutes an independent unit. A large number of layers can be contained in a given volume and consequently a large power output per unit volume can be obtained. The limiting factor in the number of layers that can be used in a given volume is primarily the large rate of the heat transfer required and secondarily the structural problem. Having in mind these limitations, power output as high as 5 k watts per ft^3 appear possible.

Figures 21 and 22 shown one possible method of conveying heat from the heat source to the hot plates. Rods (a) made of copper, aluminum, or other heat conducting material traverse the hot plates. A sleeve (b) of electric insulating material such as ceramic, quartz, or others, keeps the rods electrically insulated from the plates. The end of the rods are in contact with blocks (c) maintained at high temperature by any means, such as by means of hot gases, vapors, or liquid metal, fission products, circulating in the duct (d). The cathodes can also be heated by other methods such as liquid metal heat exchanges, condensation of vapors, or direct heating by combustion gases.

The cold plates can be cooled either by the same methods used for the hot plates. A heat exchanger can be used to pre-heat the fuel in a regenerative fashion and thus increase the thermal efficiency. Regenerative heating can be employed in diverse ways. The apparatus as a whole, or at least the hot part of it, is well insulated from the environment by means of a combination of vacuum, radiation shields, and thermal insulating material.

OVERALL THERMAL EFFICIENCY AND POWER OUTPUT

In the two distinct cases of constant plate width and constant magnetic field, expressions for the thermal efficiency with zero heat-transfer losses and for the net power output have been derived previously. These expressions are:

Thermal efficiency with zero heat losses, constant plate widths

$$\eta = \frac{X\left[\exp(-X) - (1-\mu)^2 \exp\left\{-Y\mu/(1-\mu)\right\}\right]}{(X+Y+2)\left[1-\exp(-X)\right]\exp(-X)} \tag{124}$$

For $\mu = 1 - T/T' > 0.5$ and $Y = \varphi/kT > 1$

which is usually the case, the efficiency can be approximated by

$$\eta = \frac{X}{(X+Y+2)\left[1-\exp(-X)\right]} \tag{125}$$

and the power output per unit emissive area

$$P_o = I_s kT \exp(-X)\, X \tag{126}$$

Under the same conditions the thermal efficiency with zero heat losses and the power output per unit area for the <u>constant magnetic field</u> case are

$$\eta = \frac{\sum_{i=1}^{n} X_i}{(Y+X_1+2) + \sum_{i=2}^{n} (Y+X_i+2)\left[1-\exp(-X_i)\right]} \tag{127}$$

$$P_o = I_s kT \exp(-X_1) \sum_{i=1}^{n} X_i \Big/ \sum_{i=1}^{n} L_i \tag{128}$$

If heat losses, q_e, are included, the efficiencies in the two cases can be evaluated from

$$\eta_a = (\eta^{-1} + q_e / P_o)^{-1} \tag{129}$$

where q_e is given by eq. (123).

In Figs. 23 and 24 the thermal efficiency with zero losses obtained by eq. (124) is shown versus the reversible efficiency for thoriated tungsten emitter and fixed heat source temperatures. The efficiency increases for an increase value of the parameter X. An increase of X, however, results in a rapid decrease of the power output.

The efficiency increases for a decrease of the heat sink temperature T', but for T/T' less than 0.5 the increase is negligible.

In Figs. 25 and 26 the thermal efficiency with radiation losses is shown versus the reversible efficiency. The increasing of the non-loss efficiency for increasing X is now counter-balanced by the decrease of the ratio of the power output to the radiation loss resulting in a maximum efficiency for X approximately equal to 3 and μ approximately equal to 0.50.

In Figs. 27, 28, 29, and 30 the thermal efficiency with and without radiation losses and the power output are shown versus the heat source temperature for a fixed heat sink temperature of about atmospheric. The parameters in these figures are the electron emissive material, the number of plates, and the value of the dimensionless potential barrier on the first plate. The highest efficiency is obtained for the highest

value of heat source temperature, the largest number of plates, and for a value of X of about 3.

It was shown in the section on the thermodynamics of the thermo-electron engine that the thermal efficiency of the thermo-electron engine can be made to approach the reversible efficiency if a large number of engines operating in series are interposed between a given high temperature source and a given low temperature sink. A striking example of this fact is shown in Fig. 31. In this figure the thermal efficiency of an engine composed of two steps is shown as a function of heat source temperature. For a given high temperature, the increase of efficiency obtained in this fashion is of the order of 50%.

Detail listings of the important parameters of the thermo-electron engine are given in Tables IV to X, for various emitting surfaces, number of plates, etc.

EXPERIMENTAL MODELS

Due to the large number of problems that arise in an actual construction of the thermo-electron engine, it was decided that the first part of the research program would be a feasability study. In addition to showing feasability, the experimental results would be used to verify to some degree the fundamental assumptions used in the foregoing analysis.

For simplicity, it was decided to heat the emissive surfaces electrically. Practically speaking, it seems erroneous to consume electric power and receive electric power at a smaller rate. However, once the device has been studied from the electrical point of view, the conversion to gas heating or other heating means, even though it may present some difficult engineering problems, poses no basic difficulty.

Five models were built. The emissive materials used in these models were thoriated tungsten, oxide coated nickel, and impregnated tungsten.

Model 1

The emissive material used in Model 1 was thoriated tungsten. Thoriated tungsten was used because of its chemical stability and the simplicity of its activation.

The commonly used oxide coating which is a mixture of Barium, Strontium and Calcium Oxides, requires a tedious activation process, and once activated, would decompose if it came in contact with atmospheric air. As a consequence, tubes that utilize oxides on the cathodes must be permanently sealed. A permanently sealed apparatus was not desirable if the effect of variation of pressure was to be studied and also if modifications after the first experiments were to be possible.

Thoriated tungsten, however, has a number of serious disadvantages. First, due to its high work function, very high temperatures must be employed. At these high temperatures, of the order of 2500^{o}K,

all known electric insulators conduct heat. Consequently, the emissive plates must be suspended in vacuum and heated by radiation. Heating by radiation requires a much higher temperature for the heater, having as a result a rapid evaporation of the heater.

Second, thoriated tungsten is not machinable. In fact, it is extremely difficult to drill a hole into a 10 mill thick thoriated tungsten ribbon.

The plates of Model 1 were heated and formed into the desirable shape using thoriated tungsten ribbon. The plates were extended one inch beyond the hot portion and were supported by a quartz support.

Figure 33 shows the parts used for Model 1, Fig. 32, as an assembly drawing, and Fig. 34 a photograph of the actual model.

The anodes were supported by a method similar to the one used for the cathodes. The anode assembly was allowed to move with respect to the cathode assembly by means of a bellows.

The heater was made of pure tungsten ribbon. The anodes, cathodes, and heater were contained in a pyrex envelope.

Model 1 was never tested. When the cathodes were heated, the internal stresses existing in the tungsten ribbon caused a serious deformation of the cathodes and the heater, having as a result, an electrical shortening of all components.

Model 2

From the experience gained by the failure of Model 1 it was decided to build a permanently sealed tube with only two cathodes made of oxide coated nickel. Figure 35 shows the parts used for Model 2 and Fig. 36 the assembly. The two anodes and the two cathodes are supported by ceramic material. All metallic parts except for the cathodes are made of non-magnetic tantalum. One of the cathodes is treated with a double wound-wound electric heater insulated with aluminum oxide.

Figure 37 is a photograph of the actual tube.

Model 3

Model 3 is a modification of Model 2 in which each of the two cathodes is heated independently. This was done so as to be able to heat the cold cathode beyond the Curie point, about 500°C for nickel, and thus eliminate the possibility of a distortion of the magnetic field.

Model 4

Model 4 is shown in Figs. 38 through 43. Six cathodes are used, three hot and three cold. The cathodes are Molybdenum blocks with strips of impregnated tungsten (Philips L-Cathodes) attached to them, as shown in Fig. 38. The cathode widths were determined according to Table I. Six Molybdenum anodes are used. Except for the anodes and the cathodes, all other parts are made of monel.

In Model 4 a proper mechanism and bellows shown in Fig. 41, are provided so as to adjust the anode to cathode distance externally.

The cathodes are insulated from each other and from the supporting monel by aluminum oxide ceramic. This ceramic is recommended by the manufacturer of the impregnated tungsten cathodes.

Four double wound-wound heaters are used for heating the first three cathodes.

Model 5

Model 5 is shown in Figs. 44 through 47. Four identical cathodes are used. The four cathodes when assembled form a solid cylinder. The cathodes are made of nickel, and their curved surface is covered with electron emissive oxides. Each cathode is individually heated by means of a double wound-wound heater. Four tantalium anodes are used. The anodes are shaped into a circular arc and form with the cathodes an annular space. The supports for the anodes and cathodes are made of ceramic lava. The leads are made of tantalium.

EXPERIMENTAL PROCEDURE AND RESULTS

Most of the experimental data was obtained from Model 4. Some experimental data were obtained from Models 2 and 3, and some incomplete data were obtained from Model 5. As was explained earlier, Model 1 did not operate at all.

The experimental procedure used in Models 2, 3, and 4 was the

following:

One of the hot cathodes was heated to a desired temperature while all other cathodes were kept at relatively low temperature. All cathode heaters were double wound-wound in order to eliminate the possibility of a magnetic field caused by the heaters' current. The cathode temperature was measured by means of a calibrated pyrometer. The pyrometer error was of the order of $\pm 20^{\circ}F$.

The magnetic field was produced by means of Helmholtz coils. The coils were designed so that the non-uniformity of the magnetic field in the vicinity of the cathodes was much less than 1%. In order to insure constancy of the magnetic field, the necessary D.C. current was supplied from storage batteries. The intensity of the magnetic field in the vicinity of the cathodes was calculated from the geometry as a function of the coil current. This calculation was verified by a magnetic-flux meter within experimental error of the latter.

The anode potential was supplied from B-batteries to insure constancy with time.

The following quantities wer measured:

1. The current emitted by the hot cathode.
2. The current collected by the cold cathodes. This current is labeled "current output".
3. The potential difference between hot and cold cathodes.
4. The current collected by the individual anodes.

All the preceding quantities can be calculated from the presented analysis, in terms of the anode potential, the magnetic field, the cathode temperature and the load resistance.

Except for the last anode the current collected by the anodes can be evaluated from eq. (119). Since the collision cross-sections for O_2 and N_2 are about 9.7 times 10^{-16} cm^2, the collision cross-section for air was taken to be 10^{-15} cm^2.

The current collected by the last anode can be determined as the fraction of the emitted current not having sufficient kinetic energy to be absorbed by the cold cathode.

Models 2 and 3 were permanently sealed at a pressure of 5 times 10^{-7} mm Hg. However, during the experiments the pressure in the tubes was estimated at about 10^{-5} mm Hg.

Model 4 was permanently connected to the vacuum pump and the Mac Leod gage so that the pressure was known with a greater accuracy.

Tables XI to XIX show experimental results obtained with Models 3 and 4. Tables XX to XXV show corresponding calculated results.

In Figs. 48 through 69 a comparison is made of the measured and calculated quantities. In general the agreement is very good.

In Figs. 48 and 49 the emitted current for Model 3 is shown versus the magnetic field strength at constant anode potential. The emitted current was calculated from eq. (70) using α equals 3/2. For the higher values of the magnetic field strength and consequently the higher values of l/λ the agreement is excellent. For low values of

the magnetic field and consequently low values of ℓ/λ the experimental points lie above the curve α equals 3/2, and below the curve α equals 2. For values of the magnetic field not shown in Figs. 48 and 49 the experimental points are expected to lie below the curve α equals 3/2 and above the curve α equals 1. The crossing over of the experimental points and the curve α equals 3/2 is clearly seen in Figs. 48 and 49.

Figures 52, 55, 58, 61, 64, and 67, show the current emitted by cathode 2 in Model 4. For the runs 28 and 33 of intermediate magnetic field strengths and consequently intermediate values of ℓ/λ the agreement is good. For the runs 29, 30, and 31, of large magnetic field strengths and consequently large values of ℓ/λ the experimental points fall between the curves α equals 3/2 and α equals 1. For run 34 of low magnetic field strength the experimental points fall between the curves α equals 3/2 and α equals 2.

The results described above show that a definite relation exists between the value for α and the ratio ℓ/λ. This relationship could be found analytically from a complete two-dimensional solution of the equations governing the electron flow.

Figures 53, 56, 59, 62, 65, and 68, show both the measured and the calculated current absorbed by cathode 3 in Model 4. It should be pointed out that the calculated points were based on measured voltage between the emitting and the absorbing cathodes.

This measured voltage of the order of 0.1 volts was measured inaccurately on the available voltmeters. The agreement between the

calculated and the measured points is within experimental error.

Figures 54, 57, 60, 63, 66, and 69, show the anode current versus the anode potential in Model 4. Most measured currents were less or of the order of one microamp and since the available instrument was a 0-50 microammeter the experimental error is estimated to be more than 200%.

For low and medium voltages the measured and calculated results are of the same order of magnitude thus justifying the assumption that the anode current is due to collisions of electrons with gas molecules.

The relatively large anode current obtained for large anode potentail is justified as follows:

At large anode potentials the current flowing in the last anode of the tube caused an electron bombardment on this anode which resulted in an excessive release of gases. This hypothesis is substantiated by the fact that at large anode potentials a glow was observed. The local release of gases explains the excessive anode current. The experimental results obtained with Models 3 and 4 substantiate the basic assumptions made in the analysis of the thermo-electron engine.

Model 5 was designed and constructed for the purpose of showing that current absorbed by the last anode can be eliminated by using a cylindrical design.

Unfortunately only incomplete data were obtained from Model 5. Model 5 operated only for one hour, after which the anodes shorted with the corresponding cathodes. The shorting out was caused by deposits

of evaporating cathode material on the ceramics which completely enclosed the annular space between the anodes and cathodes.

The few results obtained from Model 5 are shown in Table XXVI. In these experiments anode currents were measured while all cathodes were maintained at the same elevated temperature. It should be noted that the results shown in Table XXVI were obtained before any allignment of the magnetic field, done in all the other experiments, was performed. Even under these adverse conditions the ratio of the emitted current to the current collected by the anodes was of the order of 400.

Even though the incomplete results obtained from Model 5 have small quantitative significance, their qualitative significance is important.

They indicate essentially that with a circular design the anode current can be reduced to less than $1/400^{th}$ of the total emitted current. In fact, these last results complete the feasibility study of the thermo-electron engine.

OUTLOOK IN THE FUTURE

It is mentioned earlier in the report that the first part of the basic experimental program in the development of the thermo-electron engine was:

1. A feasibility study.
2. The verification of the basic assumption made in connection of the electric study of the thermo-electron engine.

On this firm basis, the future experimental effort should be directed towards:

1. The study of all parameters effecting the electric design of the engine.
2. The study of methods for utilizing commonly available heat sources such as fuels, solar energy, atomic energy, etc.
3. An experimental thermodynamic study.

A program of this extent will require much effort. However, within the limitations of our present knowledge it is believed that the thermo-electron engine can be reduced to an efficient and extremely valuable electric power source.

BIBLIOGRAPHY

R1 J. H. Keenan, "Thermodynamics", John Wiley & Sons, New York, 1941

R2 F. Seitz, "The Modern Theory of Solids", McGraw-Hill, New York

R3 H. S. W. Massey and E. H. S. Burhop, "Electronic and Ionic Impact Phenomena", The Clarendon Press, Oxford, 1952

R4 W. H. Kohl, "Materials Technology for Electron Tubes", Reinhold Publishing Company, New York, 1951

R5 S. Dushman, "Vacuum Technique", John Wiley & Sons, New York

R6 C. Herring and M. H. Nichols, "Thermionic Emission", Rev. of Mod. Phys., Vol. 21, p. 187, 1949

R7 T. C. Slater, "Theory of the Magnetron Oscillator", R.L. Report 118, M.I.T., 1941

R8 H. J. Lemmens, M. J. Jansen, and R. Loosjes, "A New Thermionic Cathode for Heavy Loads", Philips Tech. Rev., Vol. 11, pp. 341-350, 1950

APPENDIX 1

STEADY-STATE DISTRIBUTION OF POTENTIALS

It is demonstrated in this section that at steady state the potential of the hot plates P_2----P_n are $-V_o$, $-2V_o$,----, $-(n-1)V_o$ respectively, with reference to hot plate P_1.

The value of V_o depends on the external load resistance R_L and has to satisfy the relation

$$nV_o = R_L \left[I_m - I'_m \right] \tag{1}$$

where

$$I_m = (I_s/m) = \left[\frac{r^m - 1}{r - 1} \right] \exp\left(-V_o/kT\right) \tag{2}$$

Consider the system "hot and cold plates" at steady state. Adjust the anode potential ψ_{ak} at each plate P_k so that the potential barrier δ at all these plates satisfies the expression

$$n\delta = R_L \left[I_m - I'_m \right] \tag{3}$$

Adjust also the anode potential ψ_{ak} at each condenser plate

P_k' so that the potential barrier δ' at these plates is zero. Let $-V_k$ be the potential of any plate P_k with respect to plate P_{k-1} and V_1' be the potential of plate P_1' with respect to plate P_n. It is evident from the nature of the system that V_k and V_1' can have values positive or zero. It will be shown that V_k equals V_1' equals V_o equals δ .

The net current emitted by plate P_o is $I_m - I_m'$. At steady state this current has to be conducted to P_1 from P_1' through the external load. Since the potential of P_1' with respect to P_1 equals

$$V_2 + \cdots + V_n + V_1'$$

$$I_m - I_m' = I_m - I_{m_2} = (V_2 \text{ ---- } + V_n + V_1')/R_L \tag{4}$$

Eliminating R_L from eq. (3) and eq. (4) we get

$$n\delta = V_2 + \text{----} + V_n + V_1' \tag{5}$$

Consider the value of V_1'. There can be these cases.

1. $V_1' > \delta$
2. $V_1' < \delta$
3. $V_1' = \delta$

Cases 1 and 2 lead to contradictions or false statements as shown in the following analysis.

Case 1. $V_1' > \delta$ (Fig. 71)

The net current absorbed by P_1' is:

$$I_m \exp[-(V_1' - \delta)/kT] - I_m'$$

This current has to equal the current conducted from P_1' to P_1 (eq. 4).

$$I_m \exp[-(V_1' - \delta)/kT] - I_m' = I_m - I_m'$$

or $$\exp[-(V_1' - \delta)/kT] = 1 \quad \text{or} \quad V_1' = \delta$$

which is contrary to the hypothesis.

Case 2. $V_1' < \delta$ (Fig. 72)

The current absorbed by P_1' is I_m plus some current I' greater than 0 emitted by plates preceding P_n. In this case,

$$I_m + I' - I_m = I_m - I_m'$$

which is an erroneous statement.

From the above it is concluded that V_1' equals δ

Next consider the possible values of V_n. If V_n is greater than δ (Fig. 73) the net current absorbed by P_1' is computed as follows:

Current absorbed by P_2' from P_n	zero
Current absorbed by P_2' from P_{n-1}	$I_m\left[\exp\left(-(V_n-\delta)/kT\right)-\exp(-V_n/kT)\right]$
Current absorbed by P_2' from P_{n-2}	zero
Current absorbed by P_2' from P_1'	I_m'
Current emitted by P_2'	$-I_m'$
Net current absorbed by P_2'	$I_m \exp(-V_n/kT)\left[\exp(\delta/kT)-1\right]$

The net current absorbed by P_2' should equal the net current emitted by P_n, since P_2' and P_n form an electrically isolated system.

$$I_m \exp(-V_n/kT)\left[\exp(\delta/kT)-1\right] = I_m\left[1-\exp(-V_n/kT)\right]$$

or $$\exp\left[-(V_n-\delta)/kT\right] = 1$$

or $$V_n = \delta$$

Since this result is contrary to our assumption V_n is greater than δ it is concluded that $V_n \leq \delta$

Consider now the values of V_2----V_n. Four possible situations may occur.

1. All potential differences greater than δ
   or V_2----V_n greater than δ
2. All potential differences smaller than δ
   or V_2----V_n less than δ
3. At least one plate P_k so that
   V_k greater than δ and $V_{k+1} \leq \delta$
4. All potential differences equal δ
   V_1, V_2----V_n equal δ

1. The first case, V_2----V_n greater than δ, is ruled out since we have proven $V_n \leqslant \delta$
2. The second case, V_2----V_n less than δ is in conflict with (eq. 5)
3. The third case is analyzed as follows:
   Assume V_k greater than δ and $V_{k+1} \leqslant \delta$

Since $\delta - V_{k+1} \geqslant 0$ no current emitted by P_k can reach $P_n'_{-k+2}$ since it would be absorbed by $P_n'_{-k+1}$. For that matter no current emitted by any plate succeeding P_k will reach $P_n'_{-k+2}$. Any current emitted by P_{k-2} again cannot be absorbed by $P_n'_{-k+2}$ due to the fact that plate P_{k-1} being between P_{k-2} and $P_n'_{-k+2}$ has a lower effective potential than $P_n'_{-k+2}$. This is so since $V_k - \delta$ is greater than 0. The only net current absorbed by $P_n'_{-k+2}$ will be part of the current emitted by P_k, since P_k and $P_n'_{-k+2}$ form an isolated pair, we get:

$$I_m\left[\exp(-V_k-\delta)/kT) - \exp(-V_k/kT)\right] = I_m\left[1-\exp(-V_k/kT)\right]$$

or $$\exp\left[-(V_k-\delta)/kT_1\right] = 1$$

or

$V_k = \delta$, which is contrary to our assumptions

V_k is greater than δ

From the above analysis it is concluded that the only possible steady state for the system will be one for which

$$V_2 \text{---} V_k = \delta \quad \text{and} \quad V_1' = \delta$$

APPENDIX 2

ENERGY DISTRIBUTION OF EMITTED ELECTRONS

For a Maxwellian velocity distribution in an electron gas, the number of electrons having velocity components between u_x and $u + du_x$, u_y and $u_y + du_y$, u_z and $u_z + du_z$ is:

$$dN = \exp\left[-m_e (u_x^2 + u_y^2 + u_z^2)/kT\right] du_x du_y du_z$$

Visualize a plane parallel to the emitting surface and at such a distance from it so that the electrons crossing this plane have a Maxwellian velocity distribution. The number of electrons crossing this plane, per unit time and per unit area is:

$$N_c = \int_{-\infty}^{+\infty} \int_{0}^{\infty} \int_{-\infty}^{+\infty} \exp\left[-m_e (u_x^2 + u_y^2 + u_z^2)\right] u_y du_x du_y du_z$$

where u_y is the velocity component normal to the emitting surface. The fraction of these electrons which have velocity components in the y direction between u_y and $u_y + du_y$ is:

$$(1/N_c)\left[\int_{-\infty}^{+\infty} \int_{-\infty}^{+\infty} \exp\left\{-m (u_x^2 + u_y^2 + u_z^2)/2kT\right\} du_x du_z u_y du_y =\right.$$

$$= (m/kT) u_y \exp(-mu_y^2/2kT) du_y = (1/kT) \exp\left[-(mu_y^2/2)/kT\right] d(mu_y^2/2)$$

Expressing the kinetic energy, $\frac{1}{2} m u_y^2$, in electron-volts and substituting $V = \frac{1}{2} m_e u_y^2$, the number of electrons with y components of kinetic energy between V and V + dV e.v. is found to be:

$$(1/kT) \exp(-V/kT)\, dV$$

The number of electrons having y components of energy greater than V is found, on integration from V to ∞ , to be:

$$\exp.(-V/kT)$$

The average total kinetic energy of those electrons which have velocity components in the y direction between two given velocities u_{y1} and u_{y2} is evaluated next. This energy is given by:

$$\frac{\displaystyle\int_{-\infty}^{+\infty}\int_{u_{y_1}}^{u_{y_2}}\int_{-\infty}^{+\infty} \exp\left[-\tfrac{1}{2} m_e (u_x^2+u_y^2+u_z^2)/kT\right] \tfrac{1}{2} m (u_x^2+u_y^2+u_z^2)\, u_y\, du_x du_y du_z}{\displaystyle\int_{-\infty}^{+\infty}\int_{u_{y_1}}^{u_{y_2}}\int_{-\infty}^{+\infty} \exp\left[-\tfrac{1}{2} m_e (u_x^2+u_y^2+u_z^2)/kT\right] u_y\, du_x du_y du_z}$$

Expressing the kinetic energy $\frac{1}{2} m u_y^2$ in electron volts and substituting $V = \frac{1}{2} m_e u_y^2$, the integrated result is

$$\bar{u} = \left[V' \exp(-V'/kT) - V'' \exp(-V''/kT)\right] \Big/ \left[\exp(-V'/kT) - \exp(-V''/kT)\right] + 2kT$$

which is the average kinetic energy per electron of those electrons that have y components of energy between $V' = \frac{1}{2} m u_{y'}^2$ and $V'' = \frac{1}{2} m u_{y''}^2$ e.v.

APPENDIX 3

THE VACUUM SYSTEMS

Two vacuum systems were built. The first vacuum system was used for the models that incorporated their own glass envelope whereas the second vacuum system was used to evacuate a bell jar assembly where tube components were tested.

Both vacuum systems consist of a mechanical pump, a mercury diffusion pump, a mercury cut-off valve, a MacLeod vacuum gage, and a liquid air trap. A schematic representation of both of the vacuum systems is shown in Fig. 76.

The bell jar assembly consists of a ground glass bell jar and a brass plate (Fig. 78). The seal between the glass and the metal was obtained by means of an o-ring placed in a circular grove which was machined on the brass plate.

The vacuum obtained by either vacuum system is of the order of 10^{-6} mm Hg. The pressure at this high vacua was not accurately known since the accuracy of the MacLeod gage is very poor in this low pressure region. For this matter a precise ion gage has just been installed for future use.

Figure 77 shows an overall view of the two vacuum systems.

APPENDIX 4

THE MAGNET

The Helmholtz coil used to produce the necessary magnetic field in the vicinity of the cathodes is shown schematically in Fig. 79. The basic dimensions of the winding were properly evaluated for maximum uniformity of the magnetic field in the center of the coil.

The winding of the coil is enclosed in a bran cylinder which can be filled with oil for cooling purposes (Fig. 80). Provisions have been made to circulate water through a cooling coil emersed in the oil for additional cooling, as shown in Fig. 81.

The magnetic field produced in the center of the coil is proportional to the current I_B, circulating through the winding,

$$B = \gamma I_B$$

The proportionality constant γ has been evaluated both theoretically from the geometry of the winding and experimentally by means of a magnetic flux meter. The two values of are given below:

Computed $\gamma_c = 4.87 \times 10^{-7}$ webers/amp-cm^2

Experimental $\gamma_e = 4.38 \times 10^{-7}$ webers/amp-cm^2

The two values of γ are in mutual agreement within the compounded experimental errors of the current measurements and magnetic flux measurements.

The results shown in this thesis were based on the experimental value of γ.

APPENDIX 5

CORRELATION OF MEASURED RESULTS

1. Magnetic Field Strength

$$B = 43.8\ I_B$$

where I_B is the measured current through the magnetic coil.

2. Cycloid Trajectory Chord Length

$$\psi_a / B^2 = 1/2\ \frac{Qe}{me}\ \frac{\lambda}{2\pi}\ \left(2y_{ac} - \frac{\lambda}{2\pi}\right)$$

$$= 8.73 \times 10^{-2}\ \frac{\lambda}{2\pi}\ \left(2y_{ac} - \frac{\lambda}{2\pi}\right)$$

This equation has been plotted in Figs. 50 and 51 for y_{ac} pertaining to Model 4.

3. Emitted Current

$$I_e = \frac{\epsilon_o}{8\pi^2 s \alpha}\left(\frac{Qe}{me}\right)^2 B^3 \lambda$$

The chord length λ is obtained from Figs. 50 and 51. Assuming α equal to $3/2$ and s equal to unity:

$$I_e = 7.85 \times 10^{-9}\ \lambda^2 B^3 \quad \text{amps/cm.}$$

4. Output Current

$$I_c = I_e e^{-V/kT}$$

5. Current to the Last Anode

$$I_a = I_e - \Sigma I_c$$

6. Anode Current Due to Collisions with Gas Molecules

Fraction transmitted is:

$$I/I_o = e^{-N\Omega\zeta}$$

where $N = \frac{\rho N_o}{A}$ molecules/cm^3

$\zeta = 2.5\lambda$ cm

$\Omega = 9.7 \times 10^{-16}$ cm^2

for $P = 10^{-6}$ mm Hg

$T = 600^\circ$ K

$\lambda = 0.5$ cm

$I/I_o \simeq 1 - N\Omega\zeta$

The fraction of the anode current to the emitted current is:

$$N\Omega\zeta = (1.61 \times 10^{10})\ (9.7 \times 10^{-16})\ (1.25)$$

$$= 1.95 \times 10^{-5}$$

BIOGRAPHICAL SKETCH

The author was born in Athens, Greece, in 1927, where he attended primary and secondary schools. He attended Athens Polytechnic Institute from 1945 to 1948. He entered the Massachusetts Institute of Technology in 1948 and received his Bachelor of Science and Master of Science degrees in 1950. He served in the United States Army in the period 1951-1952, and headed the Engineering Division of Matrad Corporation during 1952-1953. He returned to M.I.T. in 1953 as a research assistant, was appointed an instructor in 1954, and an assistant professor in 1955. He received his Advanced Engineers Degree in 1954. He is the author of a technical paper entitled, "A Novel Method of Obtaining an Isothermal Surface".

TABLE I

PLATE WIDTHS AND VALUES OF POTENTIAL BARRIER

Dimensionless Potential Barrier For First Plate, $X_1 = \delta_1/kT = 1$

Plate Number	Dimensionless Plate Width, L	Dimensionless Potential Barrier, $X_n = \delta_n/kT$
0	1.00	1.00
1	1.6671	1.5110
2	2.0937	1.7390
3	2.4613	1.9007
4	2.7893	2.0258
5	3.0863	2.1270
6	3.3611	2.2122
7	3.6174	2.2857
8	3.8586	2.3491
9	4.0870	2.4069
10	4.3044	2.4596
11	4.5123	2.5068
12	4.7118	2.5501
13	4.9039	2.5902
14	5.0893	2.6265
15	5.2686	2.6611
16	5.4425	2.6936
17	5.6114	2.7242
18	5.7757	2.7511
19	5.9357	2.7811
20	6.0919	2.8065
21	6.2443	2.8314
22	6.3934	2.8549
23	6.5393	2.8778
24	6.6821	2.8990
25	6.8222	2.9198
26	6.9595	2.9401
27	7.0944	2.9590
28	7.2269	2.9775
29	7.3571	2.9957
30	7.4852	3.0127

TABLE II

PLATE WIDTHS AND VALUES OF POTENTIAL BARRIER

Dimensionless Potential Barrier For First Plate, $X_1 = \delta_1/kT = 3$

Plate Number	Dimensionless Plate Width, L	Dimensionless Potential Barrier, $X_n = \delta_n/kT$
0	1.00	3.00
1	1.7237	3.5441
2	2.2183	3.7964
3	2.6230	3.9638
4	2.9740	4.0893
5	3.2882	4.1898
6	3.5754	4.2737
7	3.8414	4.3474
8	4.0902	4.4079
9	4.3249	4.4645
10	4.5404	4.5126
11	4.7605	4.5601
12	4.9640	4.6019
13	5.1696	4.6406
14	5.3448	4.6758
15	5.5270	4.6996
16	5.7067	4.7413
17	5.8779	4.7708
18	6.0442	4.7988
19	6.2062	4.8253
20	6.3640	4.8512
21	6.5181	4.8744
22	6.6685	4.8971
23	6.8158	4.9189
24	6.9600	4.9399
25	7.1012	4.9600
26	7.2397	4.9793
27	7.3756	4.9979
28	7.5091	5.0158
29	7.6402	5.0332
30	7.7692	5.0499

TABLE III

PROPERTIES OF ELECTRON EMISSIVE MATERIALS

	Work Function Volts		Richardson's Constant A amps/cm ^{o}K		Maximum Temperature ^{o}K For a Life Of 5000 hrs	Maximum Temperature ^{o}K For a Life Of 1000 hrs	Chemical Stability in Atmospheric Air	Machinability
	Range	Average	Range	Average				
OXIDE COATED NICKEL	1.0-1.5	1.17	0.01-5	3.4	1100	----	Bad	Good
IMPREGNATED TUNGSTEN (L-cathodes)	1.6-2.0	1.7	1-15	3	1400	1500	Excellent	Good
THORIATED TUNGSTEN	2.6-2.9	2.4	3-15	5	2100	2300	Excellent	Bad

TABLE IV

COMPUTED QUANTITIES THERMO-ELECTRON ENGINE

Material:		Oxide Coating
Work Function:	φ	1.166 e.v.
Richardson's Constant:	A	3.39 amps/cm^2 $^oK^2$
Number of Plates:	n	1

Dimensionless Potential Barrier	Temperature ^oK	Output Voltage Volts	Output Current Amps	Power Watts/cm^2	Thermal Efficiency No Losses %	Thermal Efficiency With Radiation Losses %	Anode Potential Volts	Magnetic Field, B Gauss
0.5	973	0.0418	1.812	0.076	3.05	0.997	1044	962
0.5	1073	0.0462	7.20	0.333	3.31	1.89	2619	1524
0.5	1173	0.0506	29.0	1.464	3.57	2.82	7550	2590
1.0	973	0.0836	1.10	0.092	5.92	1.38	744	813
1.0	1073	0.0924	4,82	0.446	6.41	3.07	1985	1328
1.0	1173	0.1012	17.6	1.778	6.90	4.87	4715	2045
3.0	973	0.251	0.15	0.0378	15.88	0.702	196	417
3.0	1073	0.278	0.654	0.1816	17.06	2.105	525	689
3.0	1173	0.303	2.38	0.7210	18.19	4.88	1240	1050
5.0	1073	0.463	0.084	0.0388	25.5	0.505	132	342
7.0	1073	0.648	0.011	0.00697	32.4	0.085	33.75	174
9.0	1073	0.834	0.0015	0.00128	38.1	0.015	8.43	86.5

TABLE V

COMPUTED QUANTITIES THERMO-ELECTRON ENGINE

Material: Impregnated Tungsten
Work Function: φ 1.73 e.v.
Richardson's Constant: A 9.12 amps/cm^2 $^oK^2$
Number of Plates: n 3

Dimensionless Potential Barrier	Temperature ^oK	Current Output I_c, amps	Load Resistance R_o, ohms	Power Output watts/cm^2	Thermal Efficiency Without Losses (%)
0.5	1930	0.0582	4.51	0.0153	5.58
0.5	2160	0.3469	0.83	0.0994	6.04
0.5	2290	1.515	0.21	0.4711	6.46
1.0	1930	0.0353	11.36	0.0142	7.55
1.0	2160	0.211	2.08	0.0924	8.14
1.0	2290	0.92	0.52	0.437	8.70
3.0	1930	0.0479	5.79	0.0133	14.64
3.0	2160	0.285	1.06	0.0835	15.69
3.0	2290	1.25	0.26	0.411	16.66

TABLE VI

COMPUTED QUANTITIES THERMO-ELECTRON ENGINE

Material: Impregnated Tungsten
Work Function: φ 1.7 e.v.
Richardson's Constant: A 5 amps/cm^2 $^oK^2$
Number of Plates: n 10

Dimensionless Potential Barrier	Temperature ^oK	Current Output I_c, amps	Load Resistance R_o, ohms	Power Output watts/cm^2	Thermal Efficiency Without Losses (%)	Thermal Efficiency With Radiation Losses (%)
1	1500	9.748	0.2633	0.8929	13.14	11.45
1	1650	38.770	0.07283	3.9067	14.12	13.52
1	2000	448.81	0.00708	50.895	16.24	16.08
1	2500	4713.5	0.000908	719.62	18.91	18.87
3	1500	1.320	3.986	0.234	21.46	11.16
3	1650	5.248	1.102	1.024	22.89	17.95
3	2000	60.756	0.1154	14.367	25.89	24.48
3	2500	638.06	0.01374	188.60	29.53	29.18

TABLE VII

COMPUTED QUANTITIES THERMO-ELECTRON ENGINE

Material: Impregnated Tungsten
Work Function: φ 1.7 e.v.
Richardson's Constant: A 5 amps/cm^2 $^oK^2$
Number of Plates: n 30

Dimensionless Potential Barrier	Temperature ^oK	Current Output I_c, amps	Load Resistance R_o, ohms	Power Output watts/cm^2	Thermal Efficiency Without Losses (%)	Thermal Efficiency With Radiation Losses (%)
1	1500	9.748	1.009	0.6525	15.59	14.40
1	1650	38.77	0.2791	2.855	16.72	16.31
1	2000	448.8	0.0292	40.06	19.14	19.04
1	2500	4713	0.00348	525.8	22.97	22.94
3	1500	1.320	13.56	0.1534	23.56	15.44
3	1650	5.248	3.751	0.6711	25.07	21.68
3	2000	60.76	0.393	9.416	28.25	27.36
3	2500	638.1	0.0467	123.6	32.09	31.88

TABLE VIII

COMPUTED QUANTITIES THERMO-ELECTRON ENGINE

Material: Thoriated Tungsten
Work Function: φ 2.4 e.v.
Richardson's Constant: A 3 amps/cm^2 $^oK^2$
Number of Plates: n 3

Dimensionless Potential Barrier	Temperature ^oK	Current Output I_c, amps	Load Resistance R_o, ohms	Power Output watts/cm^2	Thermal Efficiency Without Losses (%)	Thermal Efficiency With Radiation Losses (%)
1	1500	0.0278	20.05	0.00326	7.53	0.106
1	2000	4.814	0.1545	0.7521	9.54	4.30
1	2500	117.67	0.0079	22.98	11.37	10.19
1	3000	1072.7	0.00104	251.4	13.03	12.71
3	1500	0.0038	360.3	0.00103	14.78	0.33
3	2000	0.6517	2.777	0.2386	18.24	2.15
3	2500	15.93	0.142	7.290	21.36	12.56
3	3000	145.2	0.019	79.76	24.04	20.92

TABLE IX

COMPUTED QUANTITIES THERMO-ELECTRON ENGINE

Material: Thoriated Tungsten
Work Function: φ 2.4 e.v.
Richardson's Constant: A 3 amps/cm^2 $^oK^2$
Number of Plates: n 10

Dimensionless Potential Barrier	Temperature ^oK	Current Output I_c, amps	Load Resistance R_o, ohms	Power Output watts/cm^2	Thermal Efficiency Without Losses (%)	Thermal Efficiency With Radiation Losses (%)
1	1500	0.0278	92.25	0.00255	9.99	0.247
1	2000	4.814	0.711	0.588	12.57	7.48
1	2500	117.7	0.0364	17.96	14.88	13,98
1	3000	1073	0.0048	196.5	16.96	16.73
3	1500	.0038	1396.0	0.0007	16.75	0.07
3	2000	.6517	10.76	0.1541	20.63	3.92
3	2500	15.93	0.5504	4.708	23.98	17.18
3	3000	145.2	0.0724	51.51	26.86	24.78

TABLE X

COMPUTED QUANTITIES THERMO-ELECTRON ENGINE

Material: Thoriated Tungsten
Work Function: φ 2.4 e.v.
Richardson's Constant: A 3 amps/cm^2 $^oK^2$
Number of Plates: n 30

Dimensionless Potential Barrier	Temperature ^oK	Current Output I_c, amps	Load Resistance R_o, ohms	Power Output watts/cm^2	Thermal Efficiency Without Losses (%)	Thermal Efficiency With Radiation Losses (%)
1	1500	0.0278	353.6	0.00186	11.94	0.52
1	2000	4.814	2.725	0.4297	14.93	10.82
1	2500	117.7	0.1394	13.13	17.58	16.98
1	3000	107.2	0.0183	143.6	19.94	19.79
3	1500	0.0038		0.00044	18.50	0.127
3	2000	0.6517	36.62	0.1010	22.67	6.611
3	2500	15.93	1.873	3.086	26.22	21.42
3	3000	145.2	0.2465	33.76	29.28	27.95

TABLE XI

EXPERIMENTAL RESULTS FROM MODEL 3

Run No. 10 Date: December 1, 1955

Anode Potential Anodes 1 2 Volts	Magnetic Field Gauss	Emitted Current Cathode 1 amps x 10^{-3} milliamps	Output Current Cathode 2 amps x 10^{-3} milliamps	Anode Current Anodes 1 2 amps x 10^{-3} milliamps
90	87.6	45	0	45
90	118.1	44	0	44
90	157.7	43	0	43
90	197.0	40	0	40
90	228	32.9	0.9	32
90	263	23.4	3.4	20
90	306	18	3.0	15
90	346	10.6	3.6	7
90	385	8.8	3.2	5.6
90	416	7.8	3.2	4.6
90	447	7.05	2.9	4.15
90	486	6.4	2.6	3.8
90	525	5.6	2.2	3.4
90	565	4.95	1.85	3.1

TABLE XII

EXPERIMENTAL RESULTS FROM MODEL 3

Run No. 17 Date: December 5, 1955

Anode Potential Anodes 1 2 Volts	Magnetic Field Gauss	Emitted Current Cathode 1 amps x 10^{-3} milliamps	Output Current Cathode 2 amps x 10^{-3} milliamps	Anode Current Anodes 1 2 amps x 10^{-3} milliamps
96	438	7.36	3.64	3.72
96	403	8.62	4.50	4.12
96	284	18.55	6.00	12.55

TABLE XIII

EXPERIMENTAL RESULTS FROM MODEL 3

Run No. 18 Date: December 5, 1955

Magnetic Field Gauss	Potential Anode 1 Volts	Potential Anode 2 Volts	Emitted Current Cathode 1 amps x 10^{-3} milliamps	Output Current Cathode 2 amps x 10^{-3} milliamps	Anode Current Anode 1 amps x 10^{-6} microamps	Anode Current Anode amps x 10^{-3} milliamps
311	90	102	14.28	3.0	29.5	11.25
311	90	102	13.48	10.1	33.0	3.35
324	90	102	13.15	4.4	30.5	8.72
324	90	102	16.03	3.0	33.0	13.0
438	135	147	23.65	9.6	45.0	14.0
438	135	147	23.96	7.4	60.0	16.5

TABLE XIV

MEASUREMENTS FROM MODEL 4

Run No. 28 Date: February 18, 1956

Pressure in tube (m.m. Hg) - - - - - 3×10^{-6}
Cathode Temperature (^{o}K) - - - - - 1300
Magnetic Field Strength (Gauss) - - - - - 350

Anode Potential Volts A_1 - - - A_6	Current Emitted Cathode 2 amps x 10^{-3} milliamps	Current Output Cathode 3 amps x 10^{-3} milliamps	Voltage Output Volts	Anode Currents A_2 amps x 10^{-6} microamps	A_3	A_1 A_4 A_5 A_6 amps x 10^{-3} milliamps
45	0.29	0.20	0.038	0-1	0-1	0.09
90	1.10	0.76	0.144	0-1	0-1	0.34
135	2.76	2.00	0.039	0-1	0-1	0.76
180	5.70	4.30	0.084	0-1	0-1	1.40
225	9.10	7.10	0.138	0-1	0-1	2.00
270	13.20	10.20	0.199	0-1	0-1	3.00
315	18.80	14.0	0.028	0-1	0-1	4.80
405	30.30	21.0	0.042	0-1	0-1	9.30

TABLE XV

MEASUREMENTS FROM MODEL 4

Run No. 29 Date: February 18, 1956

Pressure in tube (m.m. Hg) - - - - - 3×10^{-6}
Cathode Temperature (^{o}K) - - - - - 1300
Magnetic Field Strength (Gauss) - - - - - 438

Anode Potential Volts A_1- - -A_6	Current Emitted Cathode 2 amps x 10^{-3} milliamps	Current Output Cathode 3 amps x 10^{-3} milliamps	Voltage Output Volts	Anode Currents A_2 A_3 amps x 10^{-6} microamps		A_1 A_4 A_5 A_6 amps x 10^{-3} milliamps
45	0.23	0.16	0.0304	0-1	0-1	0.07
90	0.87	0.60	0.114	0-1	0-1	0.27
135	1.91	1.35	0.026	0-1	0-1	0.56
180	3.25	2.30	0.049	0-1	0-1	0.95
225	5.85	4.35	0.085	2	1.5	1.50
270	8.30	6.30	0.123	6	4	2.00
315	10.90	8.30	0.162	7	8	2.60

TABLE XVI

MEASUREMENTS FROM MODEL 4

Run No. 30 Date: February 18, 1956

Pressure in tube (m.m. Hg) - - - - - 10^{-6}
Cathode Temperature (^{o}K) - - - - - 1300
Magnetic Field Strength (Gauss) - - - - - 525.6

Anode Potential Volts A_1- - -A_6	Current Emitted Cathode 2 amps x 10^{-3} milliamps	Current Output Cathode 3 amps x 10^{-3} milliamps	Voltage Output Volts	Anode Currents A_2 amps x 10^{-6} microamps	A_3	A_1 A_4 A_5 A_6 amps x 10^{-3} milliamps
45	0.20	0.14	0.0266	0-1	0-1	0.06
90	0.69	0.48	0.0912	0-1	0-1	0.21
135	2.28	1.80	0.0352	0-1	0-1	0.48
180	2.80	2.00	0.039	0-1	0-1	0.80
225	3.98	2.80	0.045	0-1	0-1	1.18
270	6.70	4.90	0.0455	0-1	0-1	1.80
315	9.40	7.00	0.136	5	5	2.40

TABLE XVII

MEASUREMENTS FROM MODEL 4

Run No. 31 Date: February 19, 1956

Pressure in Tube (m.m. Hg) - - - - - - 10^{-6}
Cathode Temperature (^{o}K) - - - - - - 1300
Magnetic Field Strength (Gauss) - - - - - - 613.2

Anode Potential Volts A_1 - - - A_6	Current Emitted Cathode 2 amps x 10^{-3} milliamps	Current Output Cathode 3 amps x 10^{-3} milliamps	Voltage Output Volts	Anode Currents A_2 amps x 10^{-6} microamps	A_3	A_1 A_4 A_5 A_6 amps x 10^{-3} milliamps
45	0.16	0.11	0.034	0-1	0-1	0.05
90	0.59	0.41	0.112	0-1	0-1	0.18
135	1.28	0.88	0.025	0-1	0-1	0.40
180	2.42	1.70	0.047	1.0	1.5	0.72
225	3.54	2.50	0.069	1.0	1.0	1.04
270	4.90	3.40	0.0956	1.5	2.2	1.50
315	7.30	5.30	0.142	2.0	3.5	2.0
405	13.10	9.80	0.026	10.0	7.0	3.3

TABLE XVIII

MEASUREMENTS FROM MODEL 4

Run No. 33 Date: February 19, 1956

Pressure in tube (m.m. Hg) - - - - - 10^{-6}
Cathode Temperature (^{o}K) - - - - - 1300
Magnetic Field Strength (Gauss) - - - - - 188.34

Anode Potential Volts A_1- - -A_6	Current Emitted Cathode 2 amps x 10^{-3} milliamps	Current Output Cathode 3 amps x 10^{-3} milliamps	Voltage Output Volts	Anode Currents A_2 amps x 10^{-6} microamps	A_3	A_1 A_4 A_5 A_6 amps x 10^{-3} milliamps
45	0.52	0.36	0.0684	0-1	0-1	0.16
90	2.62	2.00	0.0390	0-1	0-1	0.62
135	6.40	4.80	0.0935	0-1	0-1	1.60
180	12.50	8.70	0.170	0-1	0-1	3.5
225	21.50	14.00	0.028	0-1	0-1	7.5
270	33.50	18.50	0.037	0-1	0-1	15

TABLE XIX

MEASUREMENTS FROM MODEL 4

Run No. 34 Date: February 21, 1956

Pressure in tube (m.m. Hg) - - - - - 10^{-6}
Cathode Temperature (^{o}K) - - - - - 1300
Magnetic Field Strength (Gauss) - - - - - 131.4

Anode Potential Volts A_1 - - - A_6	Current Emitted Cathode 2 amps x 10^{-3} milliamps	Current Output Cathode 3 amps x 10^{-3} milliamps	Voltage Output Volts	Anode Currents A_2 amps x 10^{-6} microamps	A_3	A_1 A_4 A_5 A_6 amps x 10^{-3} milliamps
45	1.12	0.84	0.150	0-1	0-1	0.28
90	6.20	4.20	0.082	0-1	0-1	2.00
135	18.40	12.00	0.024	25	490	6.40
180	32.00	16.00	0.032	110	4000	16.0

TABLE XX

CALCULATED RESULTS FROM MODEL 4

Run No. 28 Date: February 18, 1956

Anode Potential $A_1 - - - A_6$ Volts	Current Emitted Cathode 2 milliamps	Current Absorbed by Cathode 3 milliamps	Total Space Current milliamps	Anode Current A_2 A_3 microamps	Ratio of Anode Current to Total Space Current x 10^5
45	0.373	0.268	9.218	0.0477	0.517
90	1.64	0.465	19.28	0.2098	1.09
135	3.70	2.63	29.00	0.473	1.62
180	6.58	3.14	38.67	0.8411	2.17
225	9.74	2.90	47.44	1.252	2.64
270	14.84	2.58	58.15	1.897	3.27
315	20.21	15.7	67.88	2.583	3.79
405	34.52	23.8	88.78	4.412	4.96

TABLE XXI

CALCULATED RESULTS FROM MODEL 4

Run No. 29

Date: February 18, 1956

Anode Potential $A_1 - - - A_6$ Volts	Current Emitted Cathode 2 milliamps	Current Absorbed by Cathode 3 milliamps	Total Space Current milliamps	Anode Current A_2 A_3 microamps	Ratio of Anode Current to Total Space Current $\times 10^5$
45	0.29	0.221	11.35	0.0370	0.326
90	1.175	0.432	22.86	0.1492	0.651
135	2.79	2.21	35.32	0.3567	1.01
180	5.62	3.65	50.00	0.7050	1.41
225	7.96	3.75	59.55	1.018	1.71
270	11.45	3.88	71.39	1.464	2.05
315	15.59	3.77	83.31	1.993	2.39

TABLE XXII

CALCULATED RESULTS FROM MODEL 4

Run No. 30 Date: February 18, 1956

Anode Potential $A_1 - - - A_6$ Volts	Current Emitted Cathode 2 milliamps	Current Absorbed by Cathode 3 milliamps	Total Space Current milliamps	Anode Current A_2 A_3 microamps	Ratio of Anode Current to Total Space Current $\times 10^5$
45	0.245	0.194	13.72	0.0104	0.0762
90	0.976	0.438	27.41	0.0415	0.152
135	2.199	1.612	41.13	0.0937	0.224
180	4.11	2.93	56.28	0.1751	0.311
225	6.47	4.34	70.52	0.2757	0.392
270	9.51	6.50	85.53	0.4153	0.474
315	12.76	3.88	99.07	0.5440	0.549

TABLE XXIII

CALCULATED RESULTS FROM MODEL 4

Run No. 31 Date: February 19, 1956

Anode Potential $A_1 - - - A_6$ Volts	Current Emitted Cathode 2 milliamps	Current Absorbed by Cathode 3 milliamps	Total Space Current milliamps	Anode Current A_2 A_3 microamps	Ratio of Anode Current to Total Space Current $\times 10^5$
45	0.214	0.158	16.16	0.0091	.0564
90	0.841	0.315	32.04	0.0358	.112
135	1.906	1.53	48.26	0.0812	.168
180	3.50	2.32	65.46	0.149	.231
225	5.46	2.96	81.70	0.233	.286
270	7.86	3.39	98.00	0.335	.342
315	10.97	3.14	115.7	0.468	.404

TABLE XXIV

CALCULATED RESULTS FROM MODEL 4

Run No. 33 Date: February 19, 1956

Anode Potential $A_1 - - - A_6$ Volts	Current Emitted Cathode 2 milliamps	Current Absorbed by Cathode 3 milliamps	Total Space Current milliamps	Anode Current A_2 A_3 microamps	Ratio of Anode Current to Total Space Current $\times 10^5$
45	0.896	0.477	5.54	0.0370	0.668
90	3.16	2.25	10.57	0.1347	1.27
135	7.15	3.15	15.91	0.3048	1.92
180	13.5	3.03	21.78	0.356	1.63
225	22.79	17.8	28.42	0.9714	3.41
270	35.3	25.6	35.33	1.505	4.27

TABLE XXV

CALCULATED RESULTS FROM MODEL 4

Run No. 34 Date: February 21, 1956

Anode Potential A_1 - - - A_6 Volts	Current Emitted Cathode 2 milliamps	Current Absorbed by Cathode 3 milliamps	Total Space Current milliamps	Anode Current A_2 A_3 microamps	Ratio of Anode Current to Total Space Current x 10^5
45	1.11	0.296	3.65	0.0472	1.29
90	4.91	2.39	7.68	0.2092	2.72
135	12.94	3.85	12.44	0.5502	4.42
180	28.0	21.17	18.20	1.834	10.1

TABLE XXVI

TOTAL EMITTED CURRENT AND ANODE CURRENT FOR CIRCULAR MODEL 5

Run No. 46 Date: March 7, 1956

Magnetic Field B (Gauss)	Anode Potential ψ_a (Volts)	Total Emitted Current (milliamps)	Measured Anode Current (milliamps)	Ratio Emitted To Anode Current
219	22.5	20.7	0.042	495
	45	35.4	0.100	354
	90	73.5	0.200	367
328	22.5	24.0	0.048	500
	45	40.8	0.100	408
	90	113.0	0.25	452
	135	167.3	0.42	398
	180	211.3	0.60	352
	225	271.9	0.87	312
	270	326.4	1.02	320
438	90	96	0.32	300
	135	200	0.51	390
	180	277	0.71	392
	225	356	0.93	385
	405	650	2.3	282

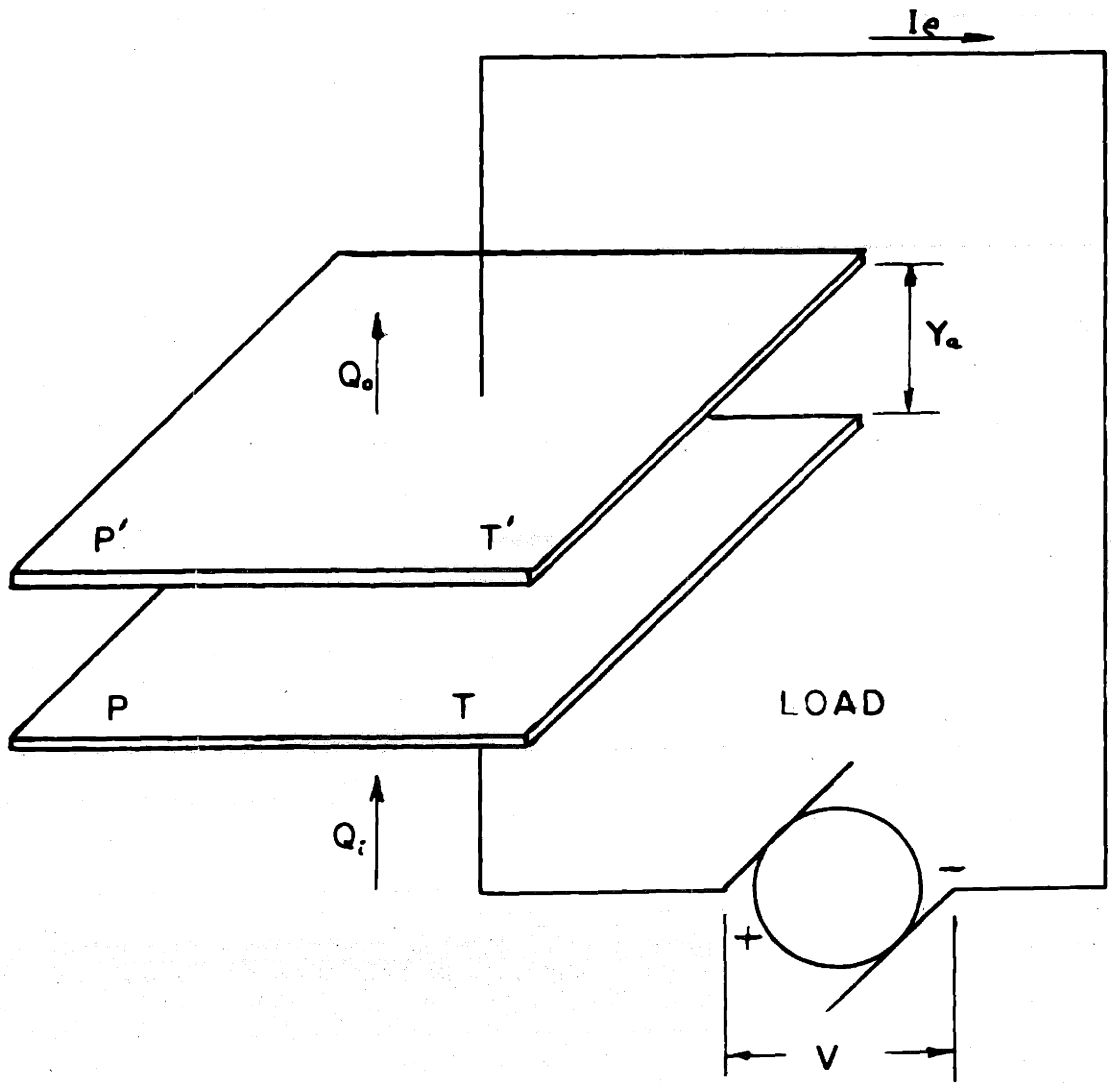

SIMPLE DIODE

FIG. 1

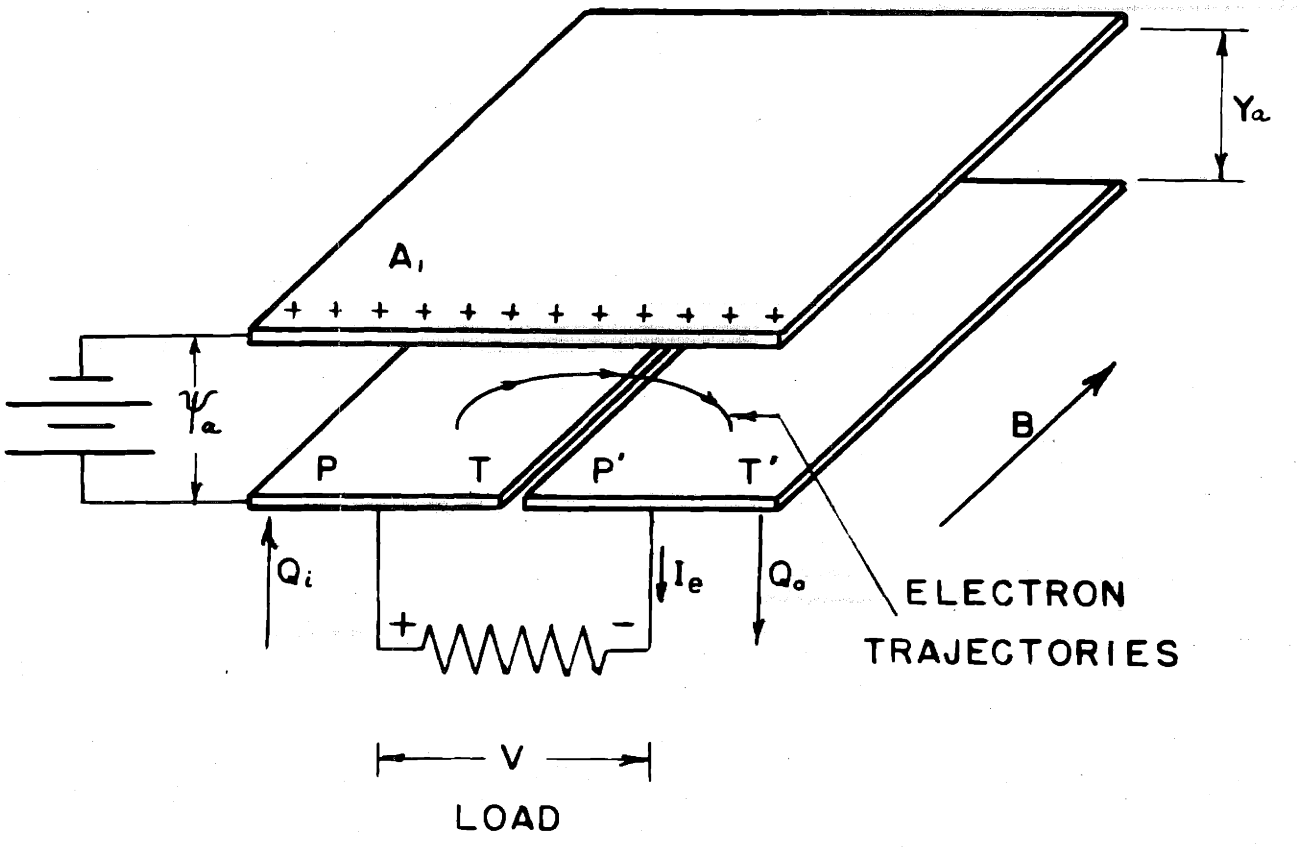

MAGNETIC TRIODE

FIG. 2

SCHEMATIC OPERATION OF THERMAL ELECTRON ENGINE

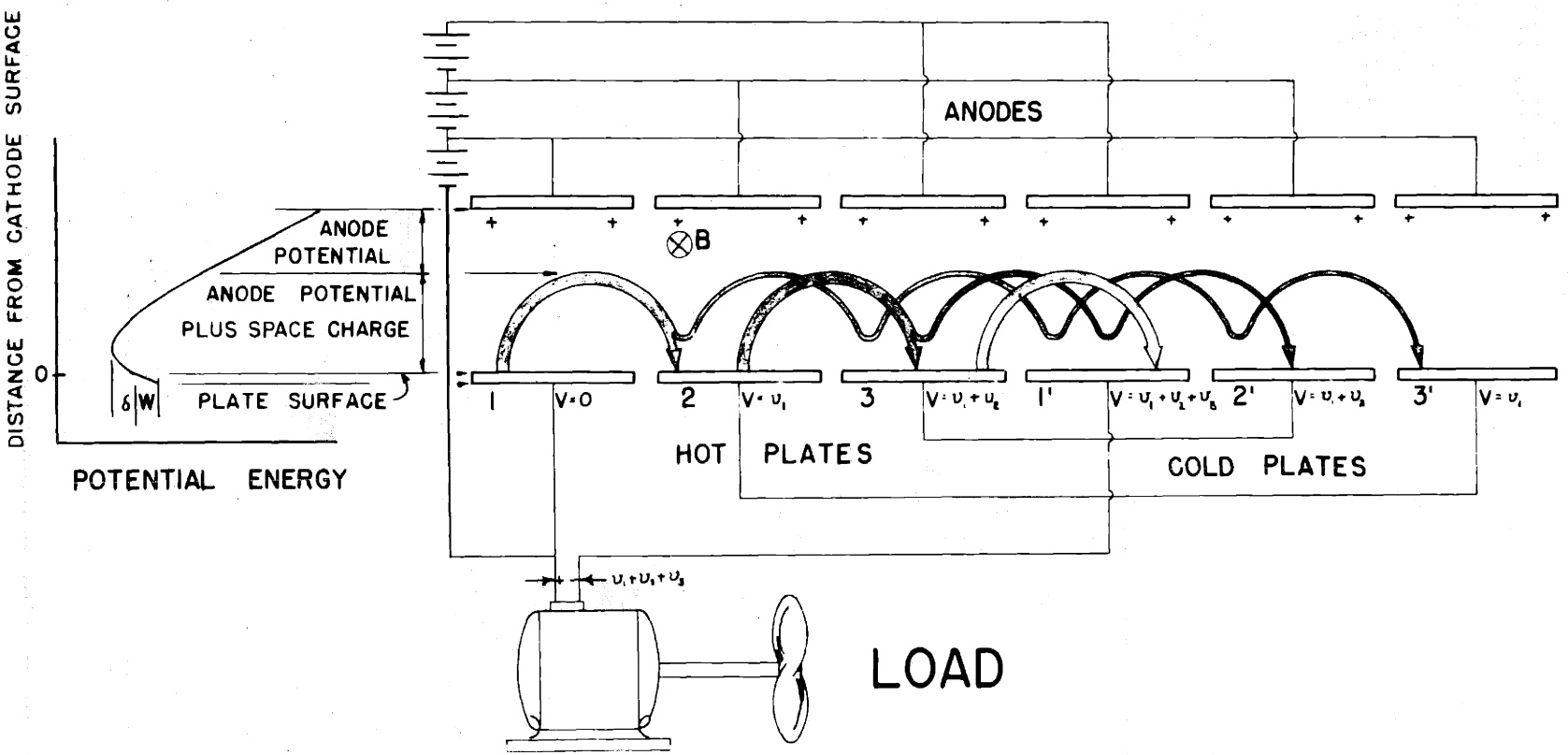

FIG. 3

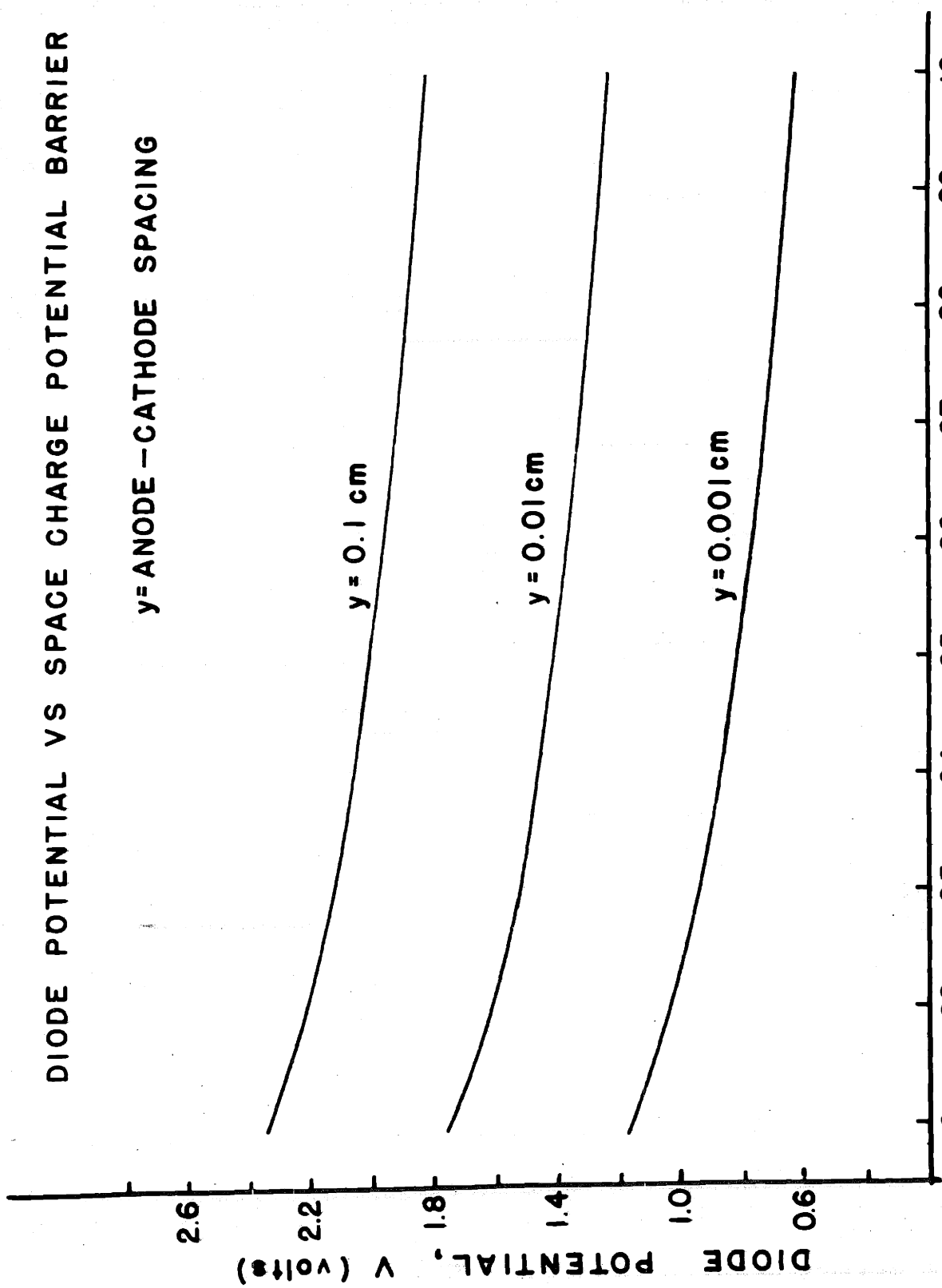
DIODE POTENTIAL VS SPACE CHARGE POTENTIAL BARRIER
y=ANODE—CATHODE SPACING
y=0.1 cm
y=0.01cm
y=0.001cm
DIODE POTENTIAL, V (volts)
2.6
2.2
1.8
1.4
1.0
0.6
.01
.02
.03
.04
.05
.06
.07
.08
.09
.10
SPACE CHARGE POTENTIAL BARRIER, δ (volts)

FIG. 4

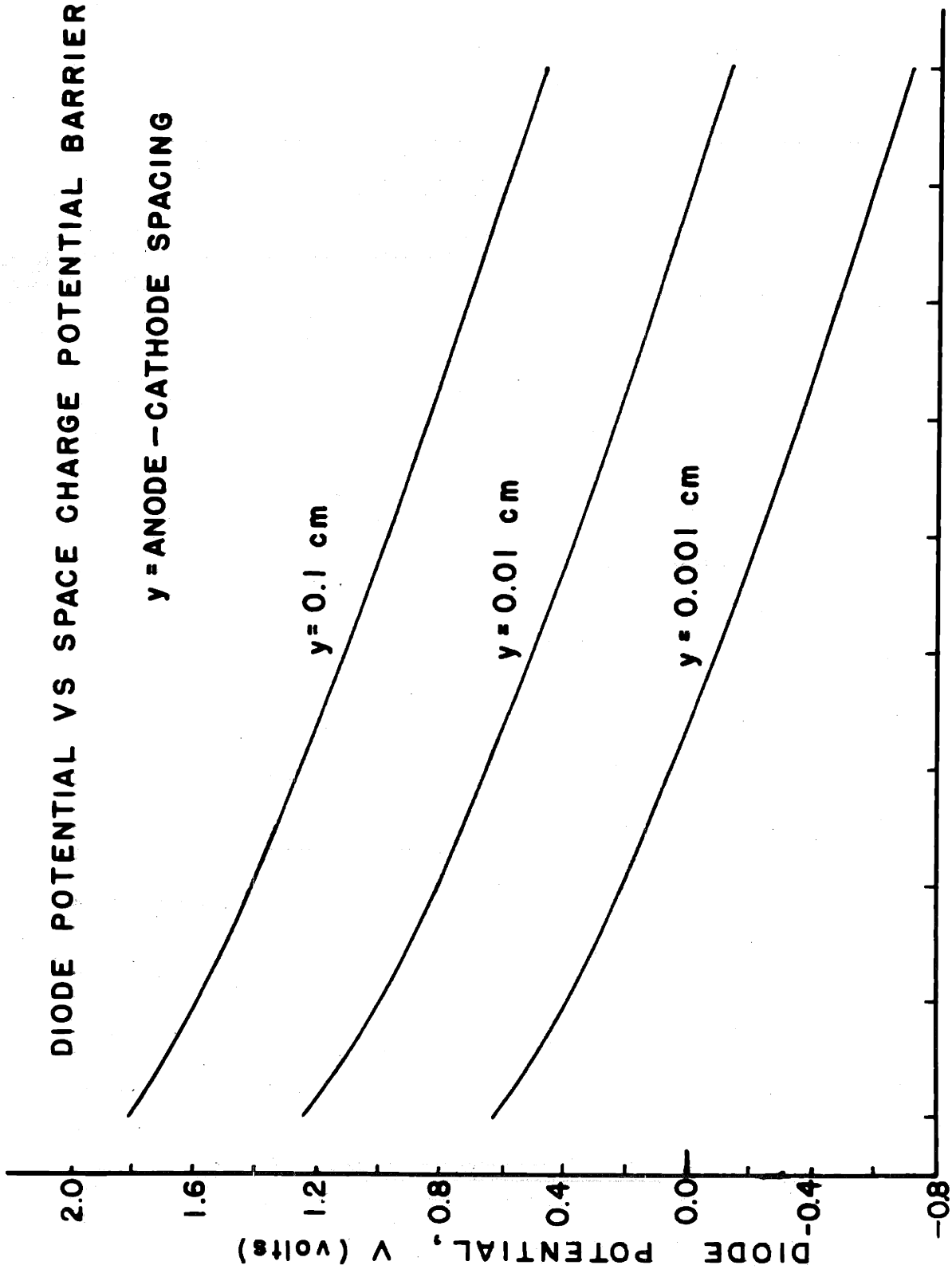
DIODE POTENTIAL VS SPACE CHARGE POTENTIAL BARRIER
y = ANODE-CATHODE SPACING
y = 0.1 cm
y = 0.01 cm
y = 0.001 cm
DIODE POTENTIAL, V (volts)
2.0
1.6
1.2
0.8
0.4
0.0
-0.4
-0.8
0.1
0.2
0.3
0.4
0.5
0.6
0.7
0.8
0.9
1.0
SPACE CHARGE POTENTIAL BARRIER, δ (volts)

FIG. 5

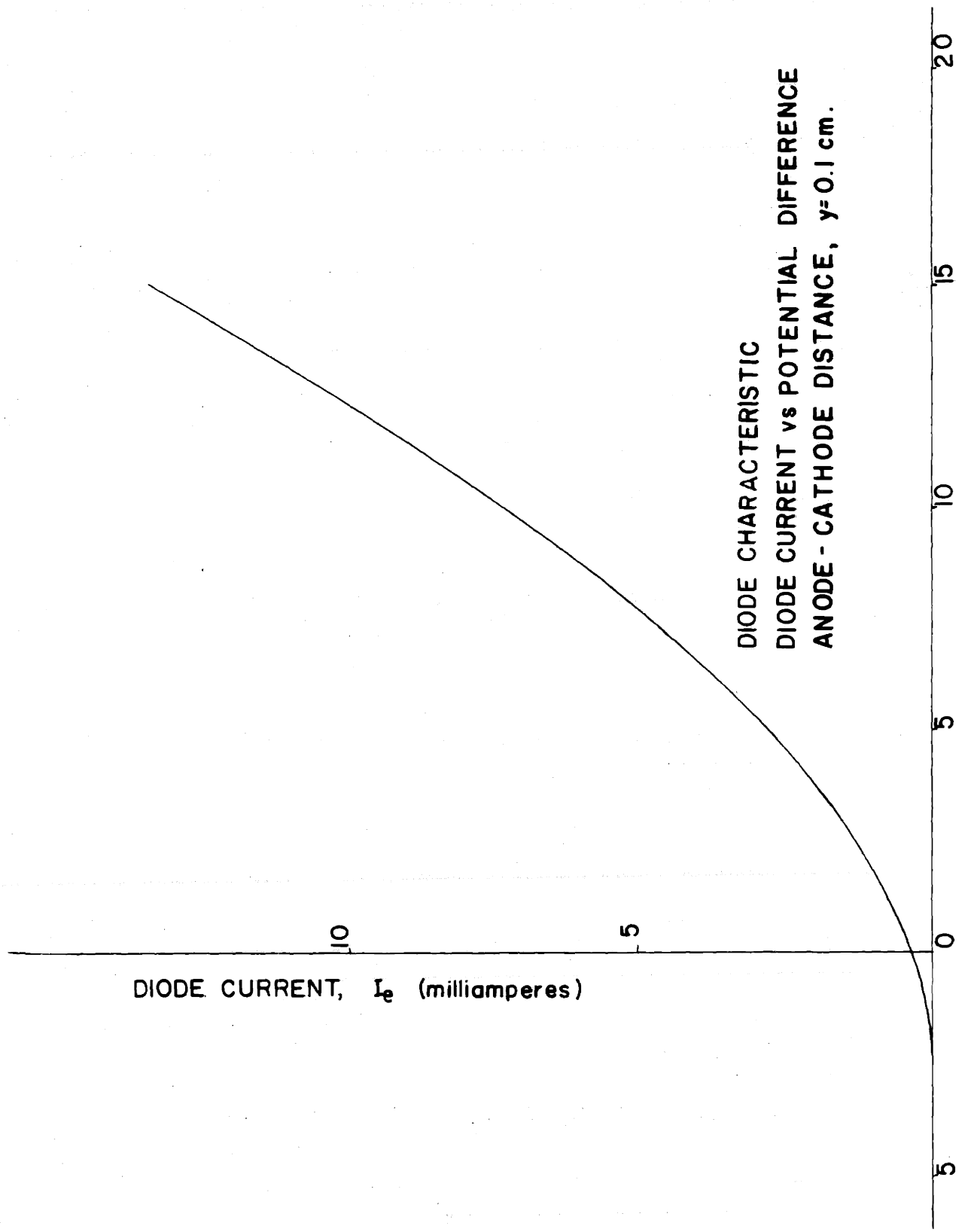
DIODE CHARACTERISTIC
DIODE CURRENT vs POTENTIAL DIFFERENCE
ANODE - CATHODE DISTANCE, y= 0.1 cm.
DIODE CURRENT, I_e (milliamperes)
10
5
0
5
10
15
20
POTENTIAL DIFFERENCE, V_1 (volts)

FIG. 6

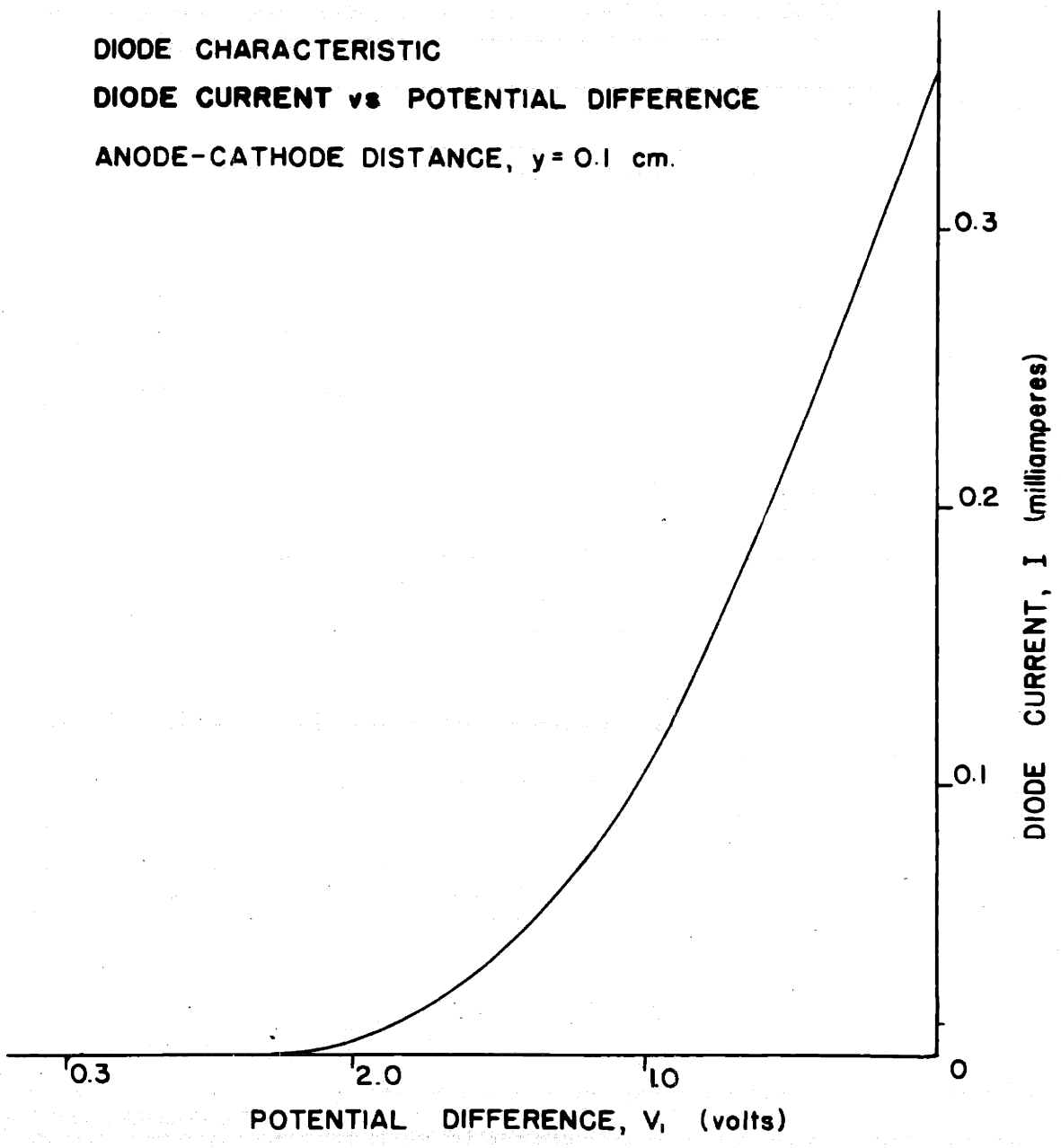
DIODE CHARACTERISTIC
DIODE CURRENT vs POTENTIAL DIFFERENCE
ANODE-CATHODE DISTANCE, y = 0.1 cm.
0.3
0.2
0.1
0
DIODE CURRENT, I (milliamperes)
0.3
2.0
1.0
POTENTIAL DIFFERENCE, V, (volts)

Fig. 7

DIODE CHARACTERISTIC
DIODE CURRENT vs POTENTIAL DIFFERENCE
ANODE-CATHODE DISTANE, y=.01cm.

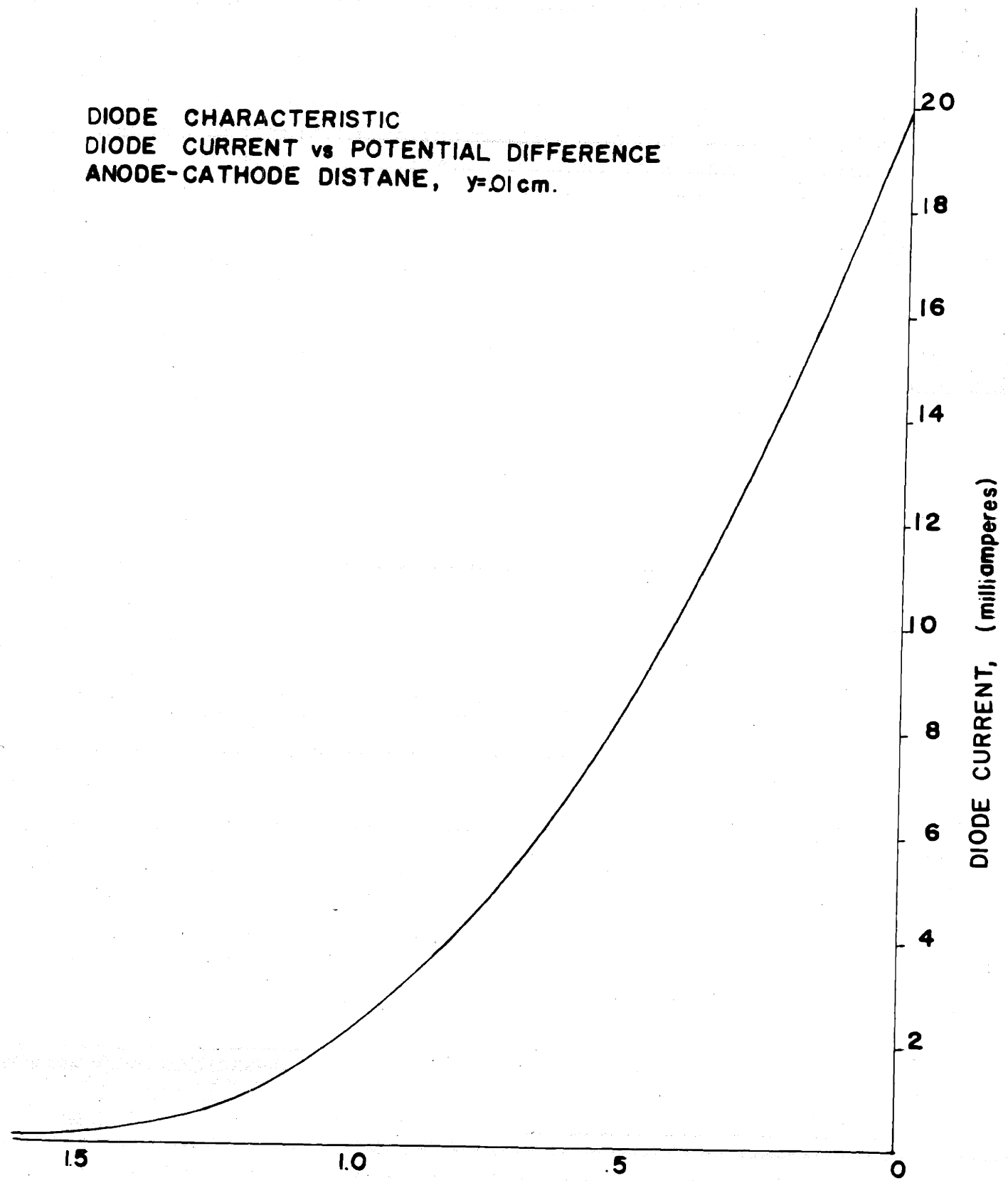

FIG. 8

DIODE CHARACTERISTIC

DIODE CURRENT vs POTENTIAL DIFFERENCE

ANODE-CATHODE DISTANCE, y= 0.001 cm.

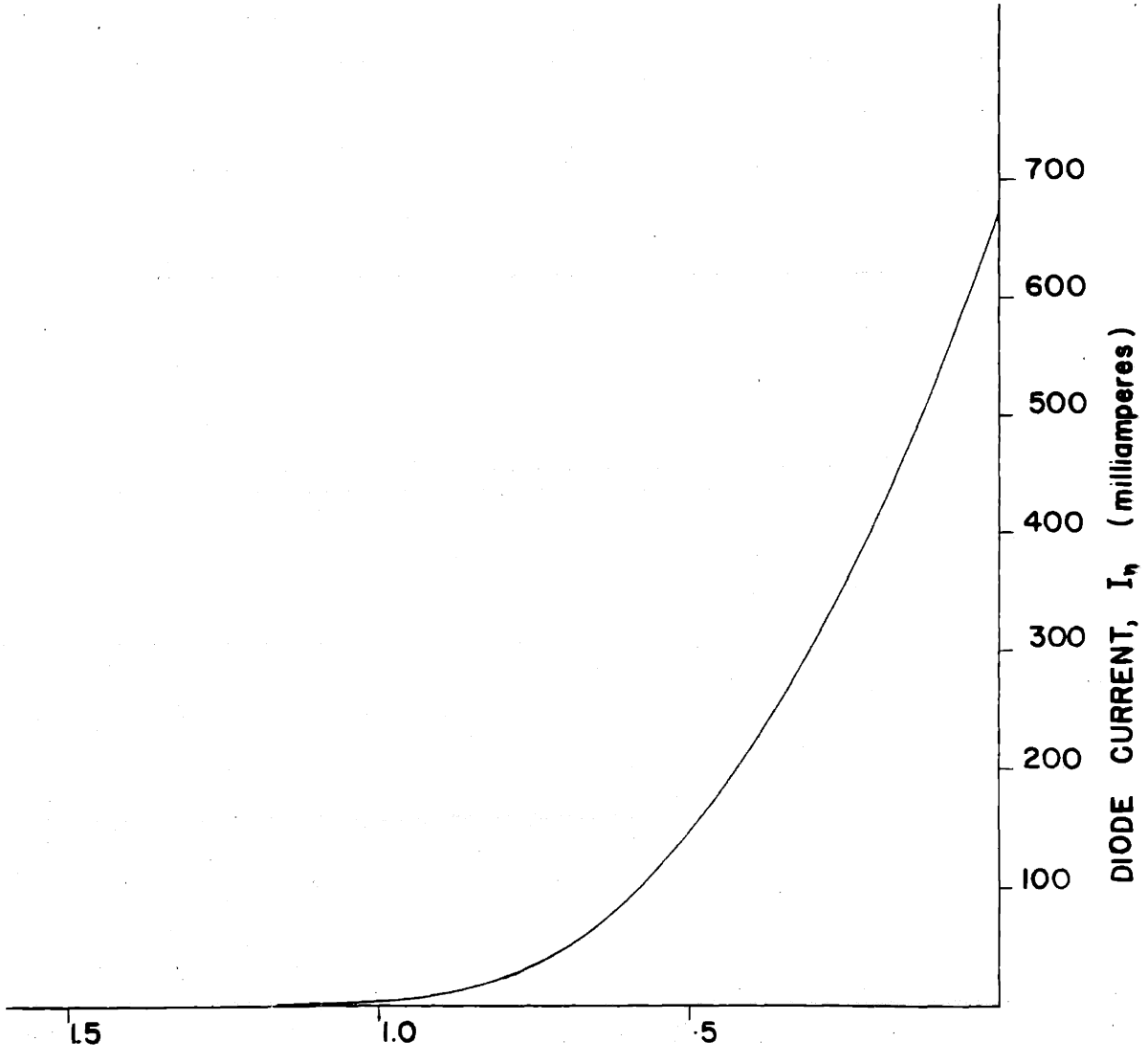

Fig. 9

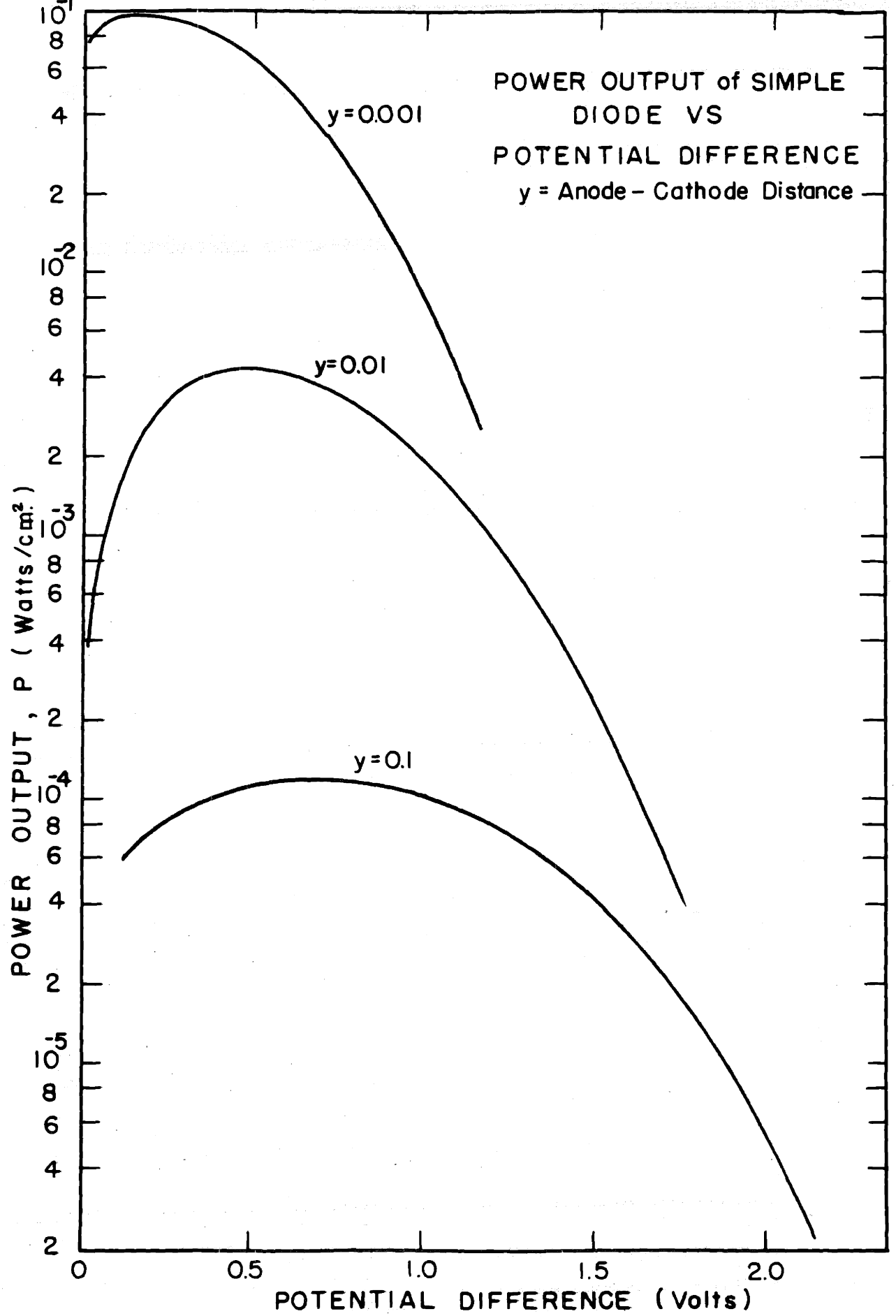
POWER OUTPUT of SIMPLE DIODE VS POTENTIAL DIFFERENCE
y = Anode – Cathode Distance
y=0.001
y=0.01
y=0.1
POWER OUTPUT, P (Watts/cm²)
POTENTIAL DIFFERENCE (Volts)
0
0.5
1.0
1.5
2.0

Fig. 10

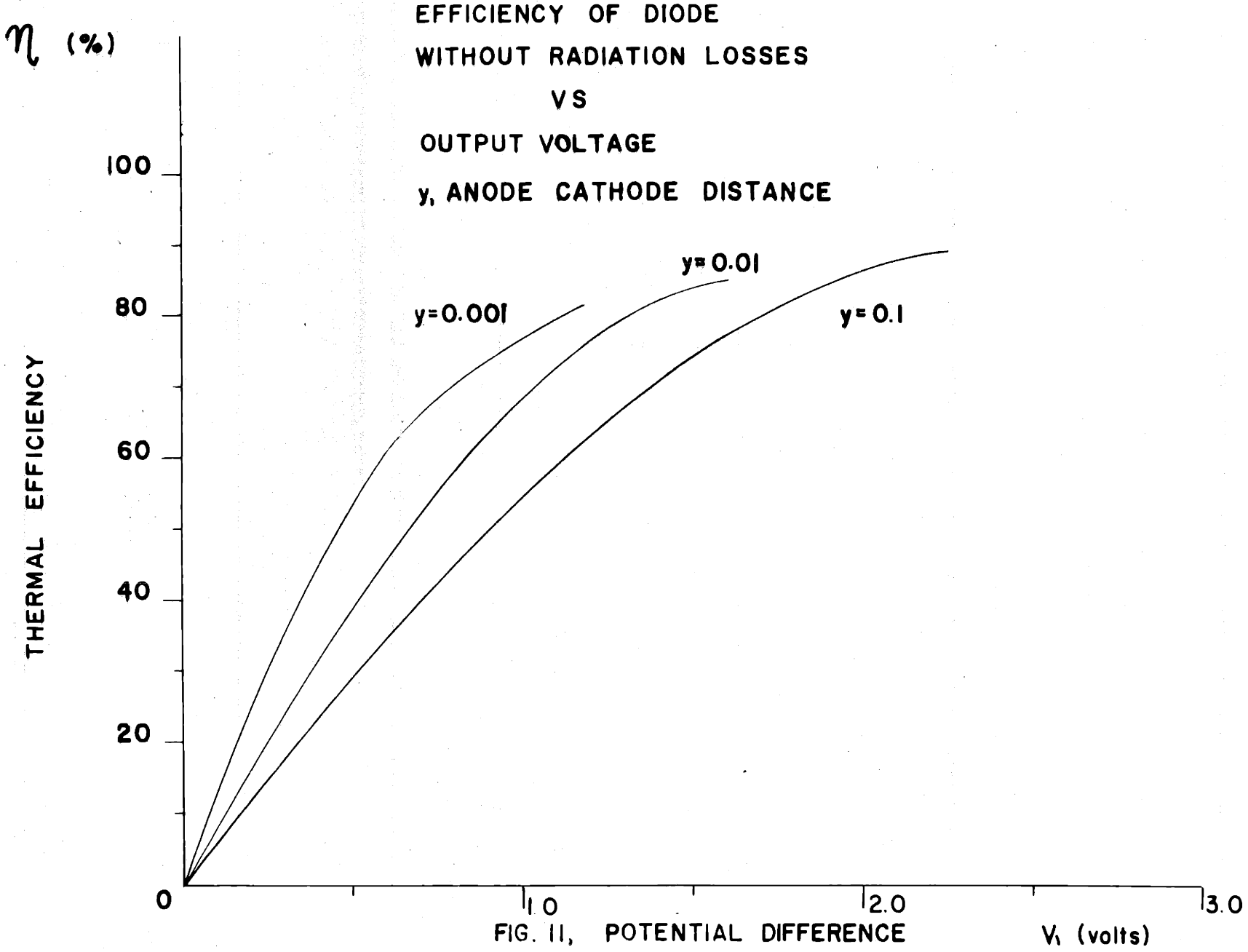

FIG. 11, POTENTIAL DIFFERENCE

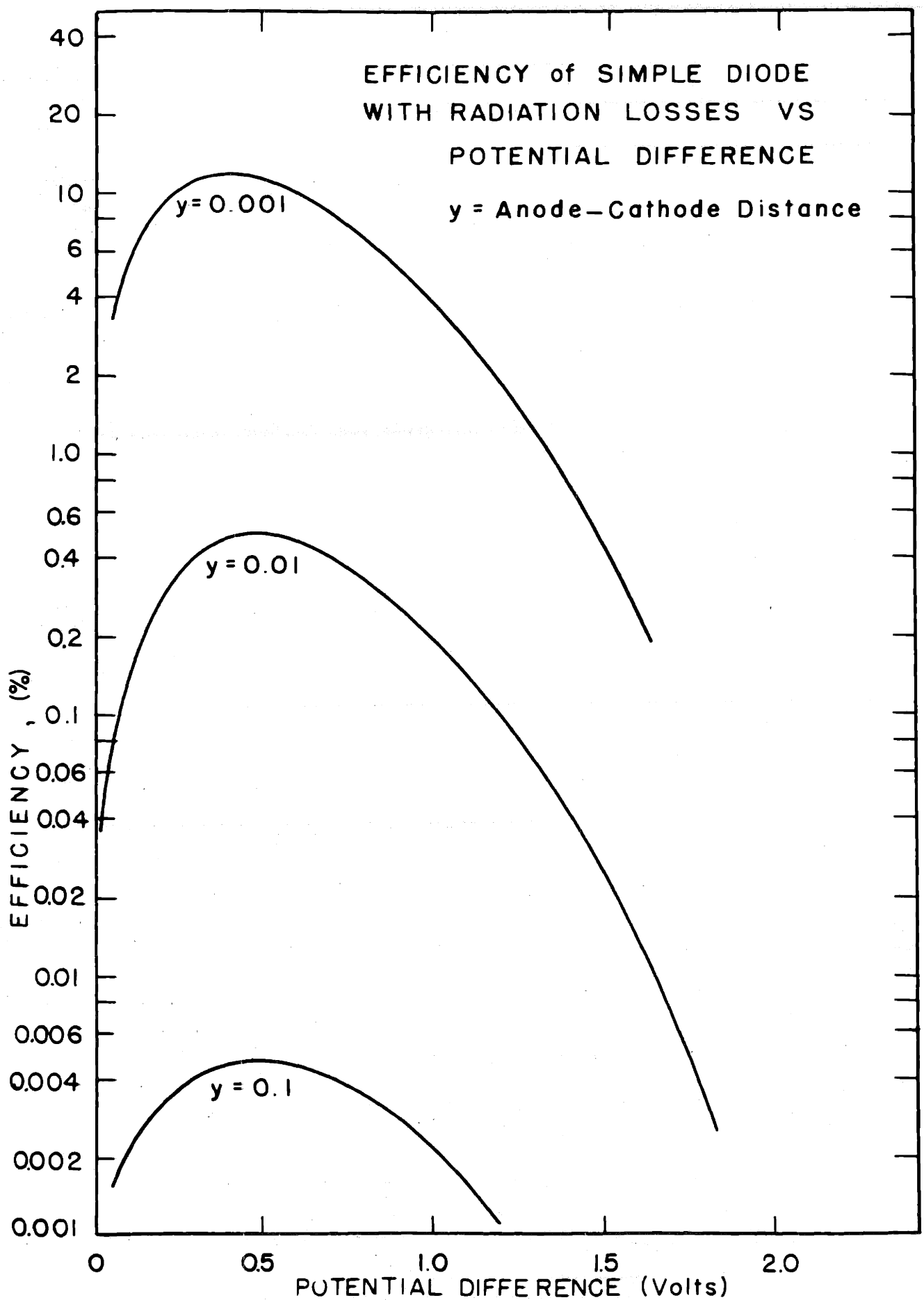
EFFICIENCY of SIMPLE DIODE
WITH RADIATION LOSSES VS
POTENTIAL DIFFERENCE
y = Anode–Cathode Distance
y = 0.001
y = 0.01
y = 0.1
EFFICIENCY , (%)
40
20
10
6
4
2
1.0
0.6
0.4
0.2
0.1
0.06
0.04
0.02
0.01
0.006
0.004
0.002
0.001
0
0.5
1.0
1.5
2.0
POTENTIAL DIFFERENCE (Volts)

Fig. 12

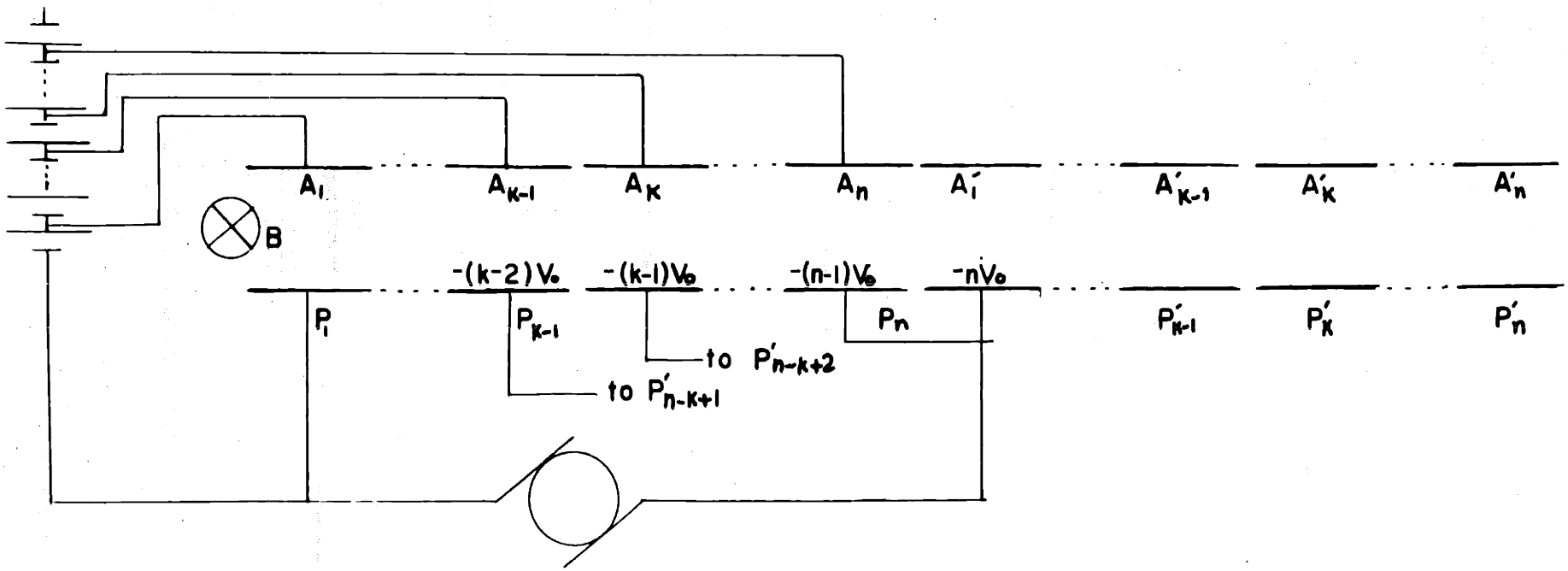

Fig. 13 Schematic Representation of T.E.E with n Hot and n Cold Plates

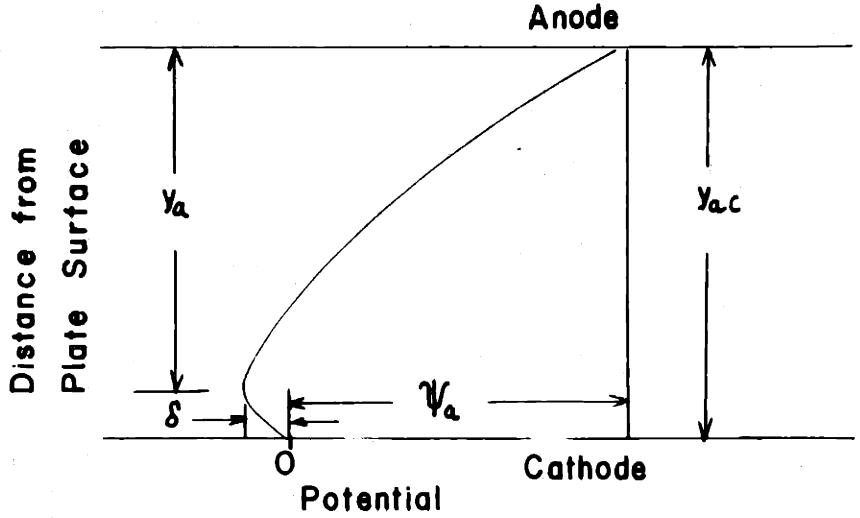

y_{ac} Distance from Anode to Cathode

ψ_a Anode Potential

δ Potential Barrier

Fig. 14 Potential Distribution above Emitting Plates

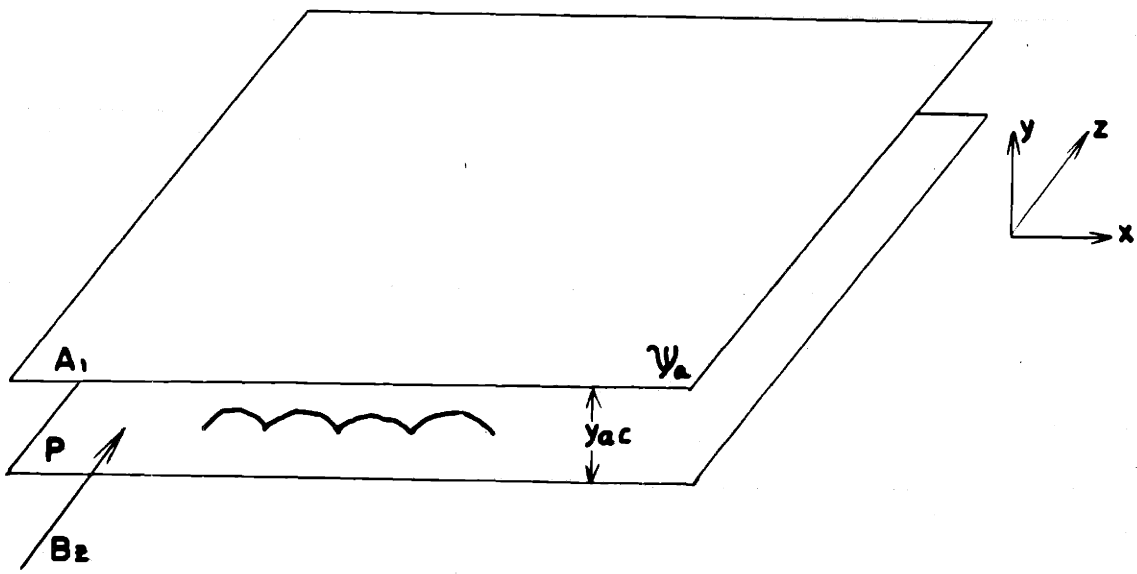

Fig. 15 One Dimensional Electron Flow

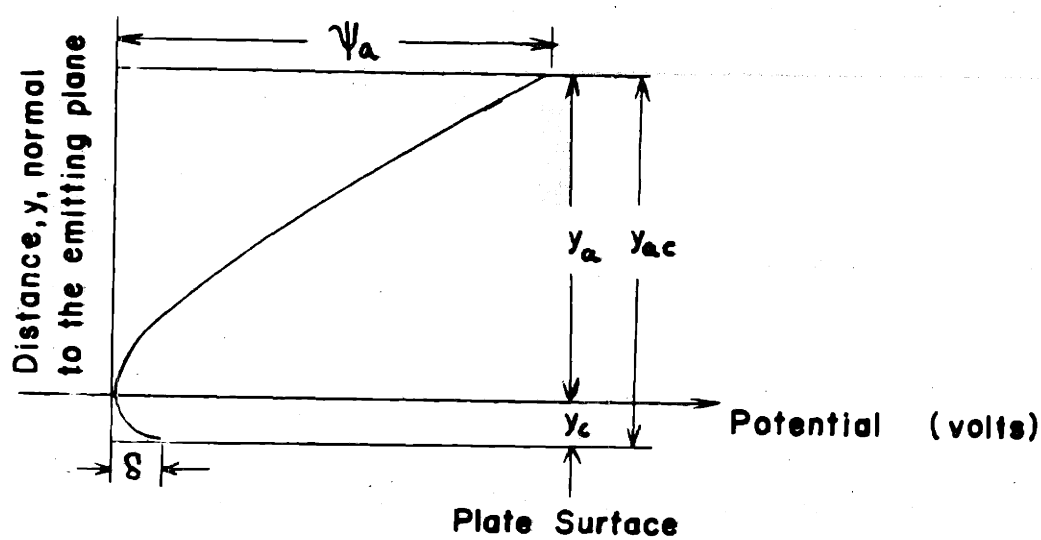

Fig. 16 Potential Distribution vs Distance, y, Normal to the Emitting Plane

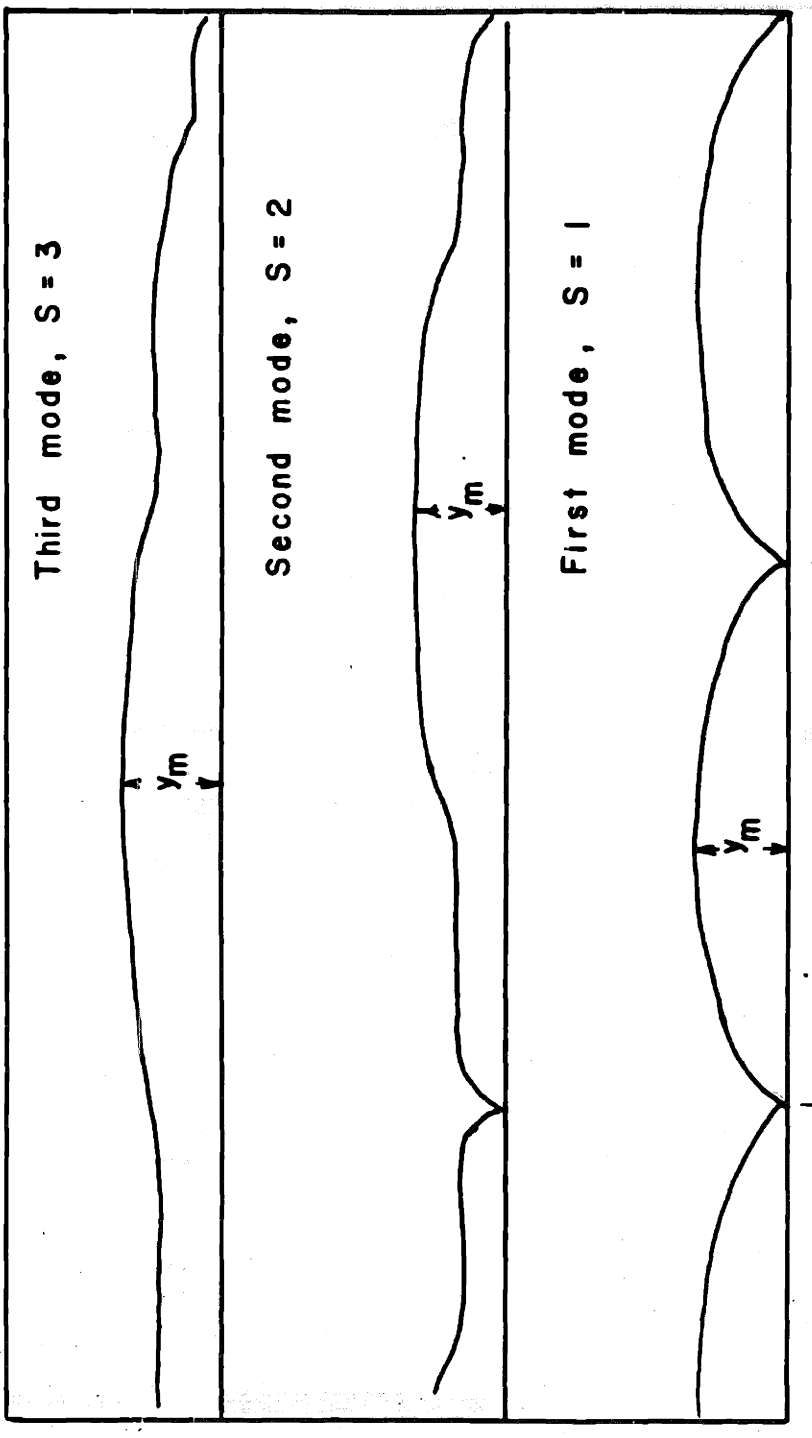

Fig. 17 ELECTRON TRAJECTORIES, ONE DIMENTIONAL ELECTRON FLOW

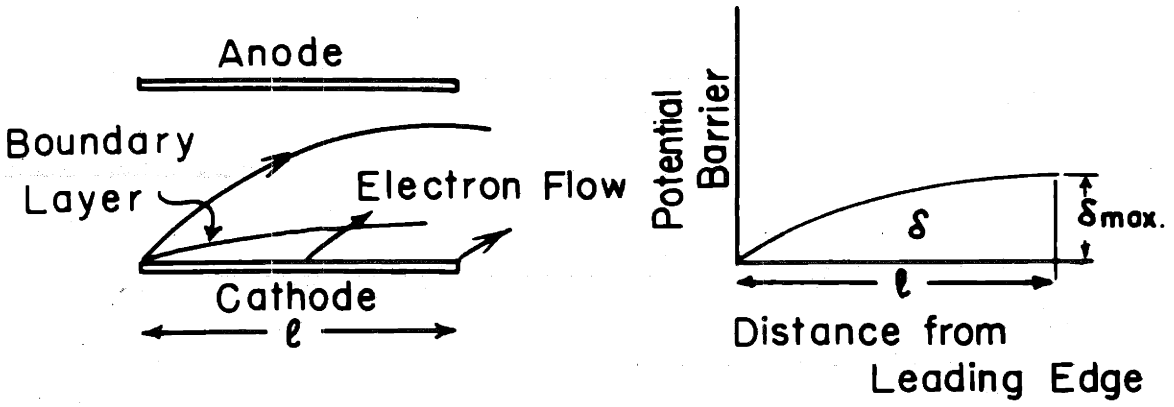

Fig.18 Electron Flow and Potential Barrier for Plates of Width Smaller than the Trajectory Chord

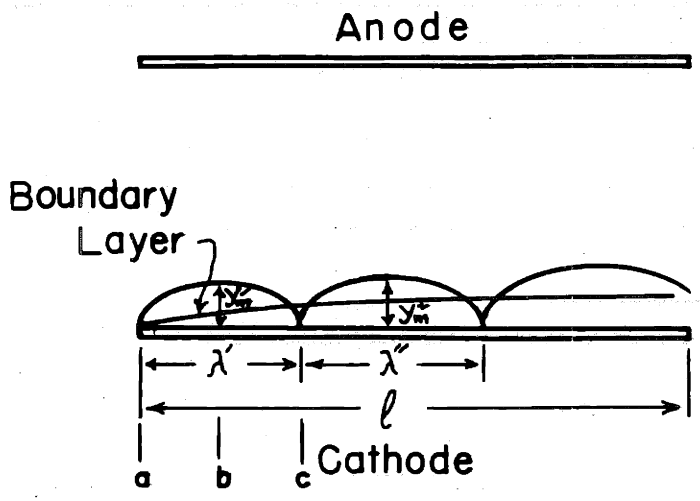

Fig. 19 Electron Flow and Potential Barrier for Plates of Width Larger than the Trajectory Chord

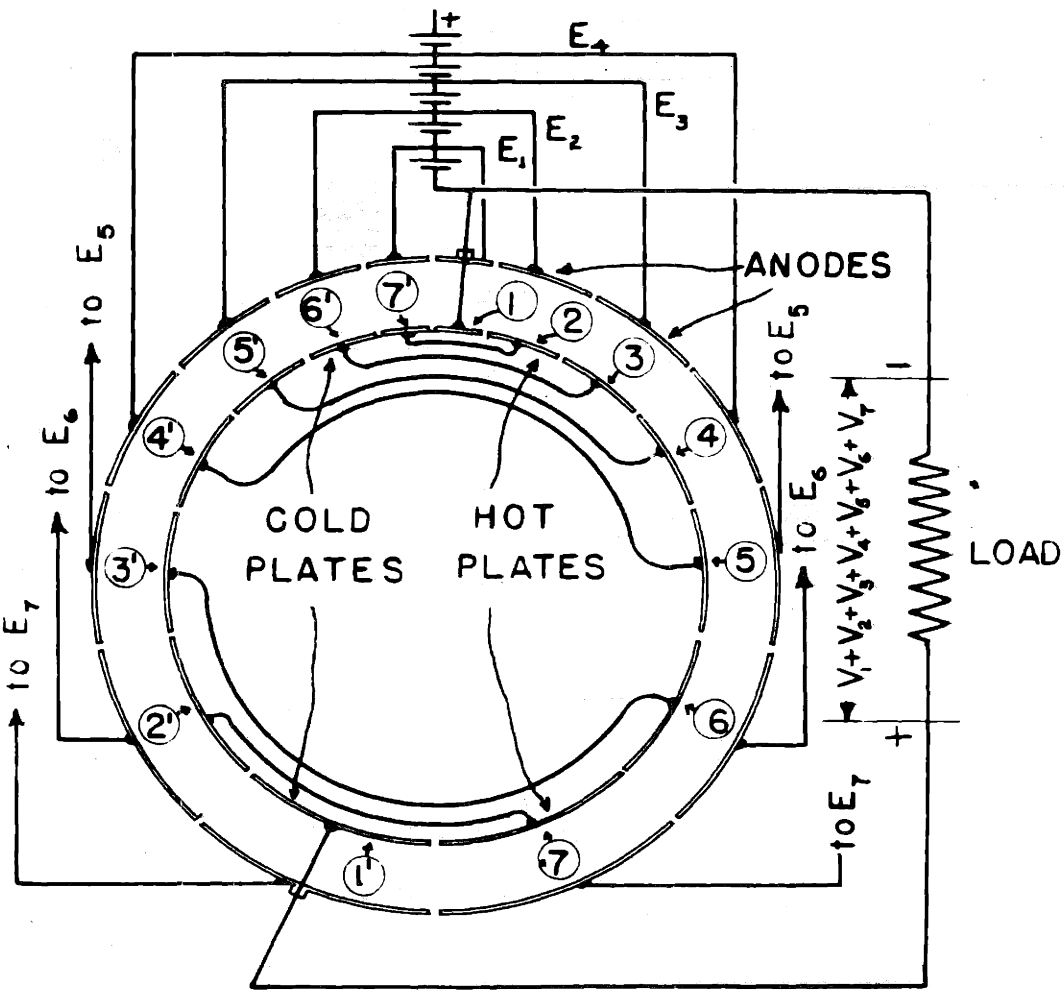

FIG. 20

CIRCULAR CONFIGURATION

THERMO-ELECTRON ENGINE

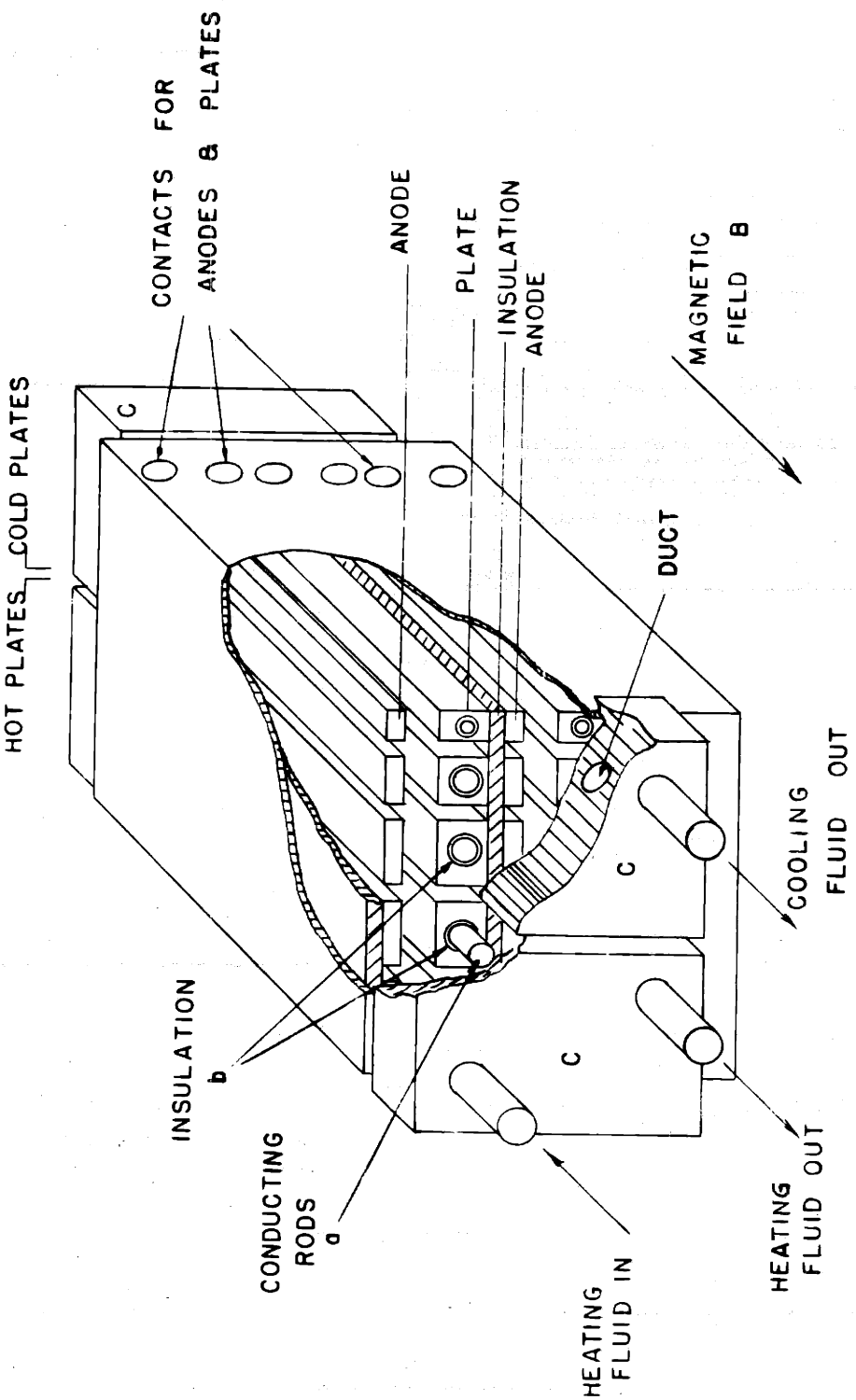

FIG. 21

SCHEMATIC REPRESENTATION, THERMO-ELECTRON ENGINE PLANE CONFIGURATION

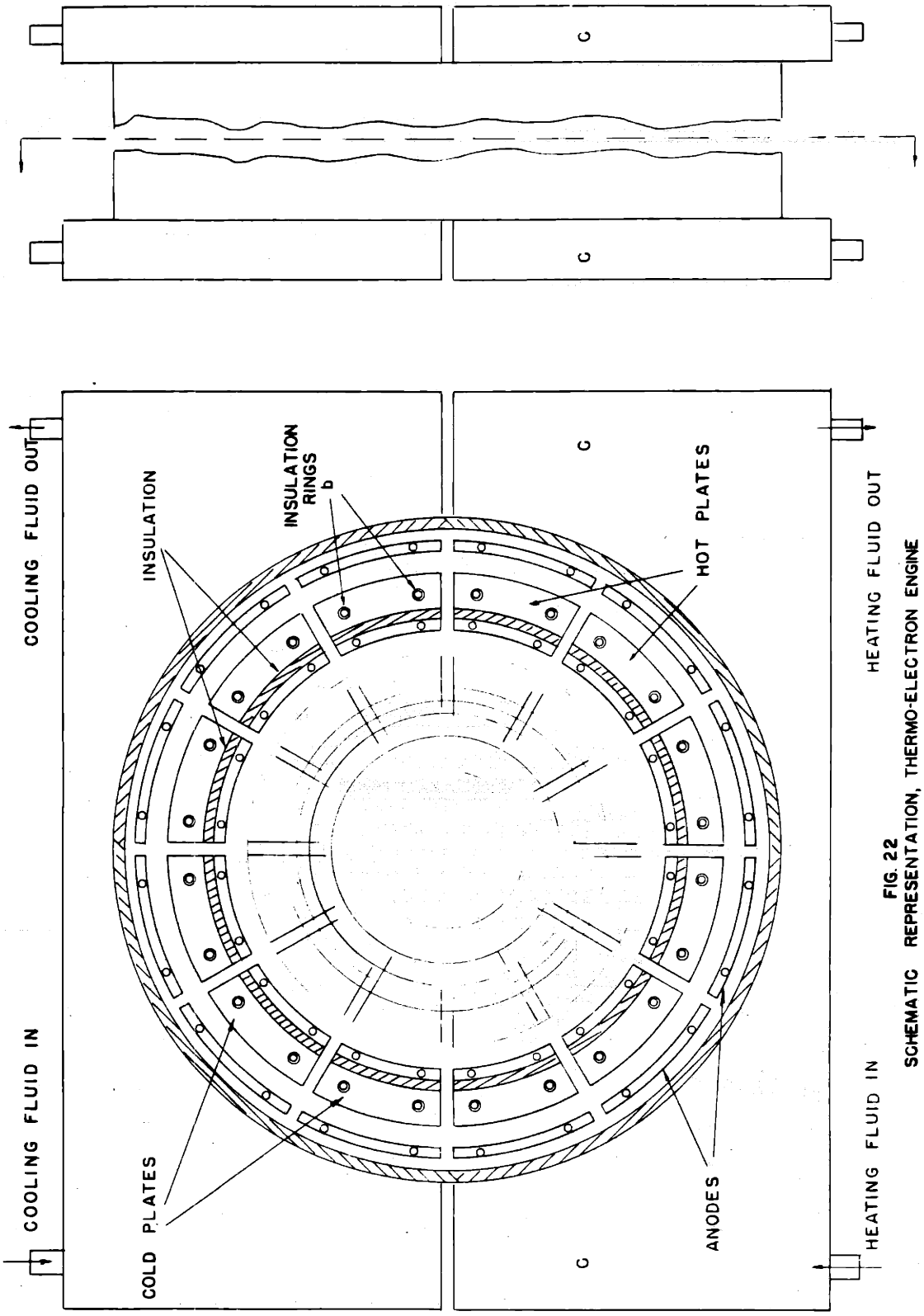

FIG. 22
SCHEMATIC REPRESENTATION, THERMO-ELECTRON ENGINE
CIRCULAR CONFIGURATION

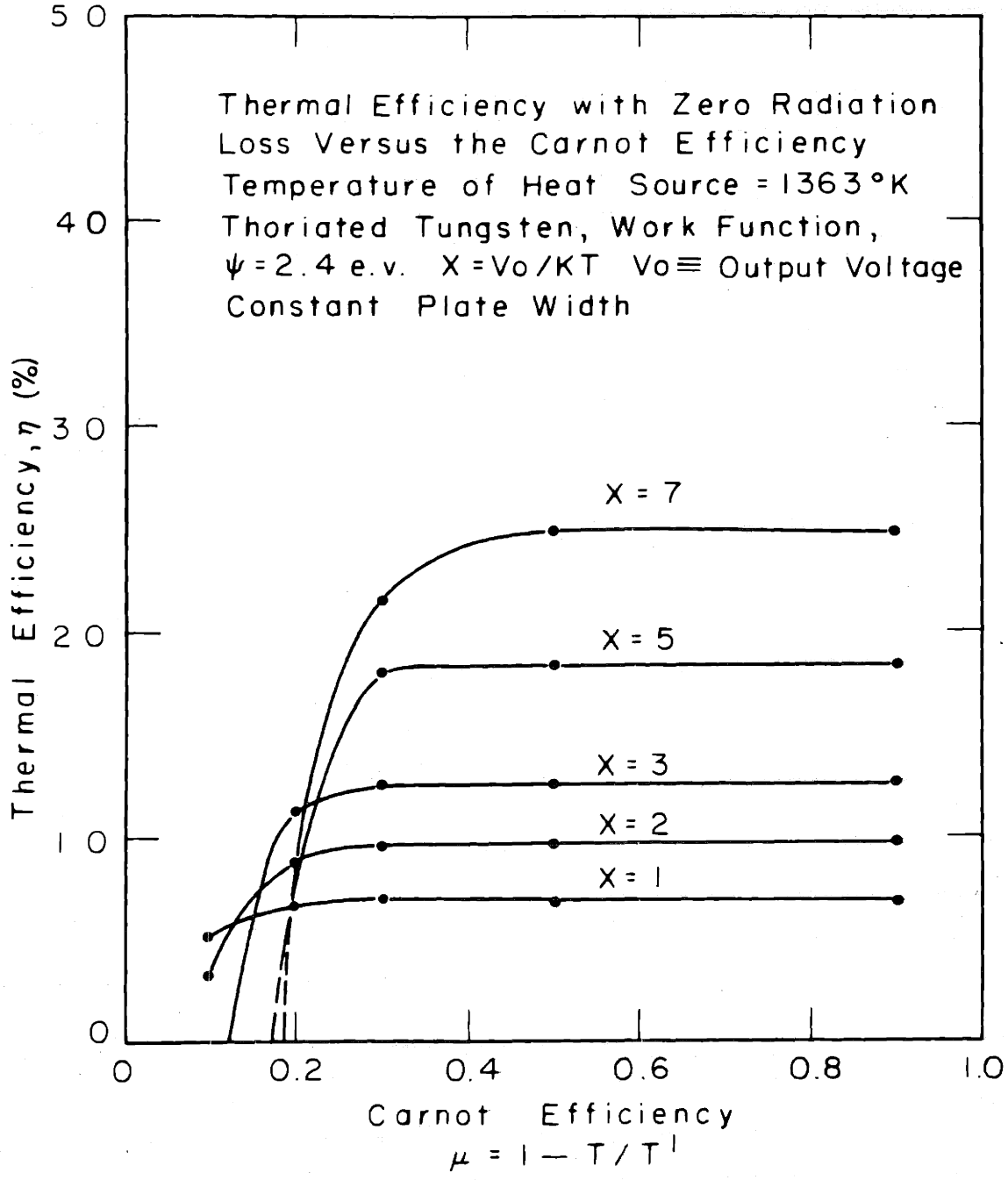
Thermal Efficiency with Zero Radiation Loss Versus the Carnot Efficiency
Temperature of Heat Source = 1363°K
Thoriated Tungsten, Work Function, ψ = 2.4 e.v. X = Vo/KT Vo ≡ Output Voltage
Constant Plate Width
X = 7
X = 5
X = 3
X = 2
X = 1
Thermal Efficiency, η (%)
0
10
20
30
40
50
0
0.2
0.4
0.6
0.8
1.0
Carnot Efficiency
μ = 1 − T/T'

Fig. 23

THERMAL EFFICIENCY WITH ZERO RADIATION LOSS
VERSUS THE CARNOT EFFICIENCY

TEMPERATURE OF HEAT SOURCE = 3000°K
THORIATED TUNGSTEN,
WORK FUNCTION, φ = 2.4 ev
$X \equiv V_o / KT$
$V_o \equiv$ OUTPUT VOLTAGE

CONSTANT PLATE WIDTH

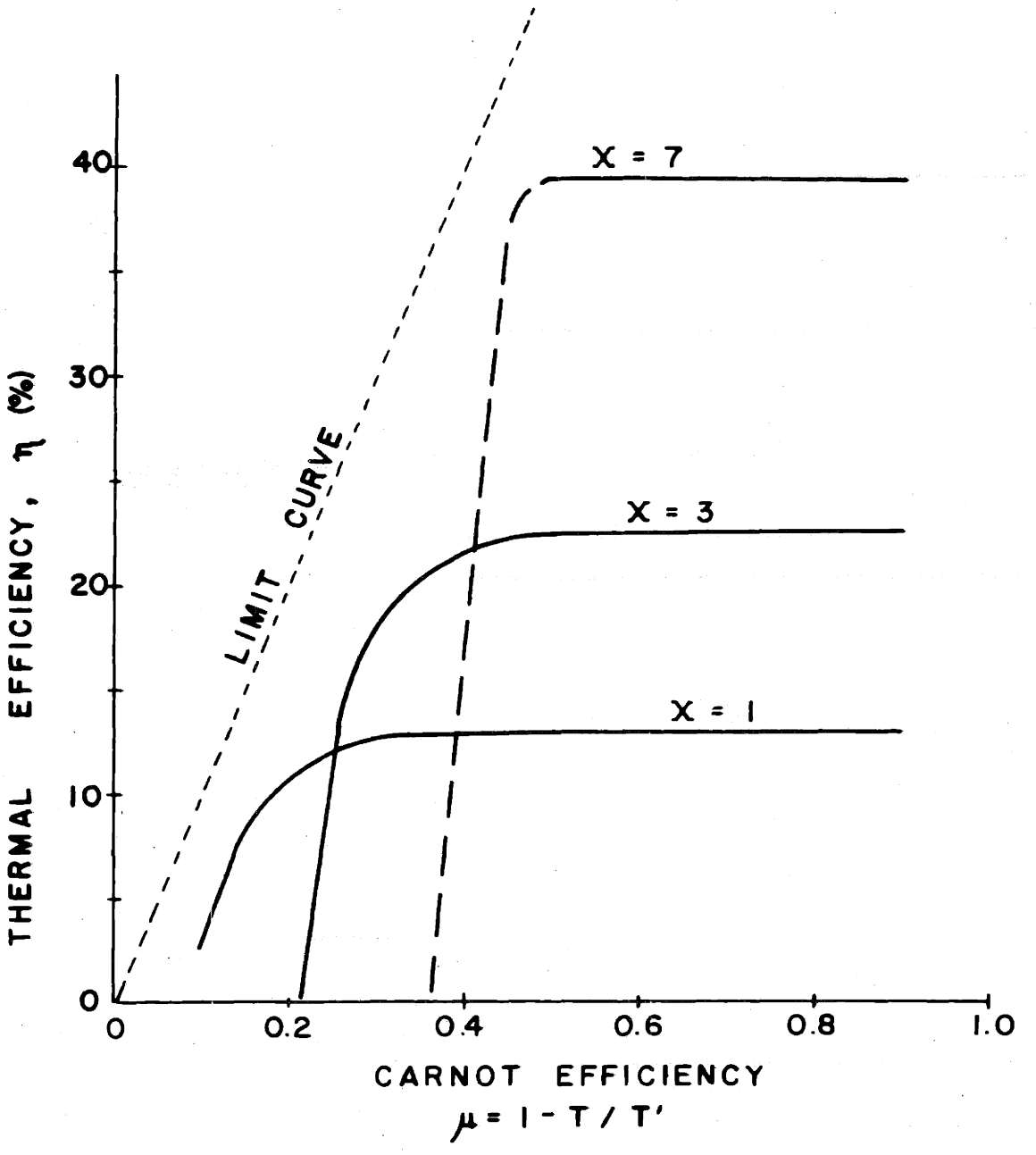

FIG. 24

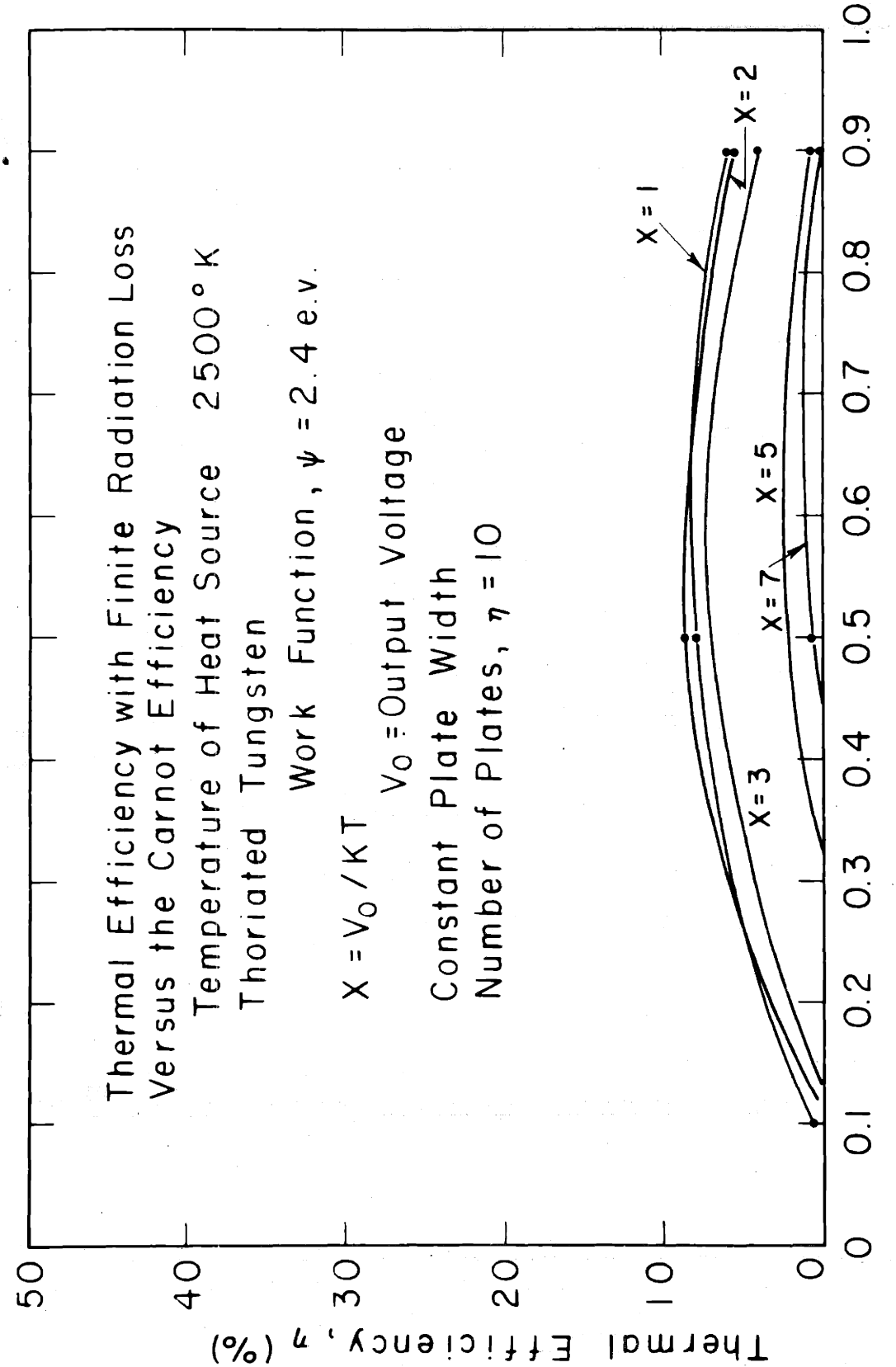
Thermal Efficiency with Finite Radiation Loss
Versus the Carnot Efficiency
Temperature of Heat Source 2500° K
Thoriated Tungsten
Work Function, ψ = 2.4 e.v.
X = V0 / KT
V0 = Output Voltage
Constant Plate Width
Number of Plates, η = 10
X = 1
X = 2
X = 3
X = 5
X = 7
Thermal Efficiency, η (%)
0
10
20
30
40
50
0
0.1
0.2
0.3
0.4
0.5
0.6
0.7
0.8
0.9
1.0
Carnot Efficiency
μ = 1 — T / T'

Fig. 25

THERMAL EFFICIENCY WITH FINITE RADIATION LOSS
VERSUS THE CARNOT EFFICIENCY

TEMPERATURE OF HEAT SOURCE = 3000°K
THORIATED TUNGSTEN,
WORK FUNCTION, φ = 2.4 ev
$X = V_o / KT$
V_o = OUTPUT VOLTAGE

CONSTANT PLATE WIDTH
NUMBER OF PLATES, n = 10

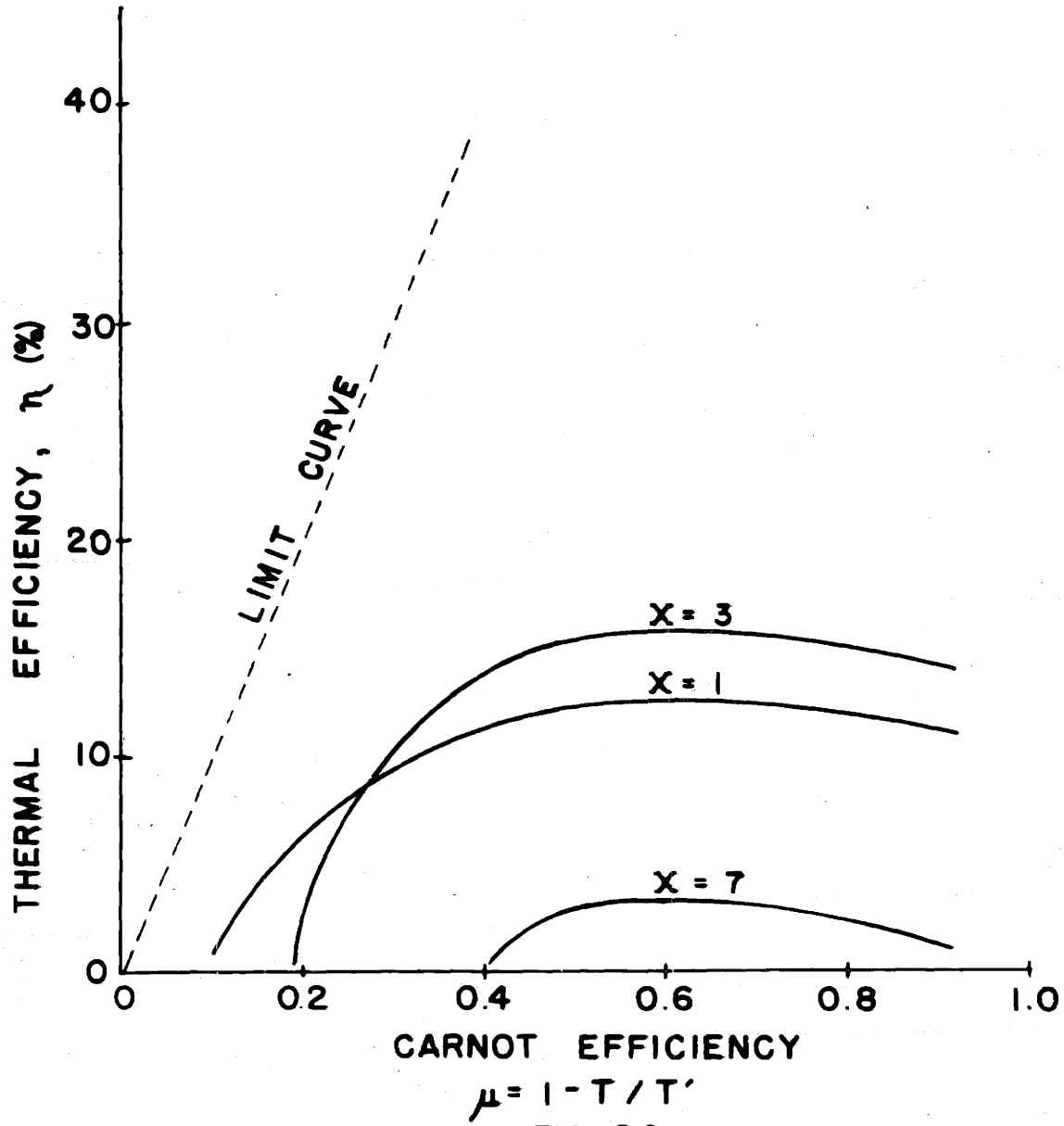

FIG. 26

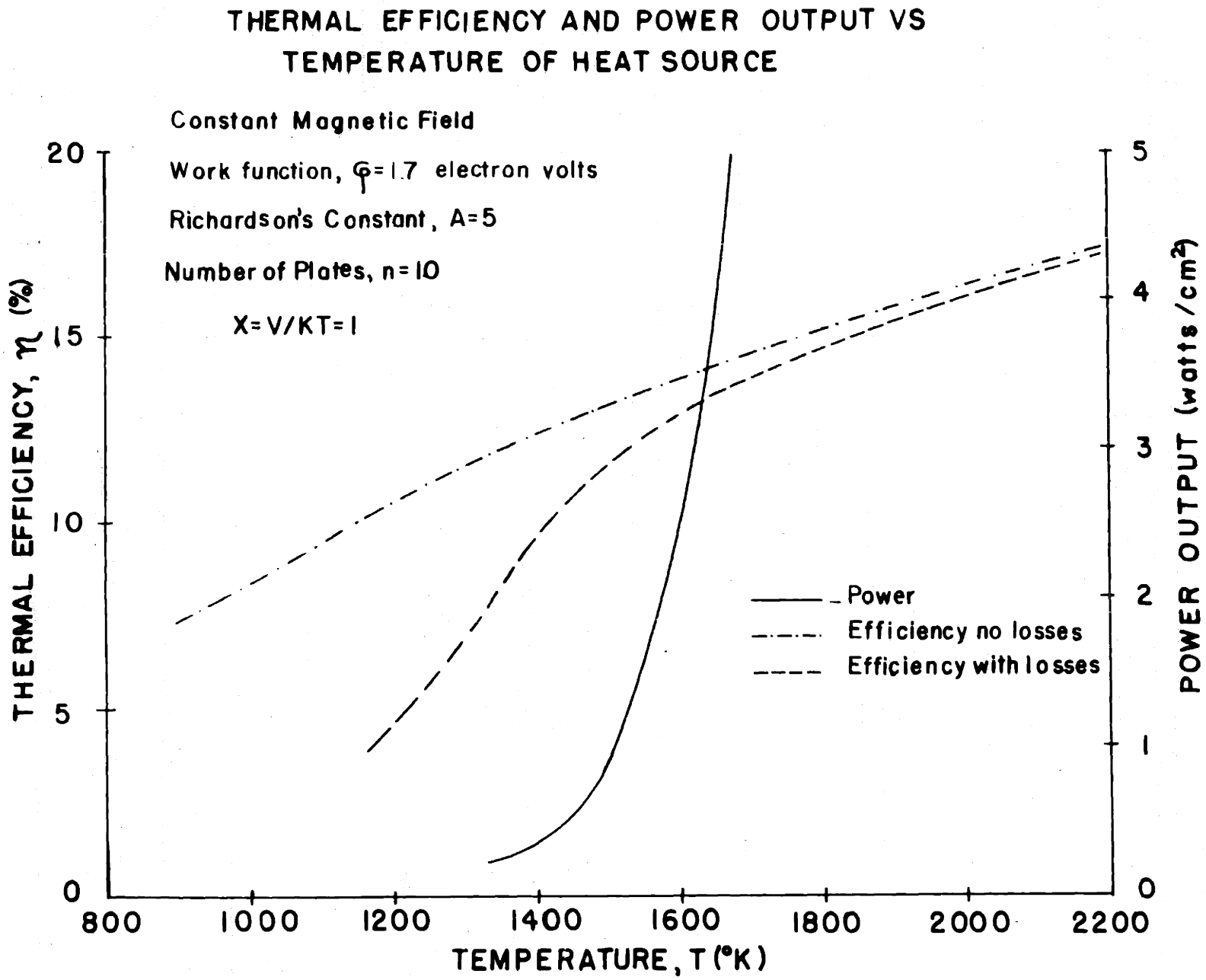
THERMAL EFFICIENCY AND POWER OUTPUT VS
TEMPERATURE OF HEAT SOURCE
Constant Magnetic Field
Work function, φ = 1.7 electron volts
Richardson's Constant, A=5
Number of Plates, n=10
X=V/KT=1
THERMAL EFFICIENCY, η (%)
POWER OUTPUT (watts/cm²)
TEMPERATURE, T (°K)
Power
Efficiency no losses
Efficiency with losses
0
5
10
15
20
800
1000
1200
1400
1600
1800
2000
2200
1
2
3
4

FIG. 27

THERMAL EFFICIENCY AND POWER OUTPUT VS TEMPERATURE OF HEAT SOURCE

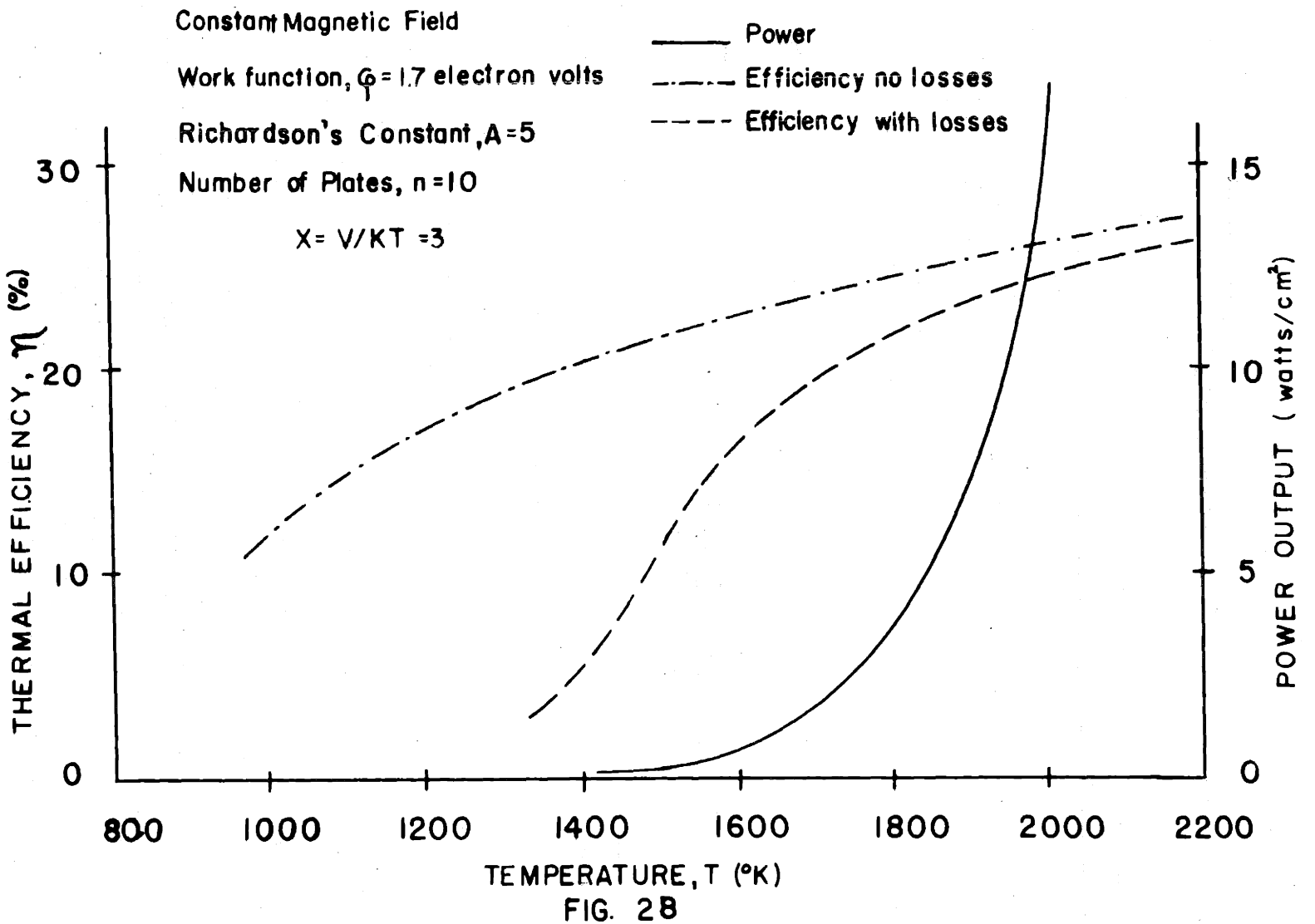

FIG. 28

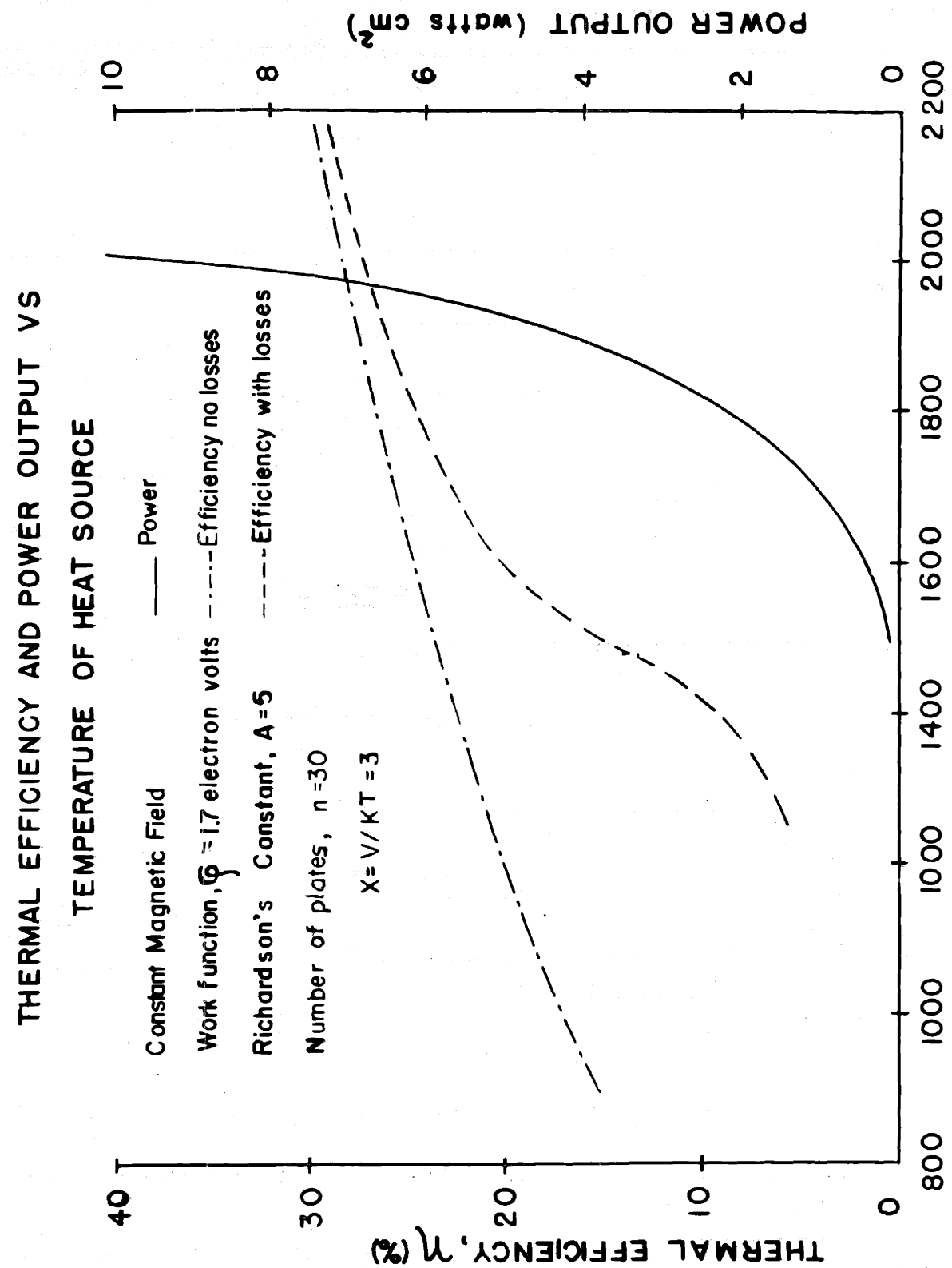
THERMAL EFFICIENCY AND POWER OUTPUT VS
TEMPERATURE OF HEAT SOURCE
Constant Magnetic Field
Work function, φ = 1.7 electron volts
Richardson's Constant, A=5
Number of plates, n=30
X= V/KT =3
—— Power
-·-·- Efficiency no losses
---- Efficiency with losses
THERMAL EFFICIENCY, η (%)
POWER OUTPUT (watts cm²)
TEMPERATURE, T (°K)
0
10
20
30
40
0
2
4
6
8
10
800
1000
1000
1400
1600
1800
2000
2200

FIG. 29

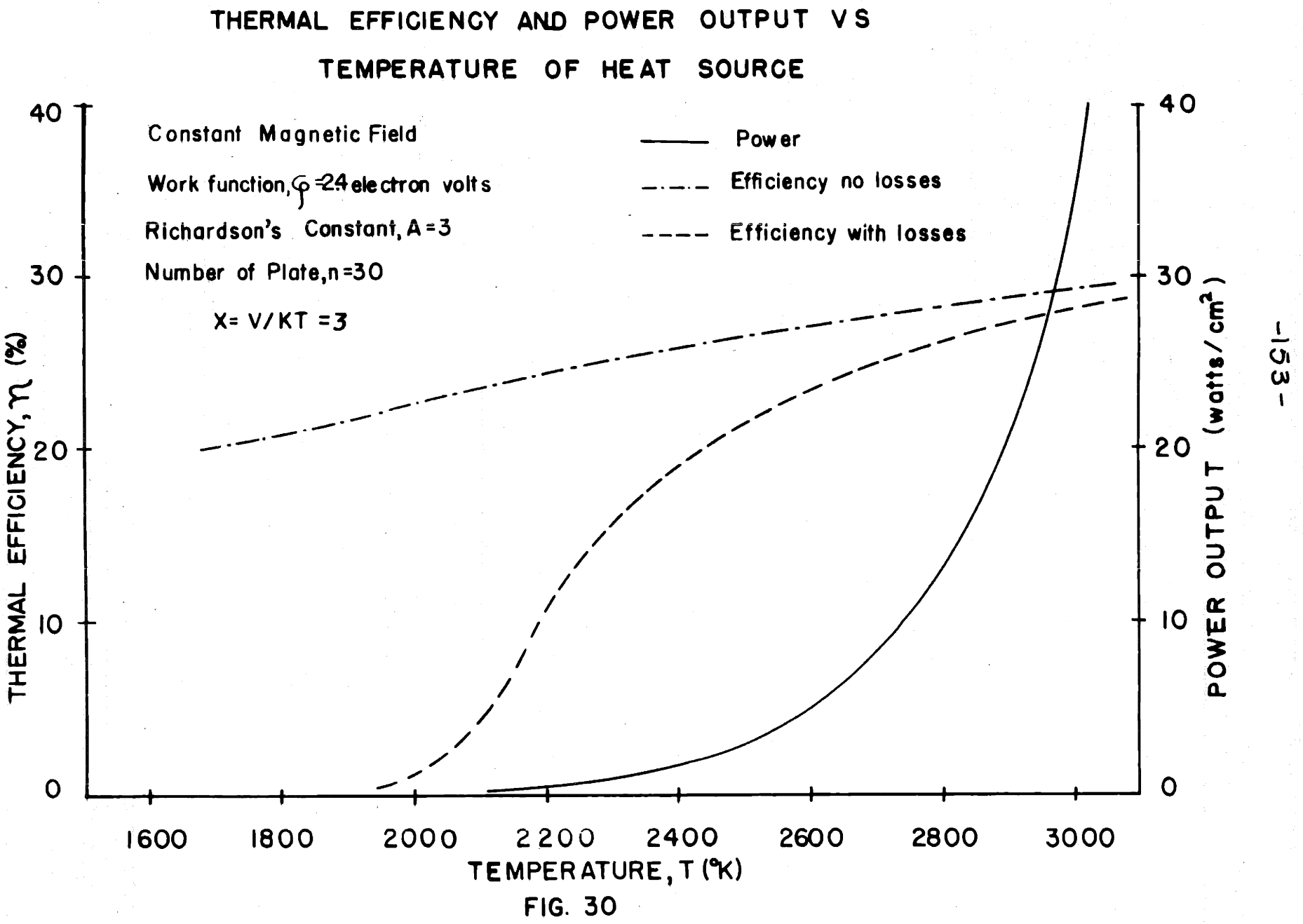
THERMAL EFFICIENCY AND POWER OUTPUT VS
TEMPERATURE OF HEAT SOURCE
Constant Magnetic Field
Work function, φ = 2.4 electron volts
Richardson's Constant, A = 3
Number of Plate, n = 30
X = V/KT = 3
Power
Efficiency no losses
Efficiency with losses
THERMAL EFFICIENCY, η (%)
POWER OUTPUT (watts/cm²)
TEMPERATURE, T (°K)
0
10
20
30
40
1600
1800
2000
2200
2400
2600
2800
3000

FIG. 30

EFFICIENCY OF COMPOSITE THERMOELECTRON ENGINE VERSUS TEMPERATURE OF HEAT SOURCE

Intermediate temperature, T_2, equal to six tenths of high temperature, T_1.

Engine one, Thoriated Tungsten, work function, φ = 2.4 e.v.

Engine two, Impregnated Tungsten, work function, φ = 1.7 e.v.

Parameter $X = V/KT = 3$

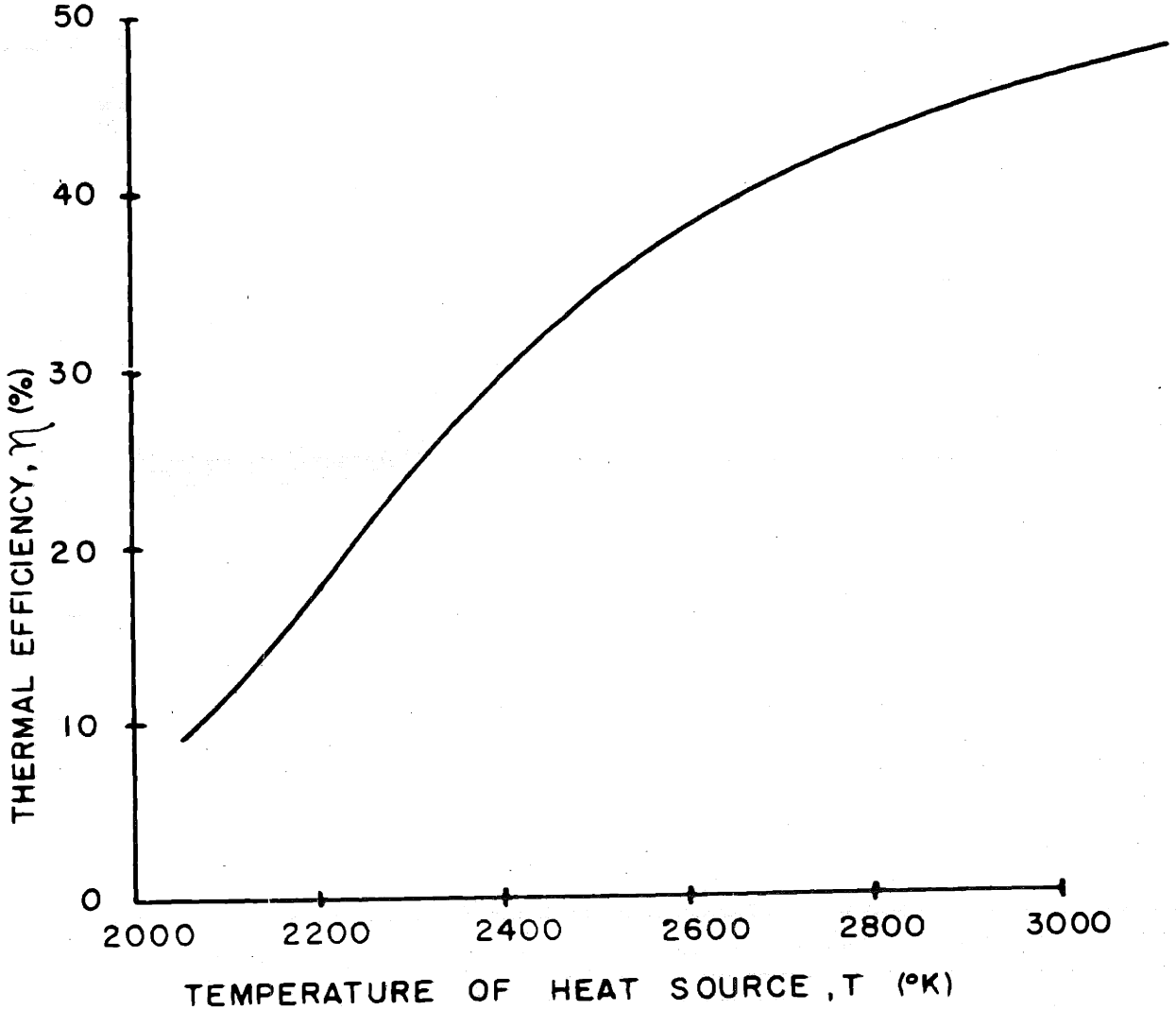

FIG. 31

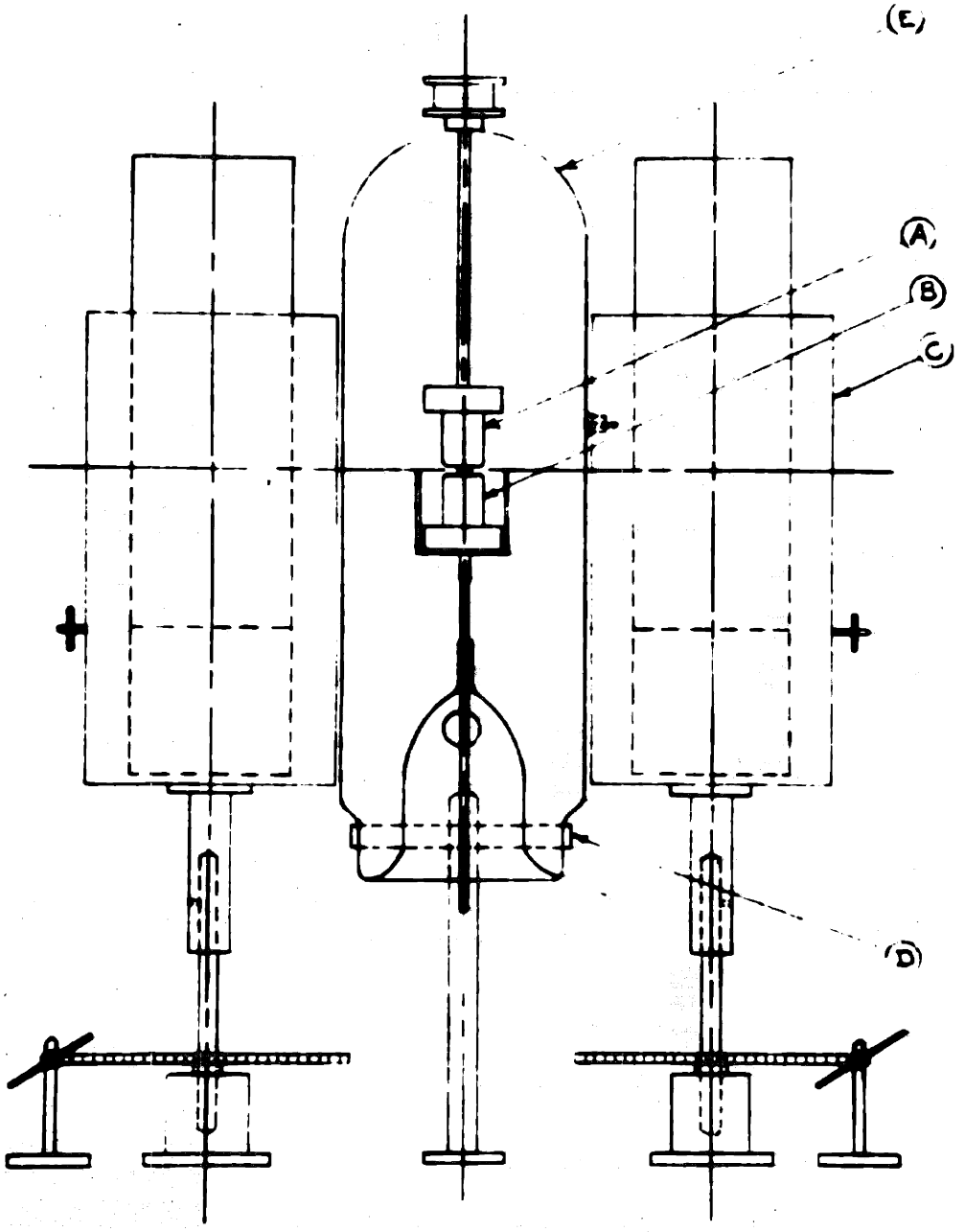

(A) Anode (C) Magnet Assembly (E) Tube
(B) Cathode (D) Tube Clamp Scale: 1" = 3"

MODEL 1 ASSEMBLY

Fig. 32

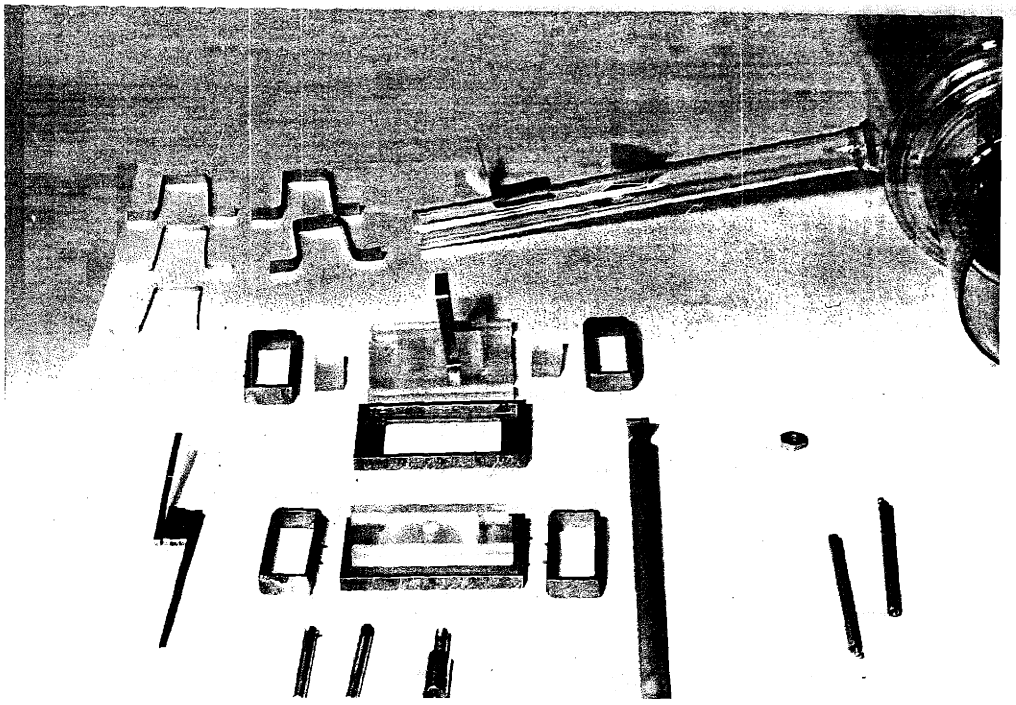

FIGURE 33 - MODEL 1 PARTS

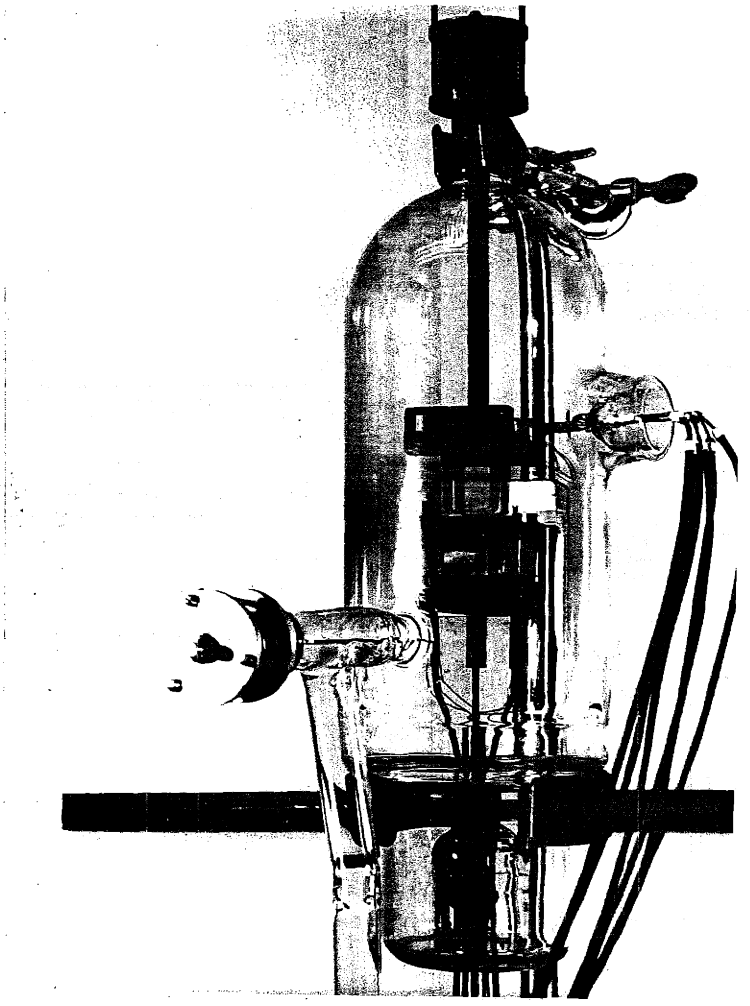

FIGURE 34 - MODEL 1 ASSEMBLED TUBE

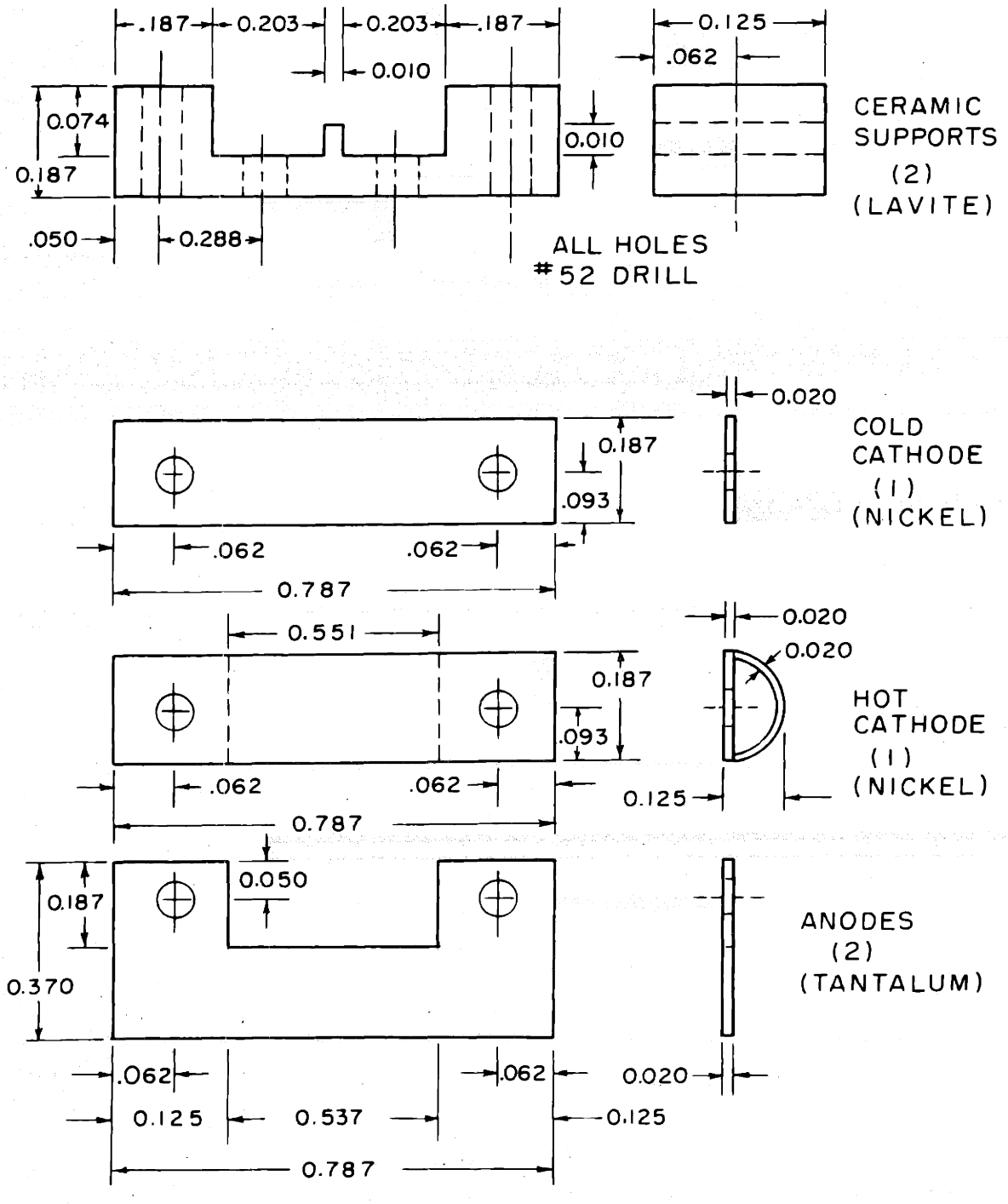

PARTS, MODEL 2

FIG. 35

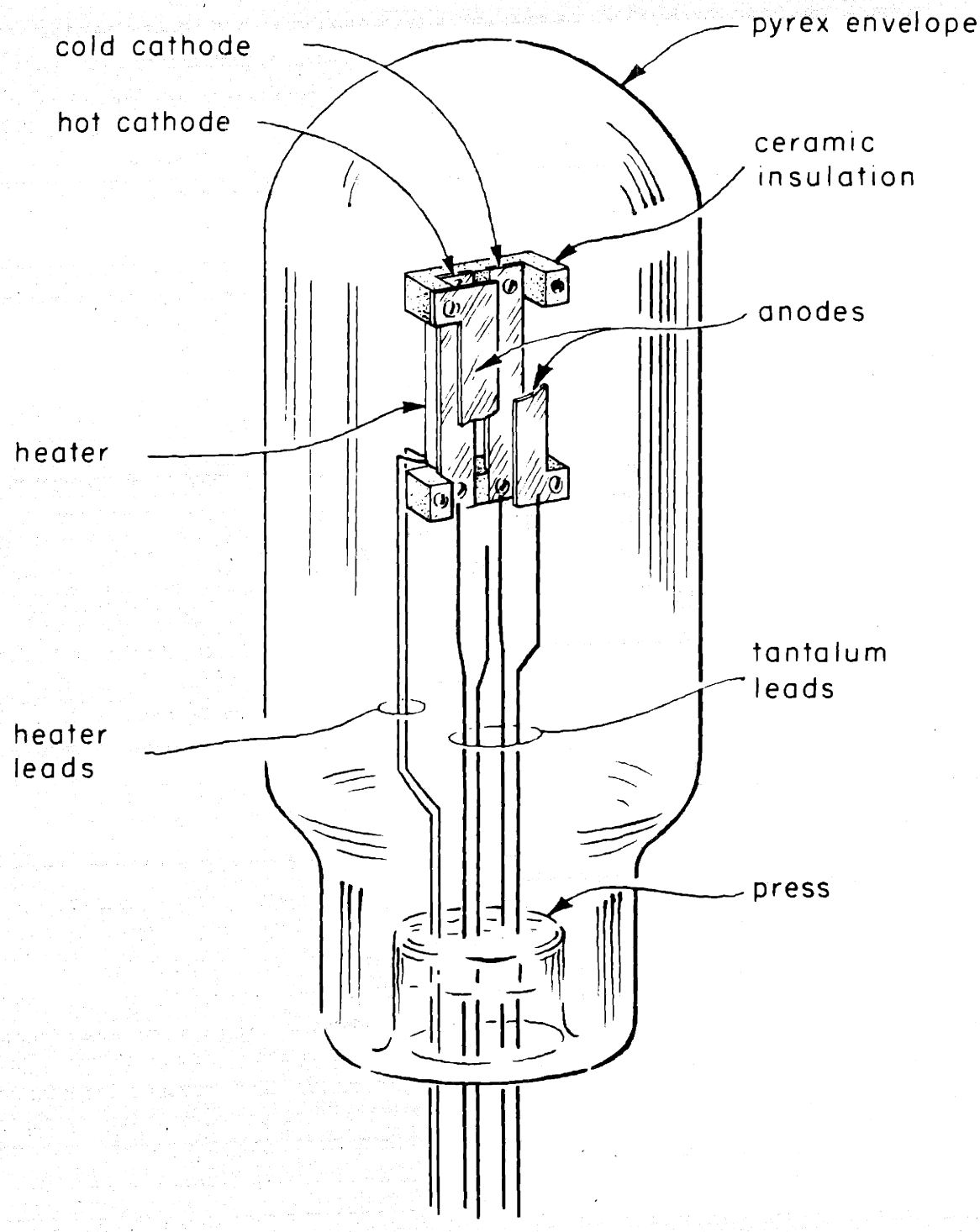

ASSEMBLY DRAWING - MODEL 2

Fig.36

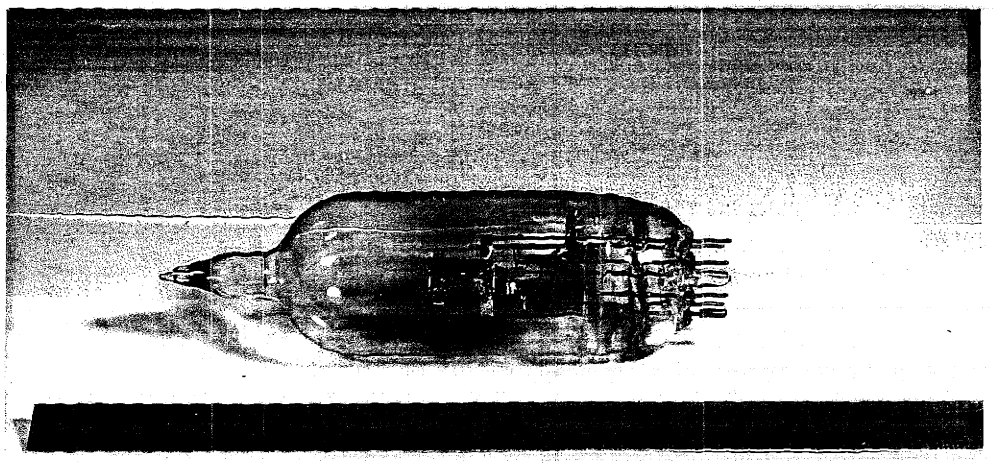

FIGURE 37 - MODEL 3 ASSEMBLY

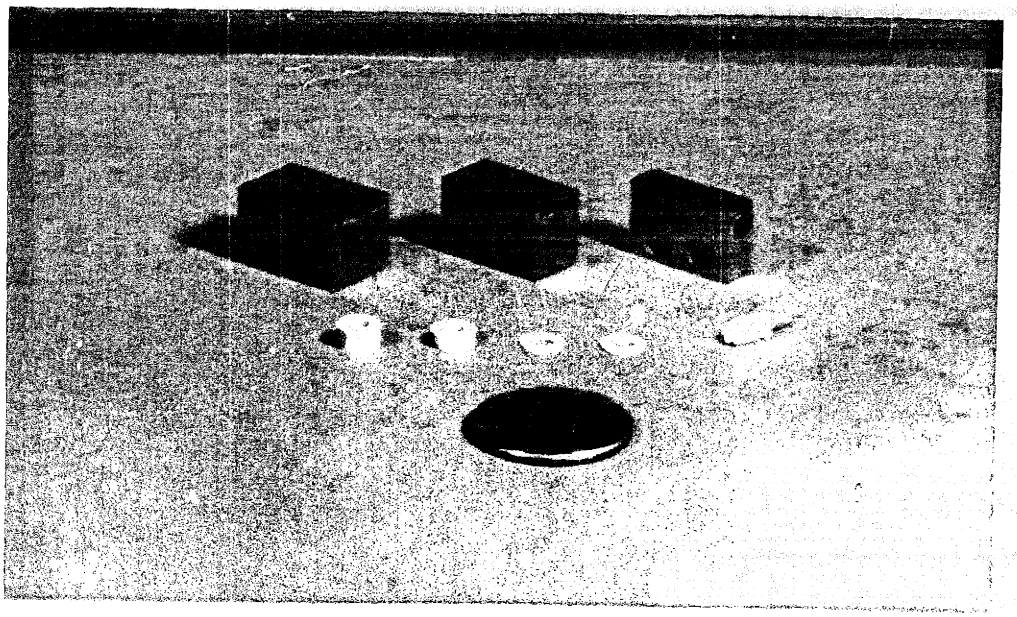

FIGURE 38 - MODEL 4 CATHODES

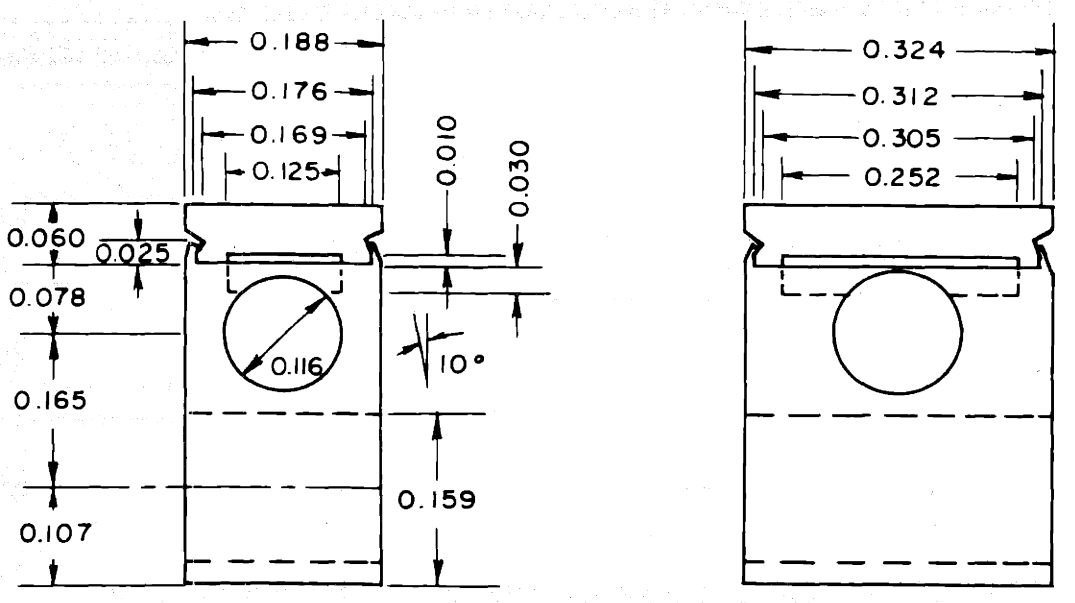

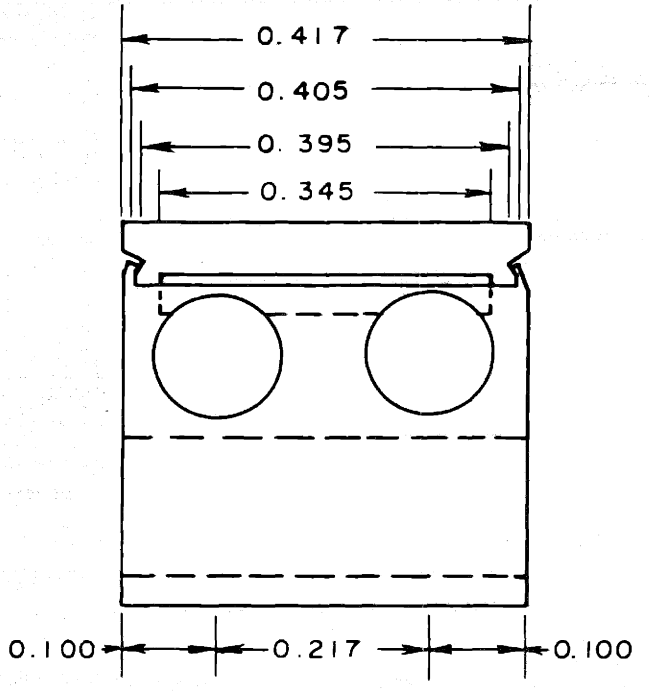

Front View

IMPREGNATED TUNGSTEN CATHODES MODEL 4

FIG. 39

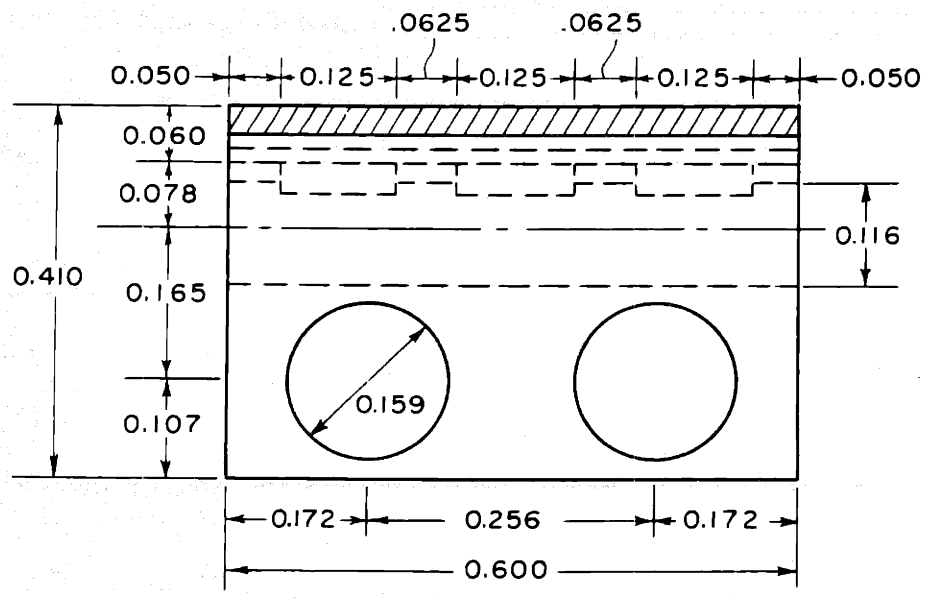

SIDE VIEW

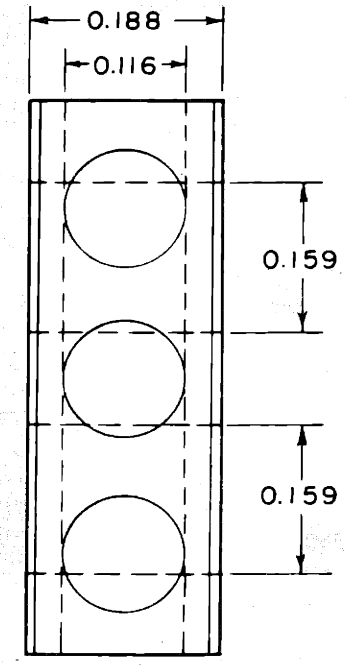

TOP VIEW

FIG. 39a

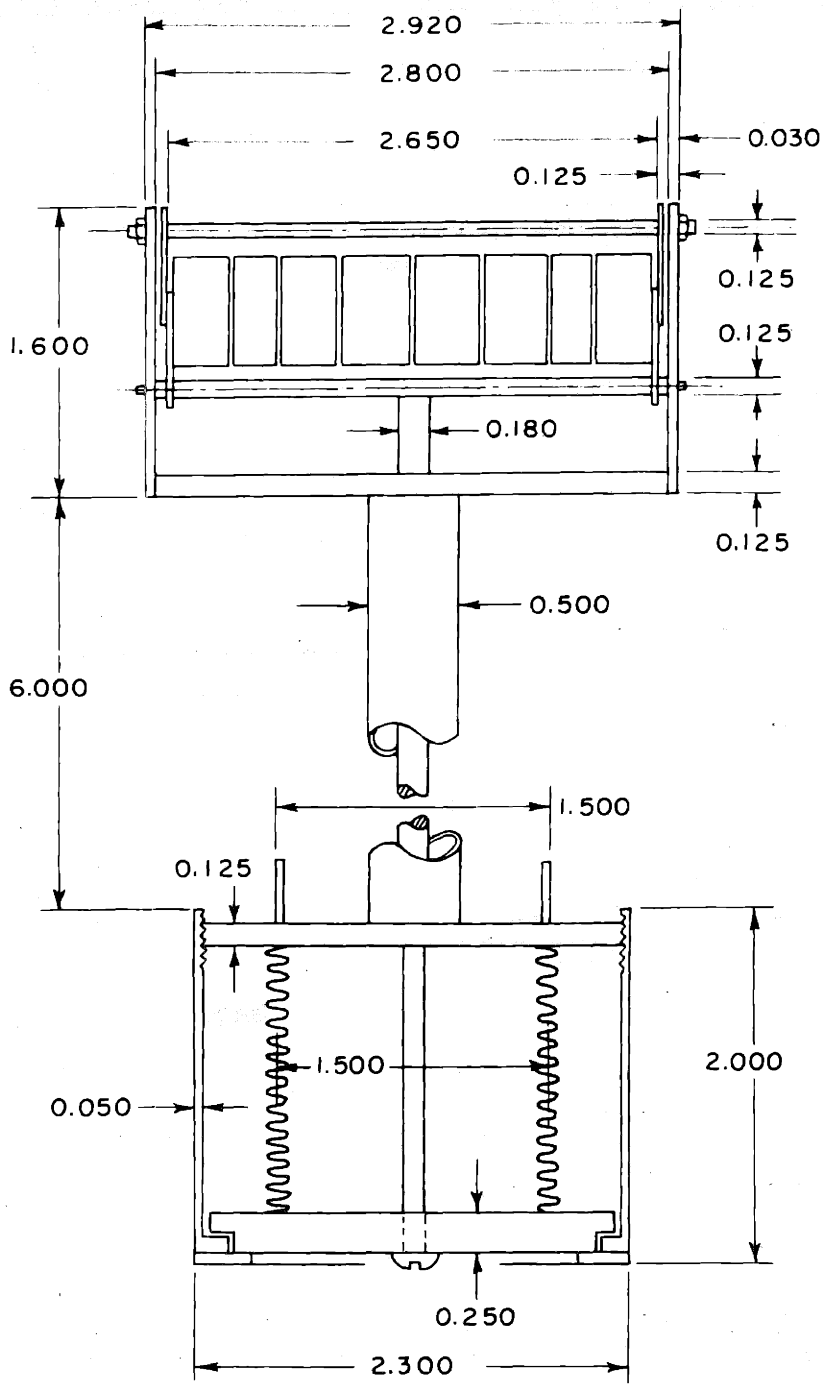

SIDE VIEW Scale 1:1

CATHODE MECHANISM, MODEL 4

FIG. 40

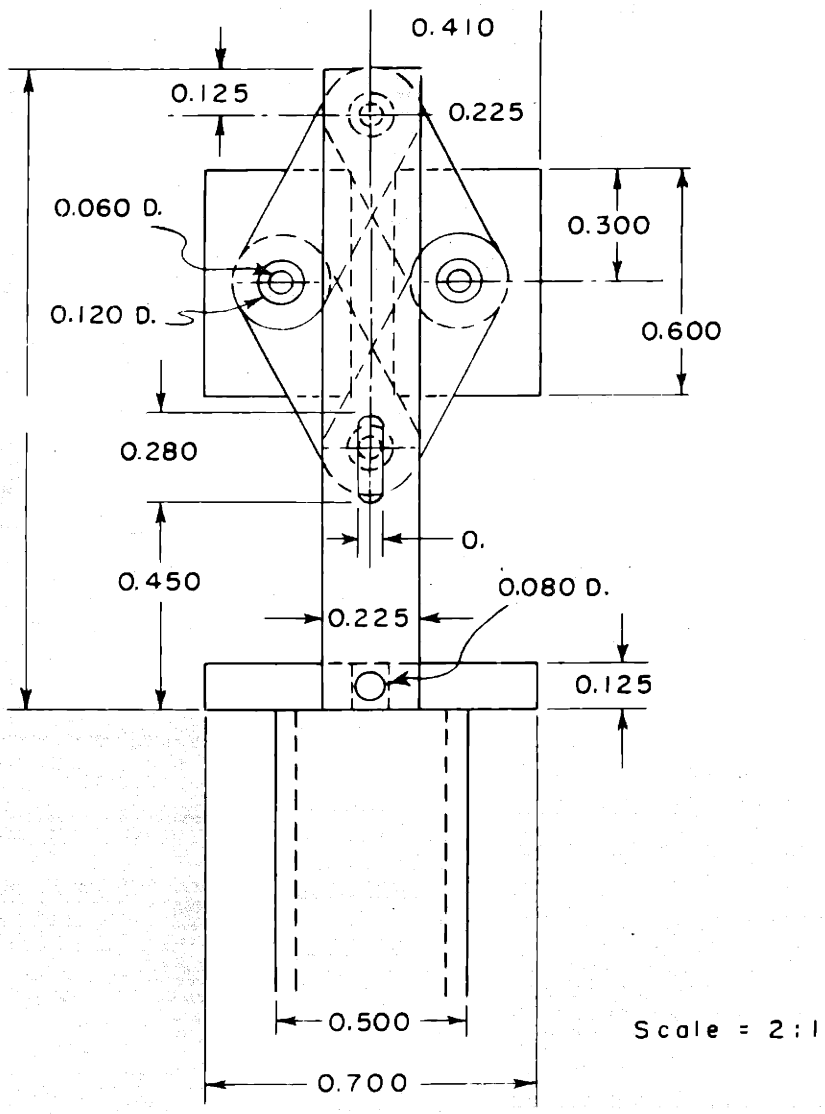

CATHODE MECHANISM, MODEL 4

FIG. 40 a

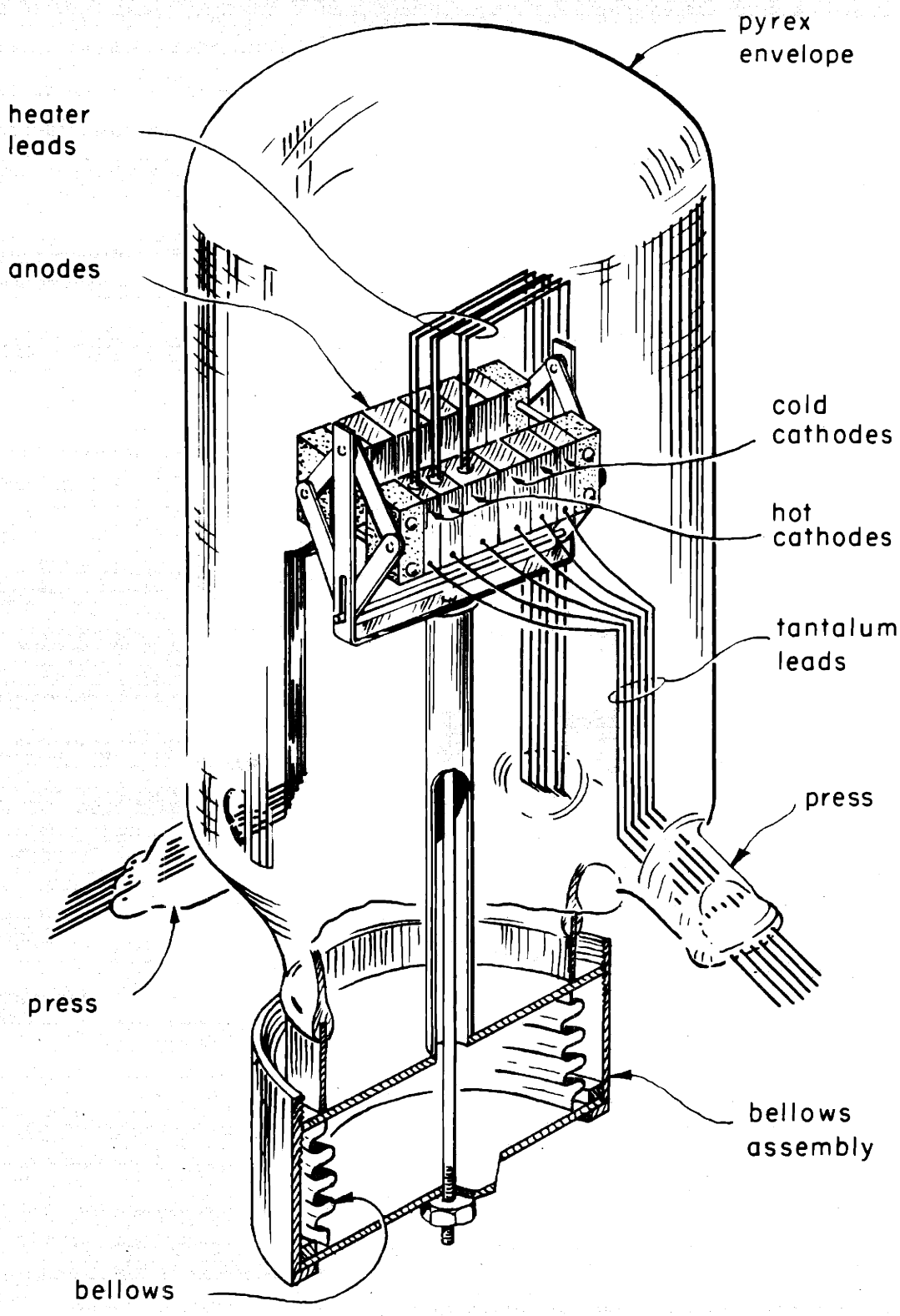

ASSEMBLY DRAWING - MODEL 4

Fig. 41

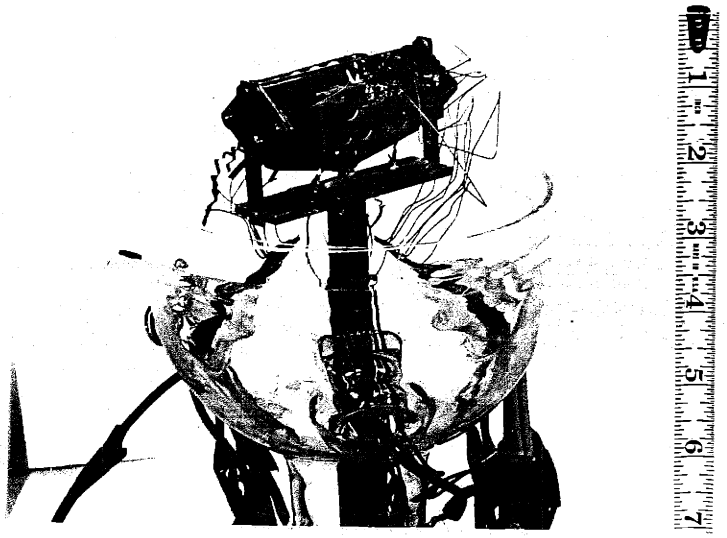

FIGURE 42 - MODEL 4 CATHODE ASSEMBLY

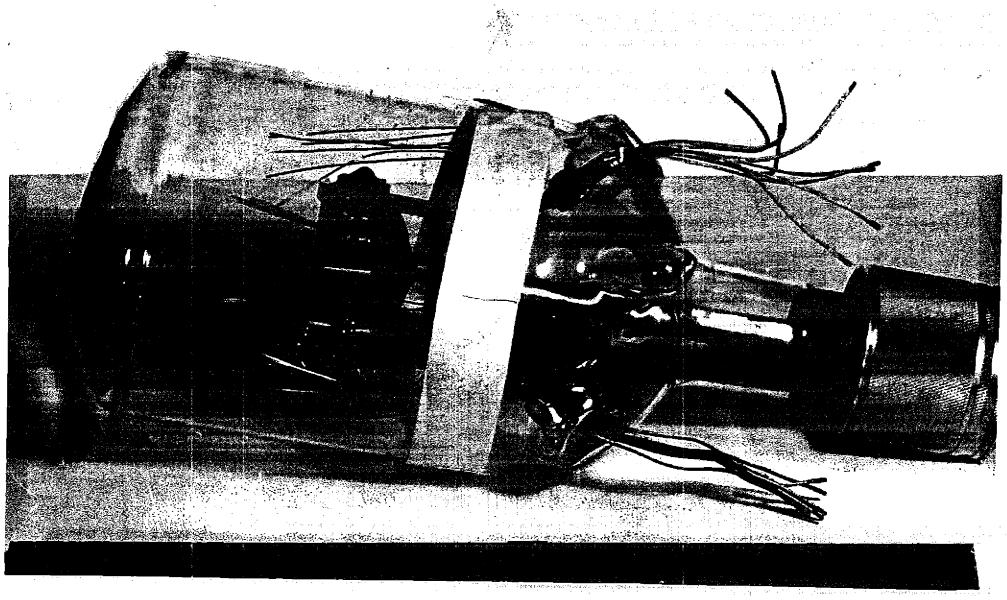

FIGURE 43 - MODEL 4 ASSEMBLY

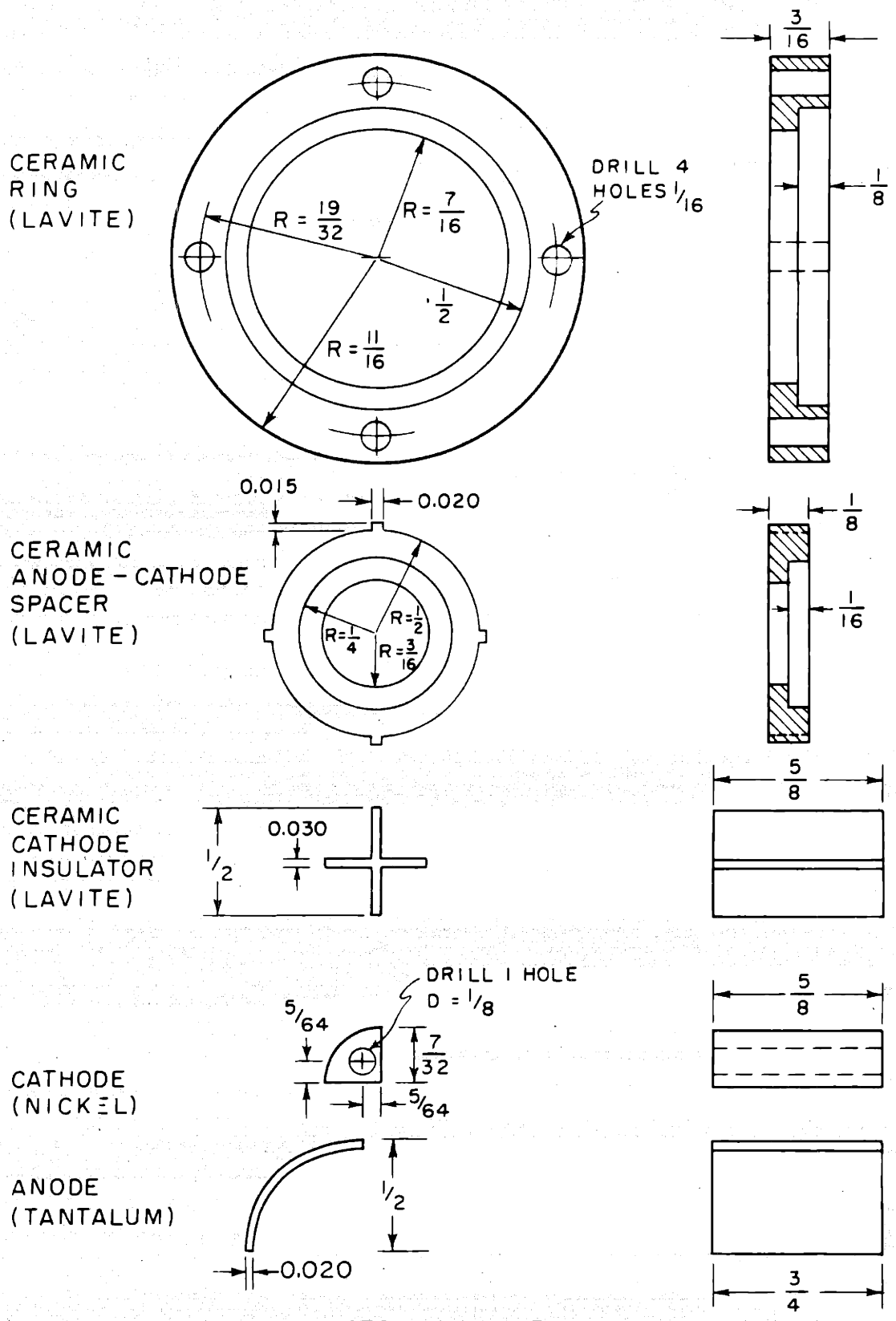

PARTS, MODEL 5

FIG. 44

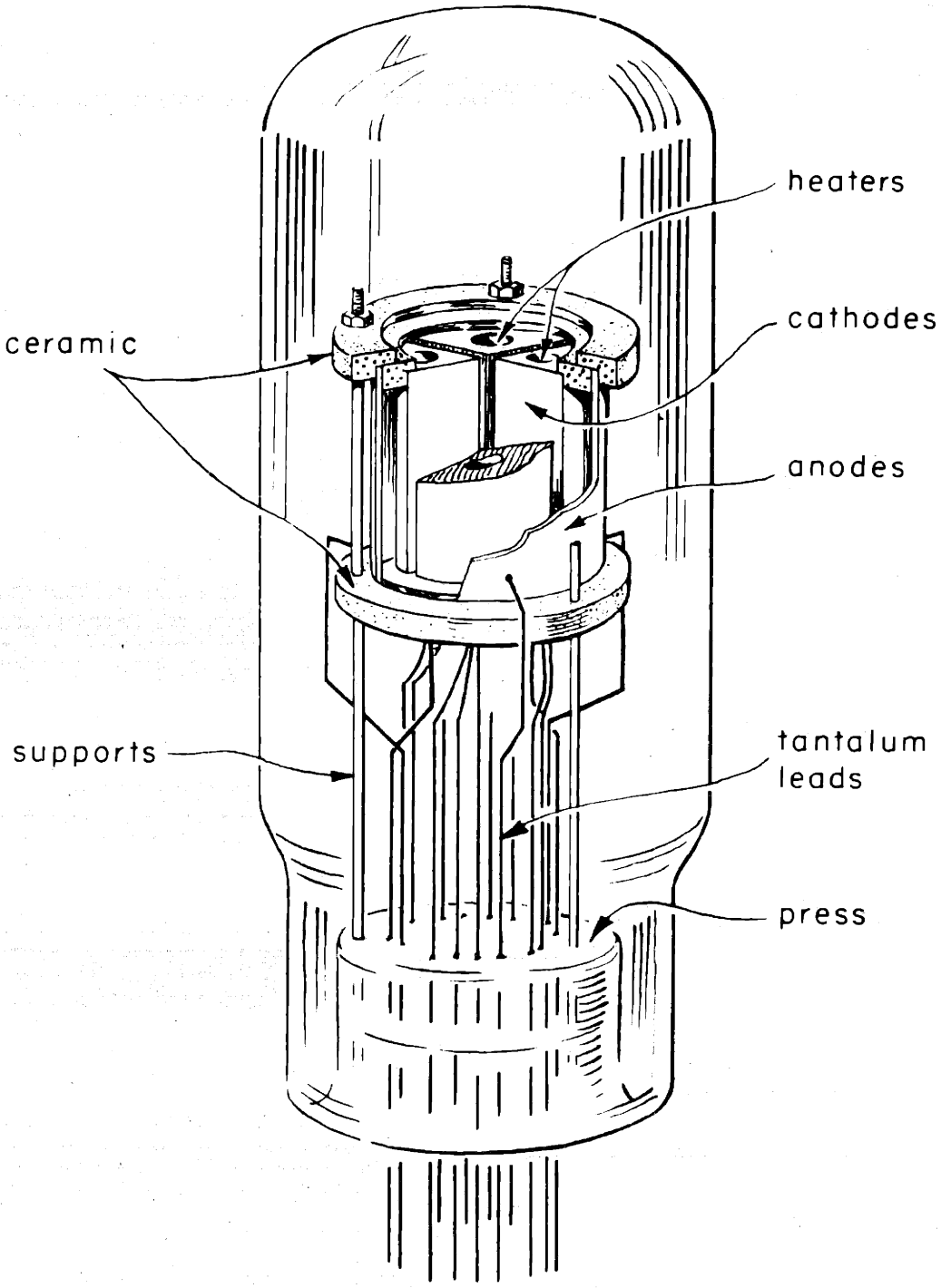

ASSEMBLY DRAWING - MODEL 5

Fig. 45

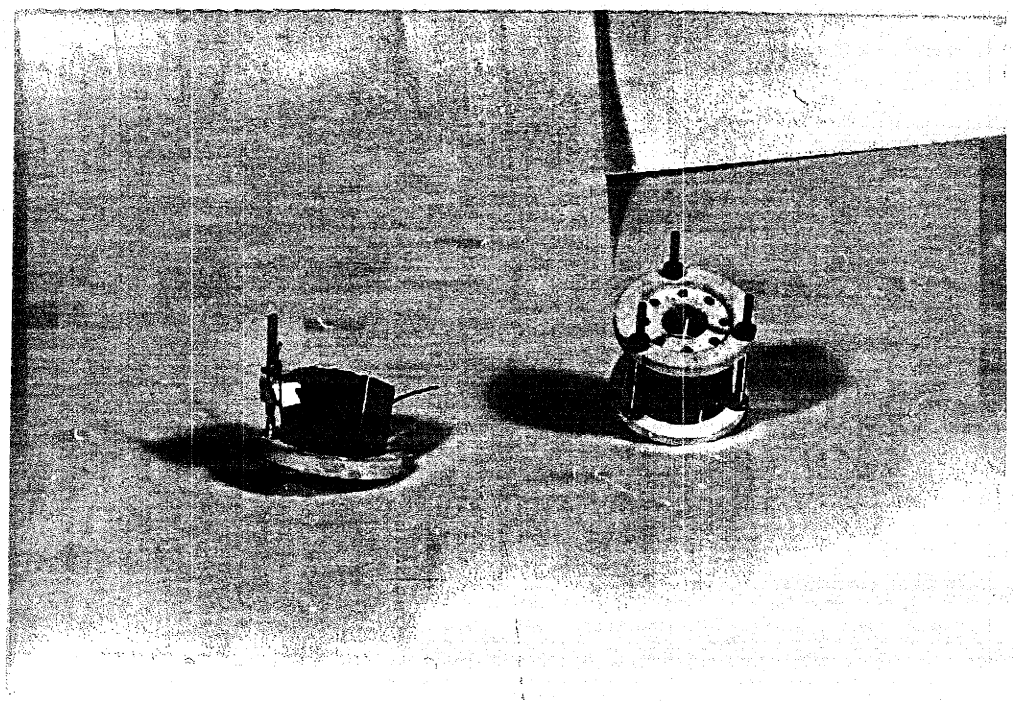

FIGURE 46 - MODEL 5 ANODE-CATHODE ASSEMBLY

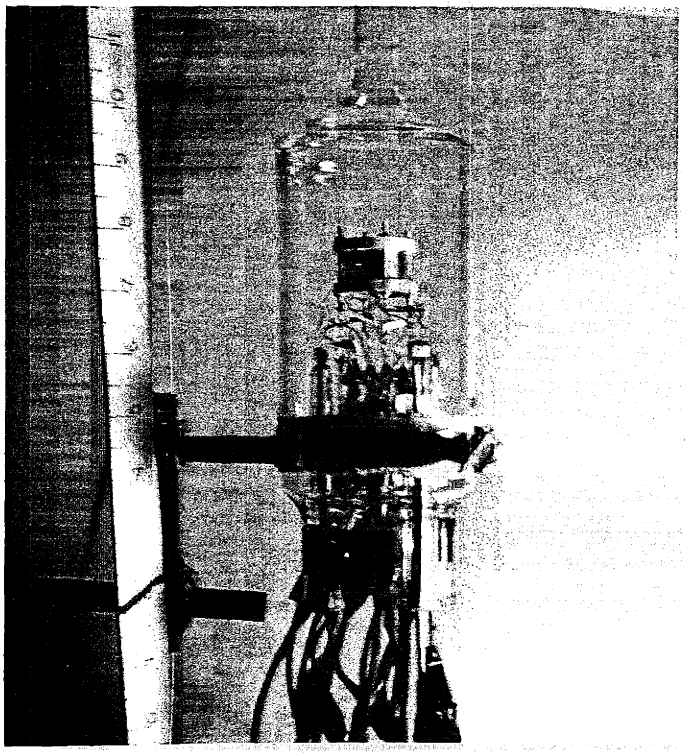

FIGURE 47 - MODEL 5 ASSEMBLY

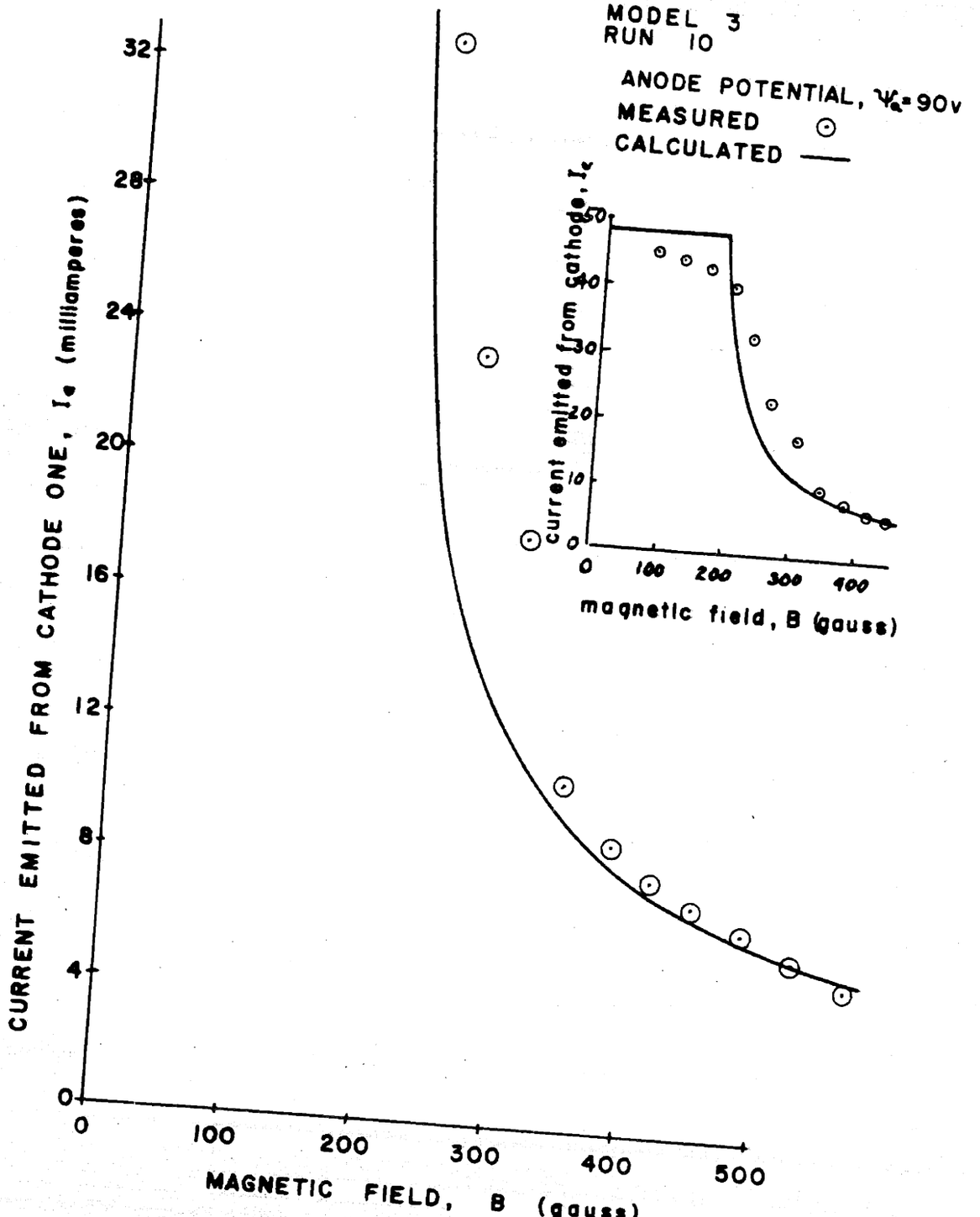
MODEL 3
RUN 10
ANODE POTENTIAL, V_a = 90v
MEASURED ⊙
CALCULATED ——
current emitted from cathode, I_e
0
10
20
30
40
50
0
100
200
300
400
magnetic field, B (gauss)
CURRENT EMITTED FROM CATHODE ONE, I_e (milliamperes)
0
4
8
12
16
20
24
28
32
0
100
200
300
400
500
MAGNETIC FIELD, B (gauss)

Fig. 48

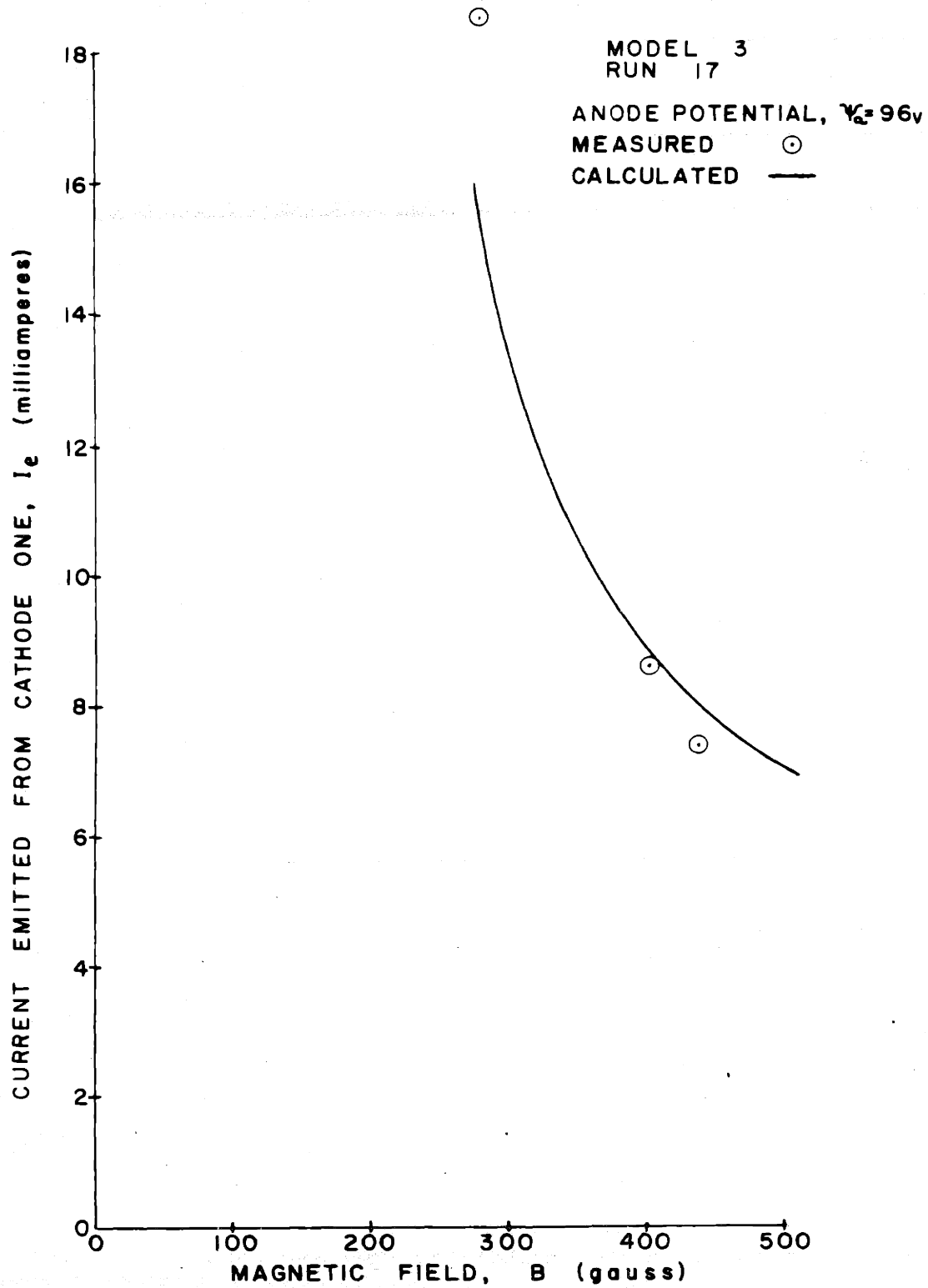
MODEL 3
RUN 17
ANODE POTENTIAL, V_a = 96v
MEASURED ⊙
CALCULATED —
CURRENT EMITTED FROM CATHODE ONE, I_e (milliamperes)
0
2
4
6
8
10
12
14
16
18
0
100
200
300
400
500
MAGNETIC FIELD, B (gauss)

Fig. 49

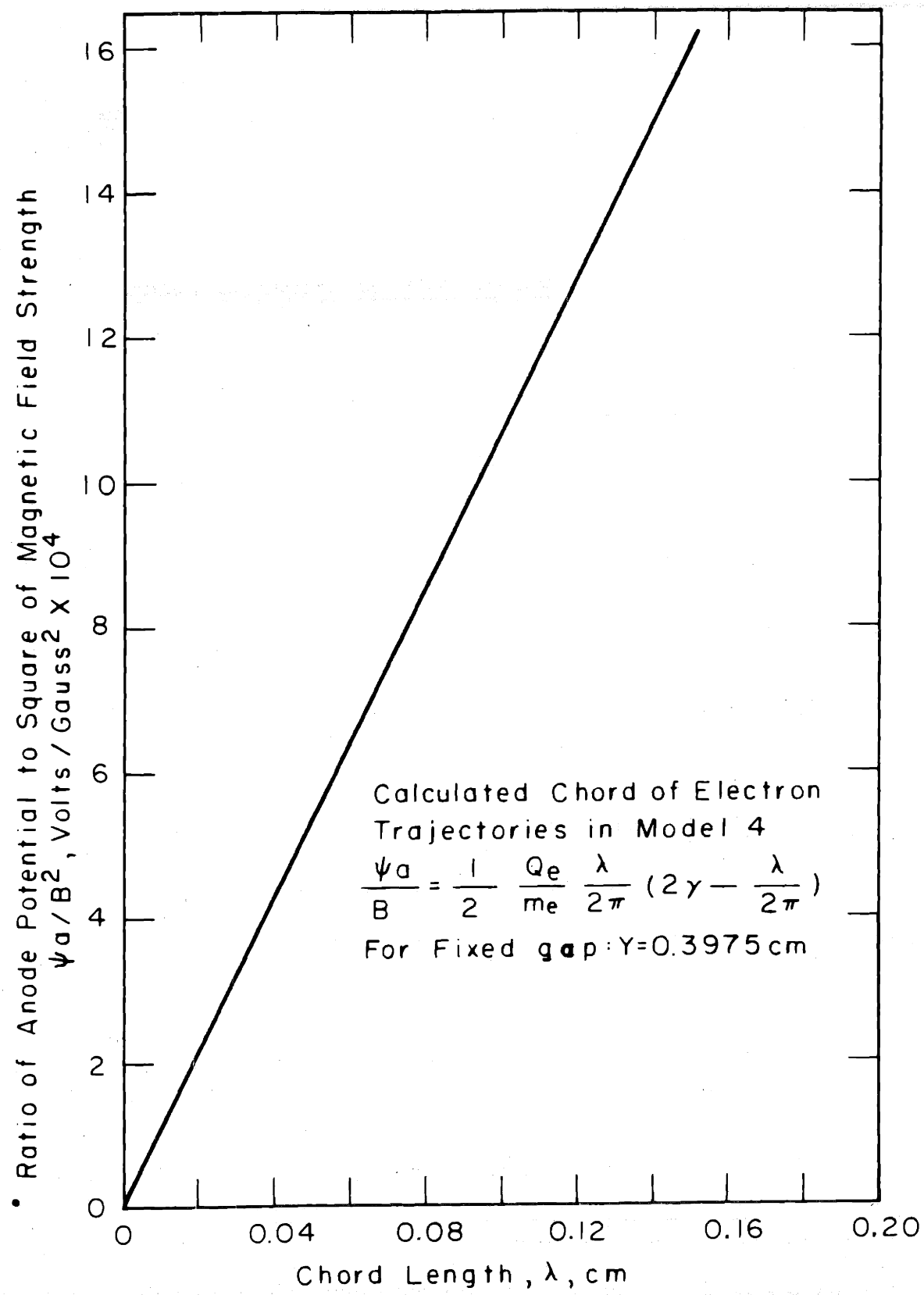
Ratio of Anode Potential to Square of Magnetic Field Strength
ψa/B², Volts/Gauss² X 10⁴
0
2
4
6
8
10
12
14
16
0
0.04
0.08
0.12
0.16
0.20
Chord Length, λ, cm
Calculated Chord of Electron Trajectories in Model 4
ψa/B = 1/2 Qe/me λ/2π (2γ − λ/2π)
For Fixed gap: Y=0.3975 cm

Fig. 50

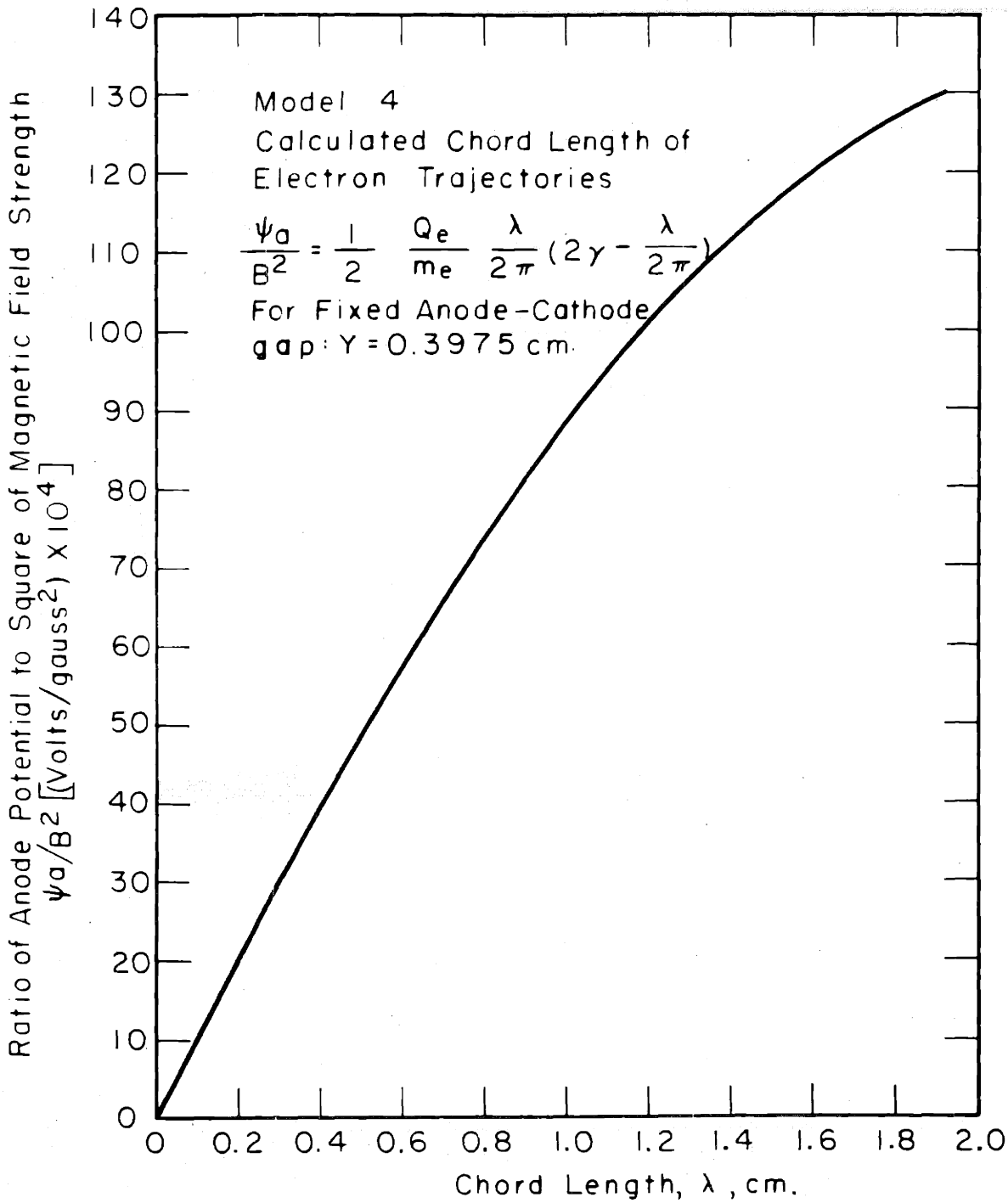
Model 4
Calculated Chord Length of
Electron Trajectories
$\frac{\psi_a}{B^2} = \frac{1}{2} \frac{Q_e}{m_e} \frac{\lambda}{2\pi}(2\gamma - \frac{\lambda}{2\pi})$
For Fixed Anode-Cathode
gap: Y = 0.3975 cm.
Ratio of Anode Potential to Square of Magnetic Field Strength
ψ_a/B^2 [(Volts/gauss^2) X 10^4]
Chord Length, λ, cm.
0
10
20
30
40
50
60
70
80
90
100
110
120
130
140
0
0.2
0.4
0.6
0.8
1.0
1.2
1.4
1.6
1.8
2.0

Fig.51

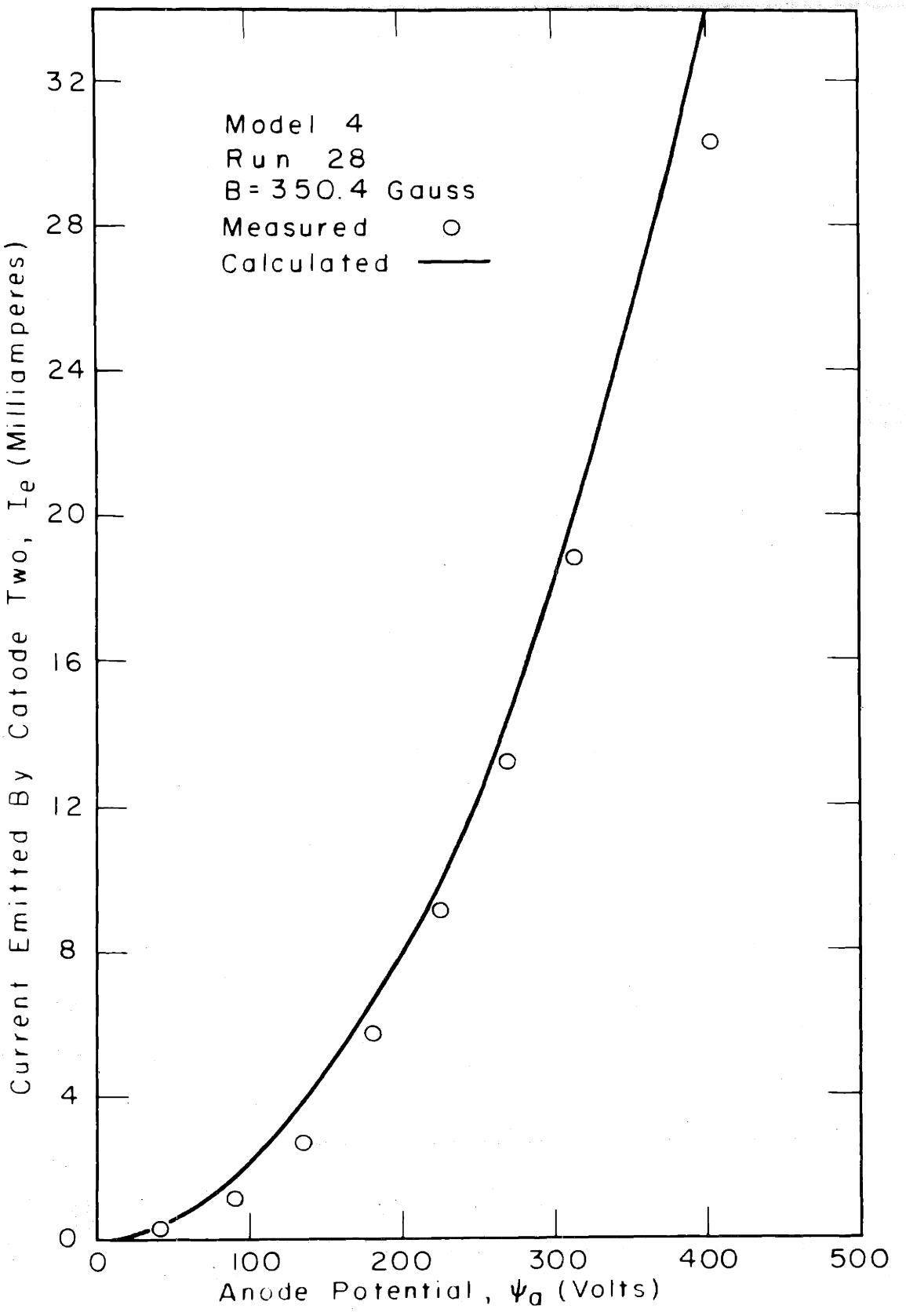
Model 4
Run 28
B = 350.4 Gauss
Measured
Calculated
Current Emitted By Catode Two, I_e (Milliamperes)
Anode Potential, ψ_a (Volts)
0
4
8
12
16
20
24
28
32
0
100
200
300
400
500

Fig. 52

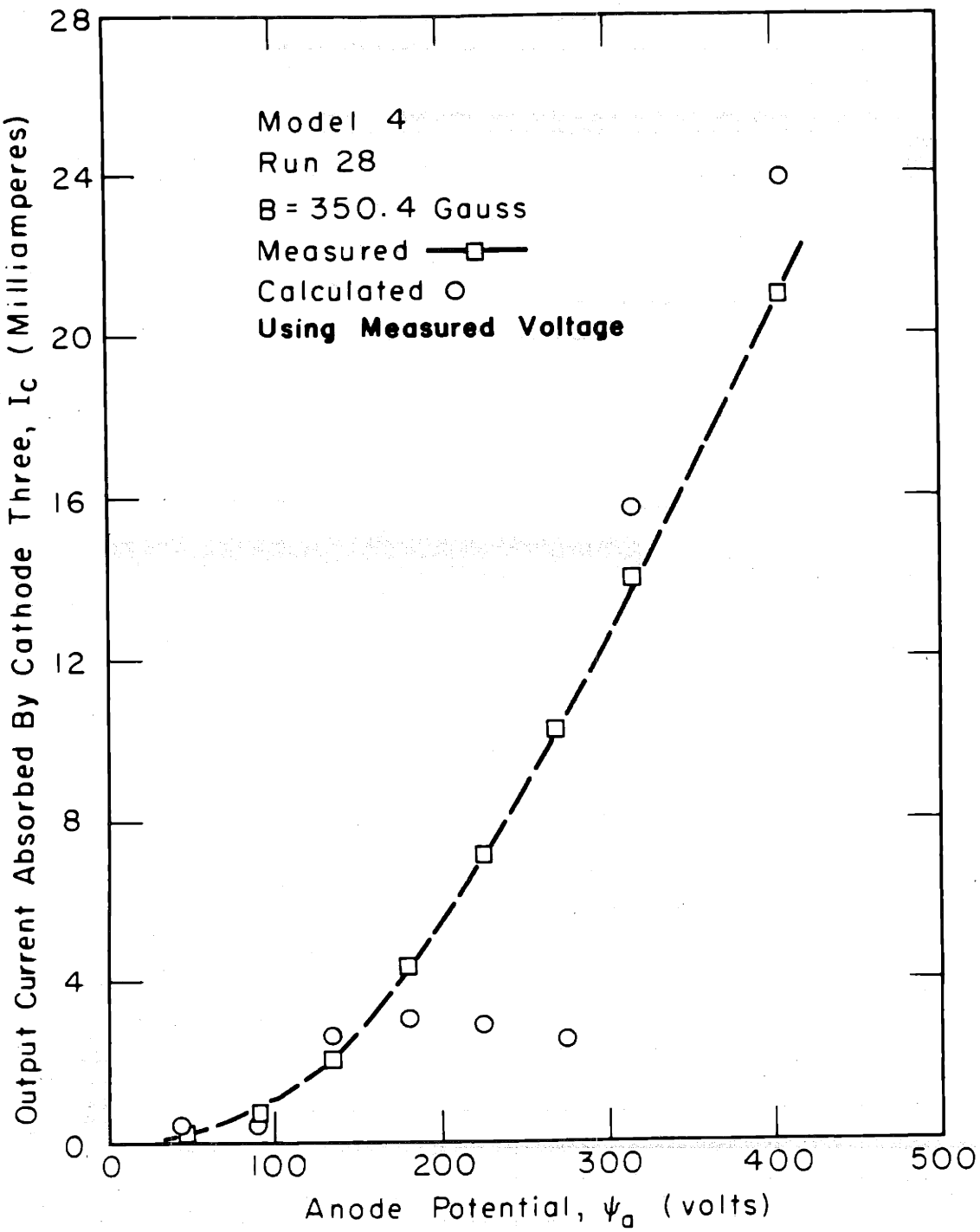
Model 4
Run 28
B = 350.4 Gauss
Measured
Calculated O
Using Measured Voltage
Output Current Absorbed By Cathode Three, I_c (Milliamperes)
Anode Potential, ψ_a (volts)
0
4
8
12
16
20
24
28
0
100
200
300
400
500

Fig. 53

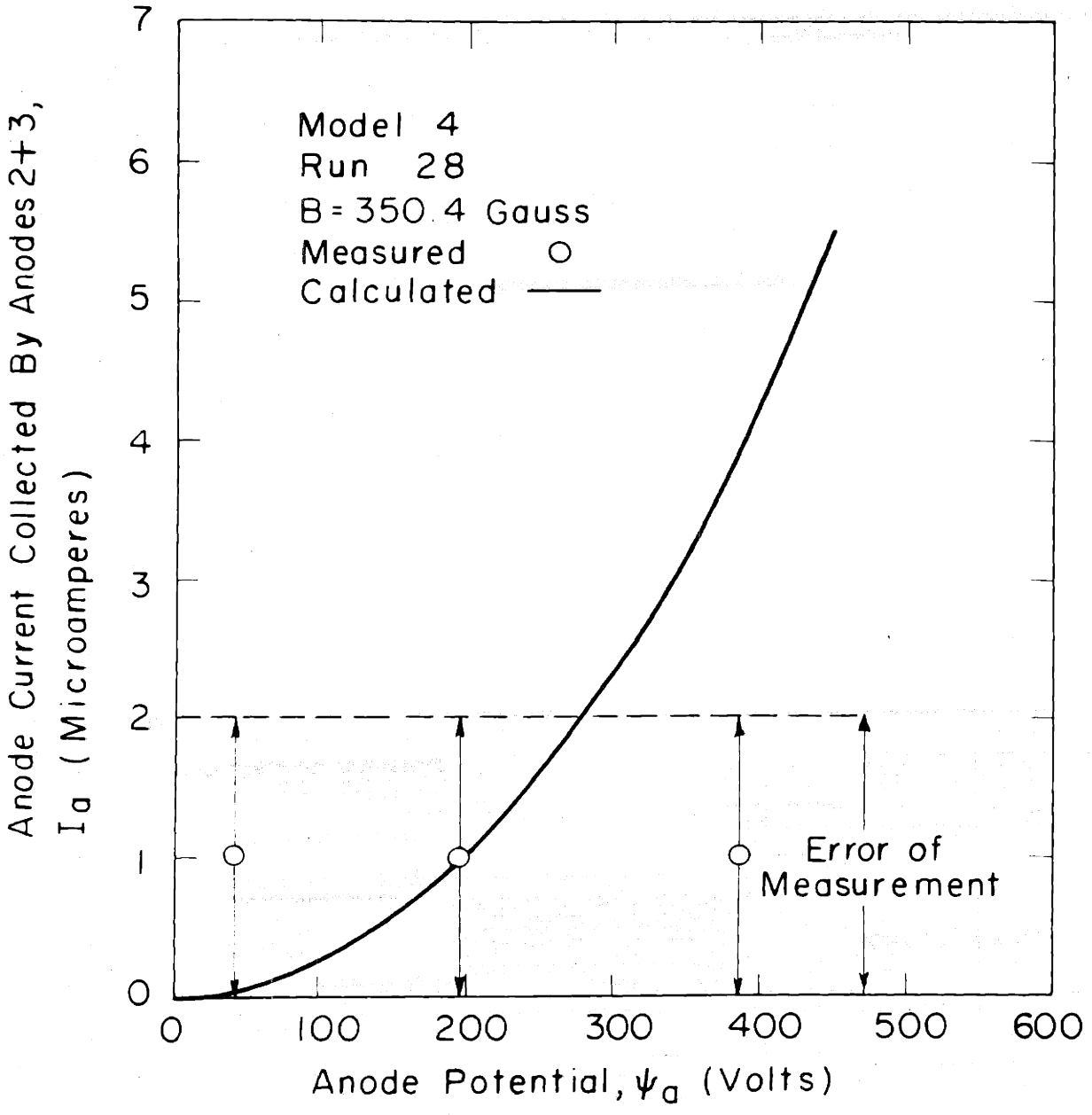
Model 4
Run 28
B = 350.4 Gauss
Measured O
Calculated
Error of Measurement
Anode Current Collected By Anodes 2+3, Ia (Microamperes)
Anode Potential, ψa (Volts)
0
1
2
3
4
5
6
7
0
100
200
300
400
500
600

Fig. 54

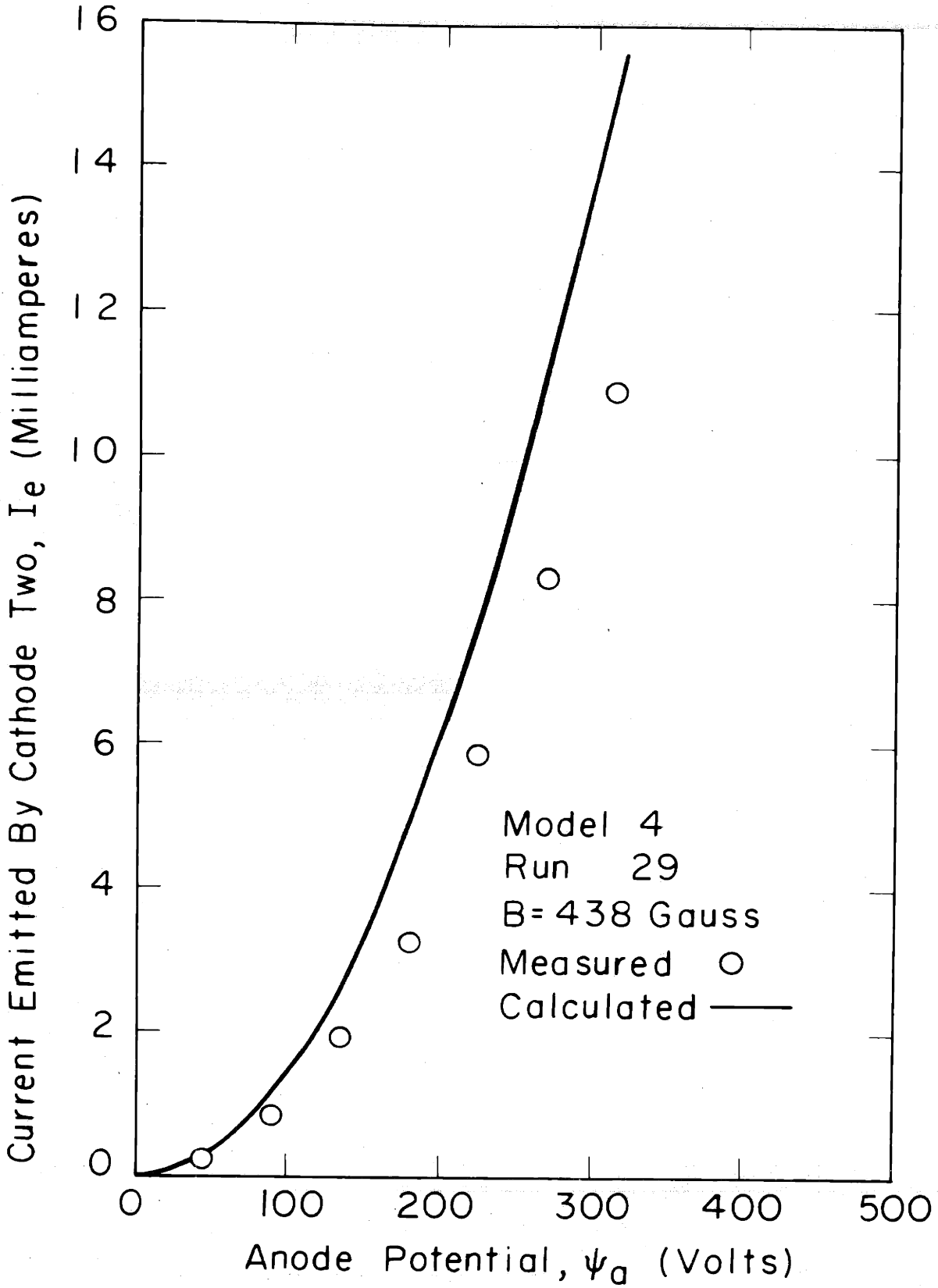
Current Emitted By Cathode Two, I_e (Milliamperes)
0
2
4
6
8
10
12
14
16
0
100
200
300
400
500
Anode Potential, ψ_a (Volts)
Model 4
Run 29
B = 438 Gauss
Measured O
Calculated ——

Fig.55

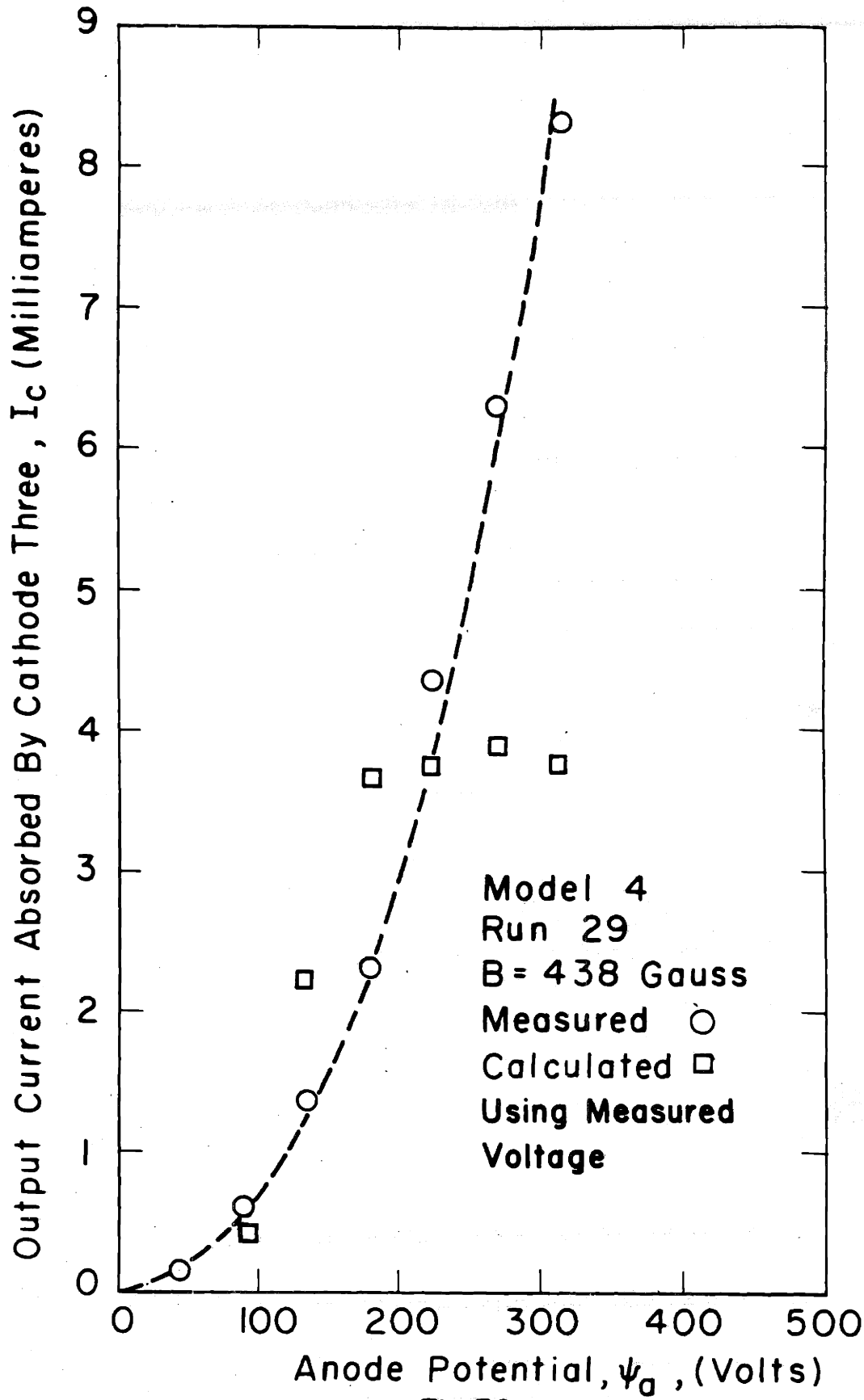
Output Current Absorbed By Cathode Three , I_c (Milliamperes)
Anode Potential, ψ_a , (Volts)
0
1
2
3
4
5
6
7
8
9
0
100
200
300
400
500
Model 4
Run 29
B = 438 Gauss
Measured
Calculated
Using Measured
Voltage

Fig.56

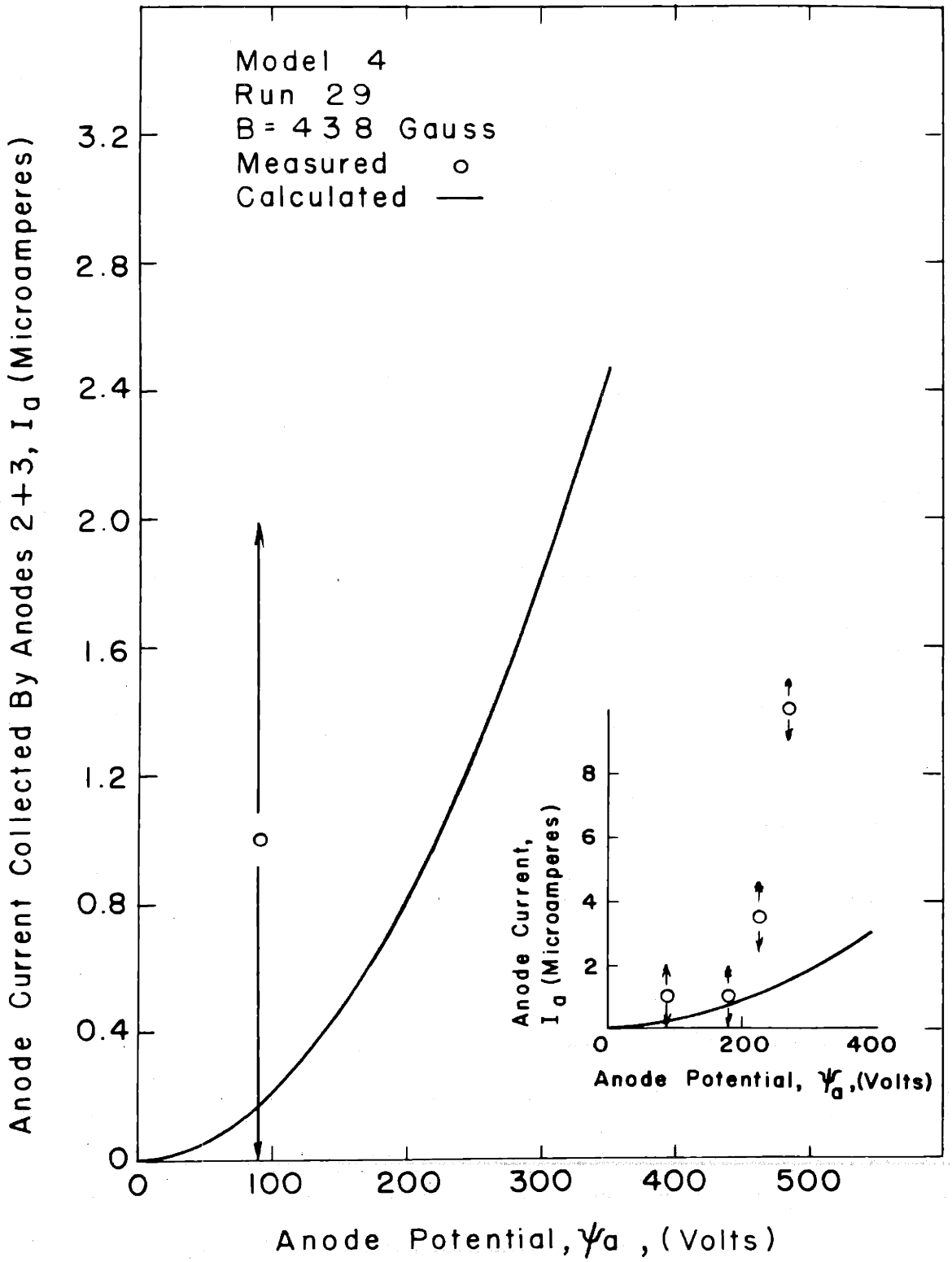
Model 4
Run 29
B = 438 Gauss
Measured o
Calculated —
Anode Current Collected By Anodes 2+3, I_a (Microamperes)
3.2
2.8
2.4
2.0
1.6
1.2
0.8
0.4
0
0
100
200
300
400
500
Anode Potential, ψ_a, (Volts)
Anode Current, I_a (Microamperes)
8
6
4
2
0
200
400
Anode Potential, ψ_a, (Volts)

Fig. 57

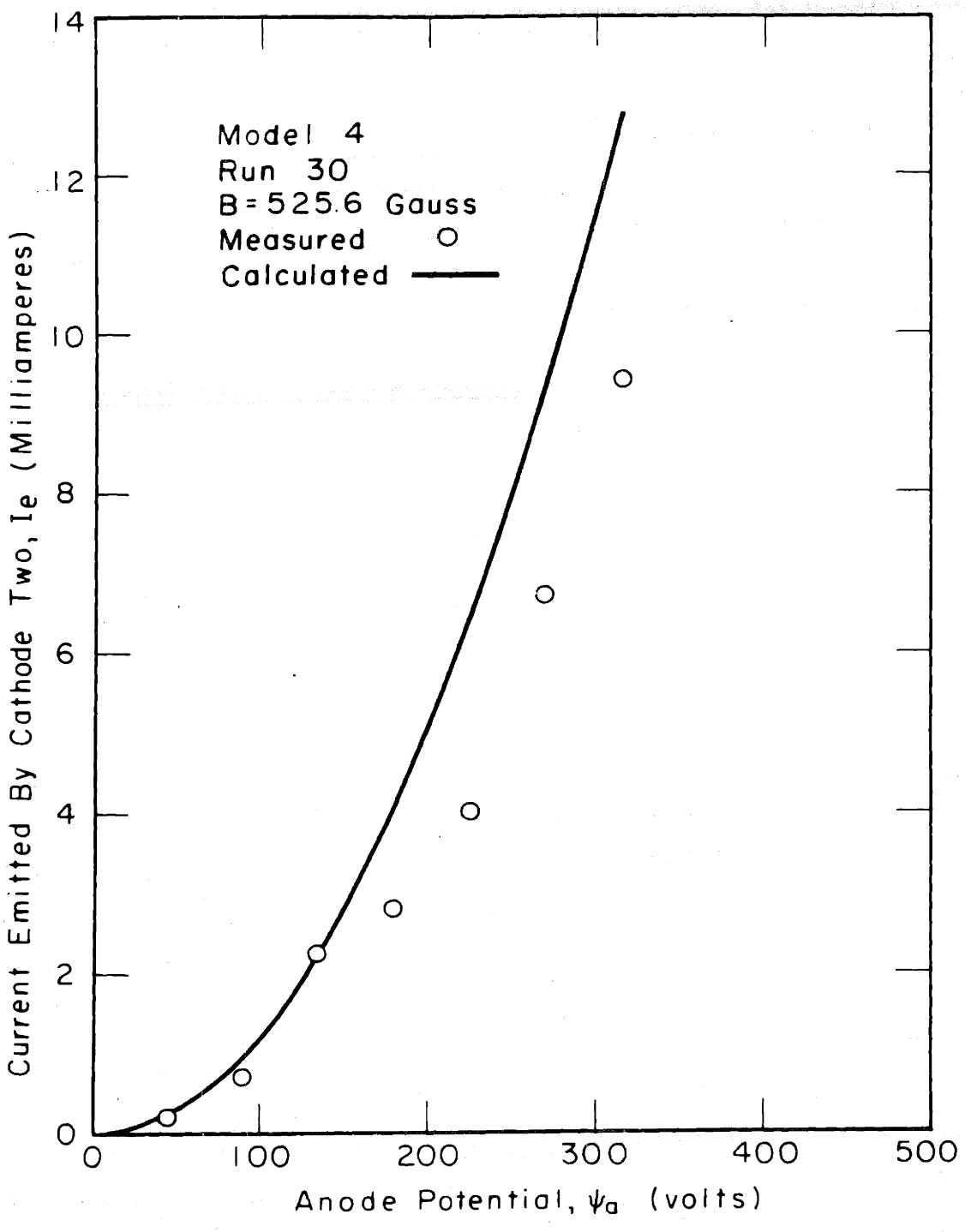
Model 4
Run 30
B = 525.6 Gauss
Measured
Calculated
Current Emitted By Cathode Two, Ie (Milliamperes)
Anode Potential, ψa (volts)
0
2
4
6
8
10
12
14
0
100
200
300
400
500

Fig. 58

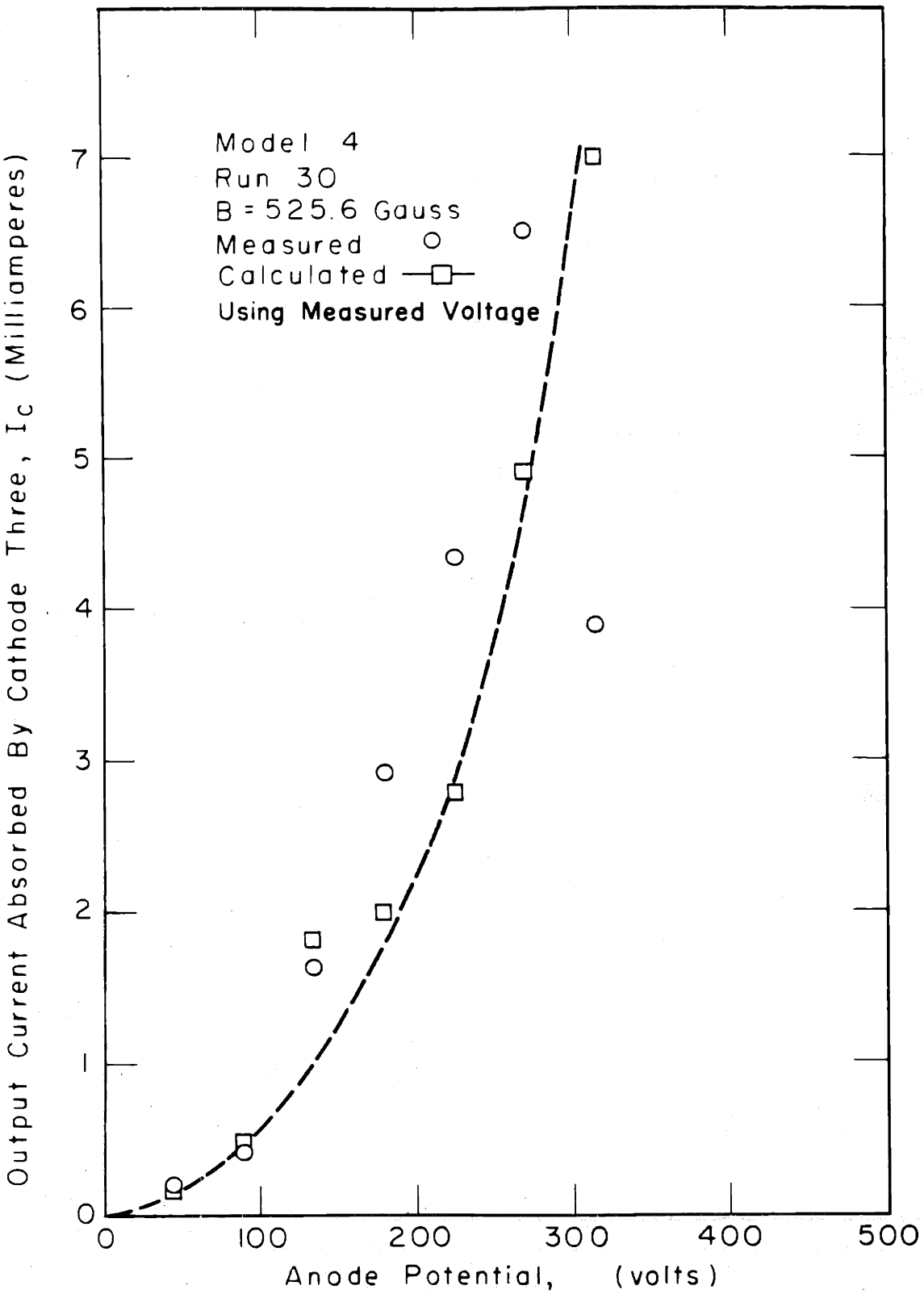
Model 4
Run 30
B = 525.6 Gauss
Measured
Calculated
Using Measured Voltage
Output Current Absorbed By Cathode Three, I_c (Milliamperes)
0
1
2
3
4
5
6
7
0
100
200
300
400
500
Anode Potential, (volts)

Fig. 59

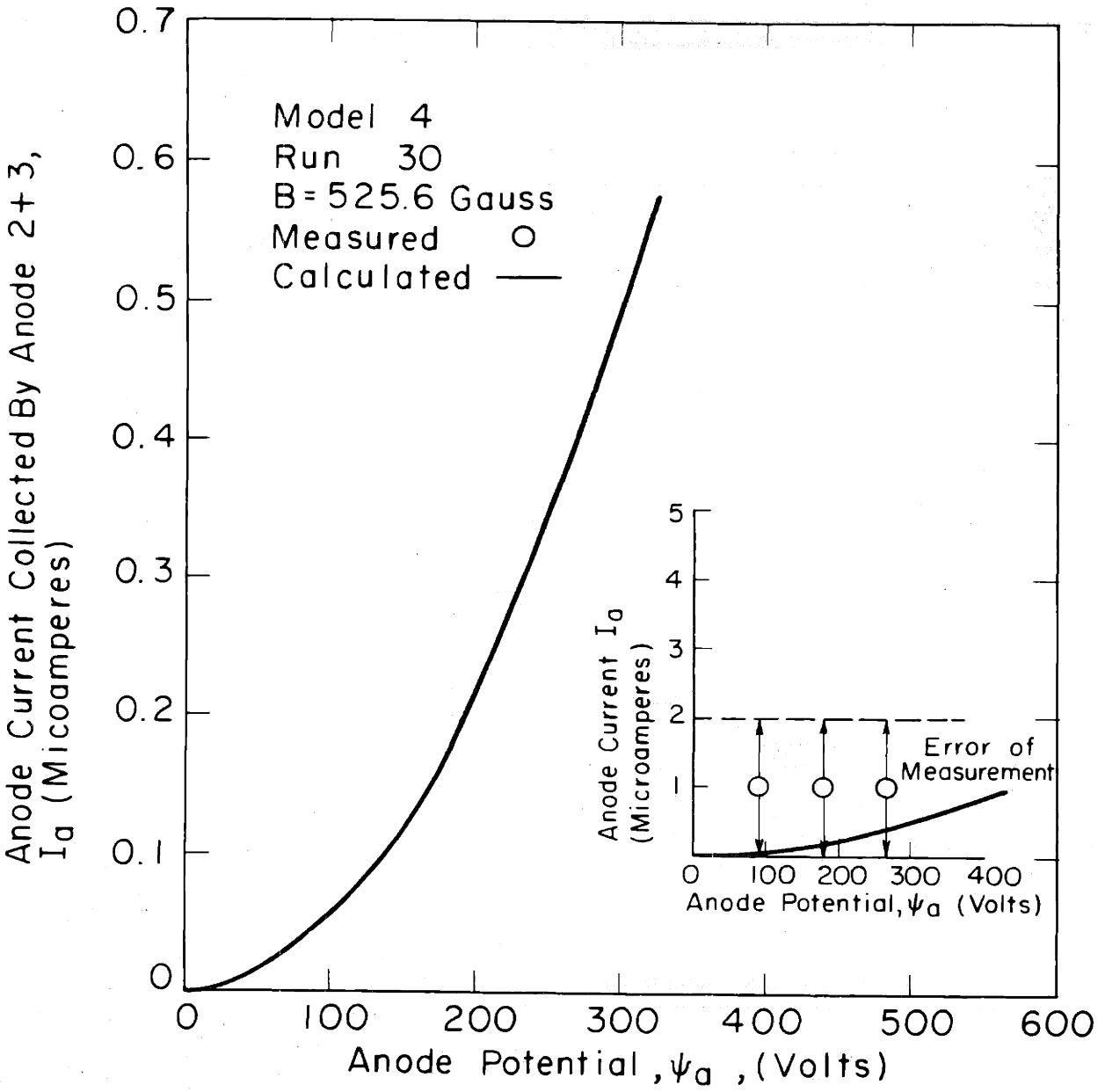
Model 4
Run 30
B = 525.6 Gauss
Measured O
Calculated —
Anode Current Collected By Anode 2+3, I_a (Micoamperes)
0.7
0.6
0.5
0.4
0.3
0.2
0.1
0
0 100 200 300 400 500 600
Anode Potential, ψ_a, (Volts)
Anode Current I_a (Microamperes)
5
4
3
2
1
0 100 200 300 400
Anode Potential, ψ_a (Volts)
Error of Measurement

Fig.60

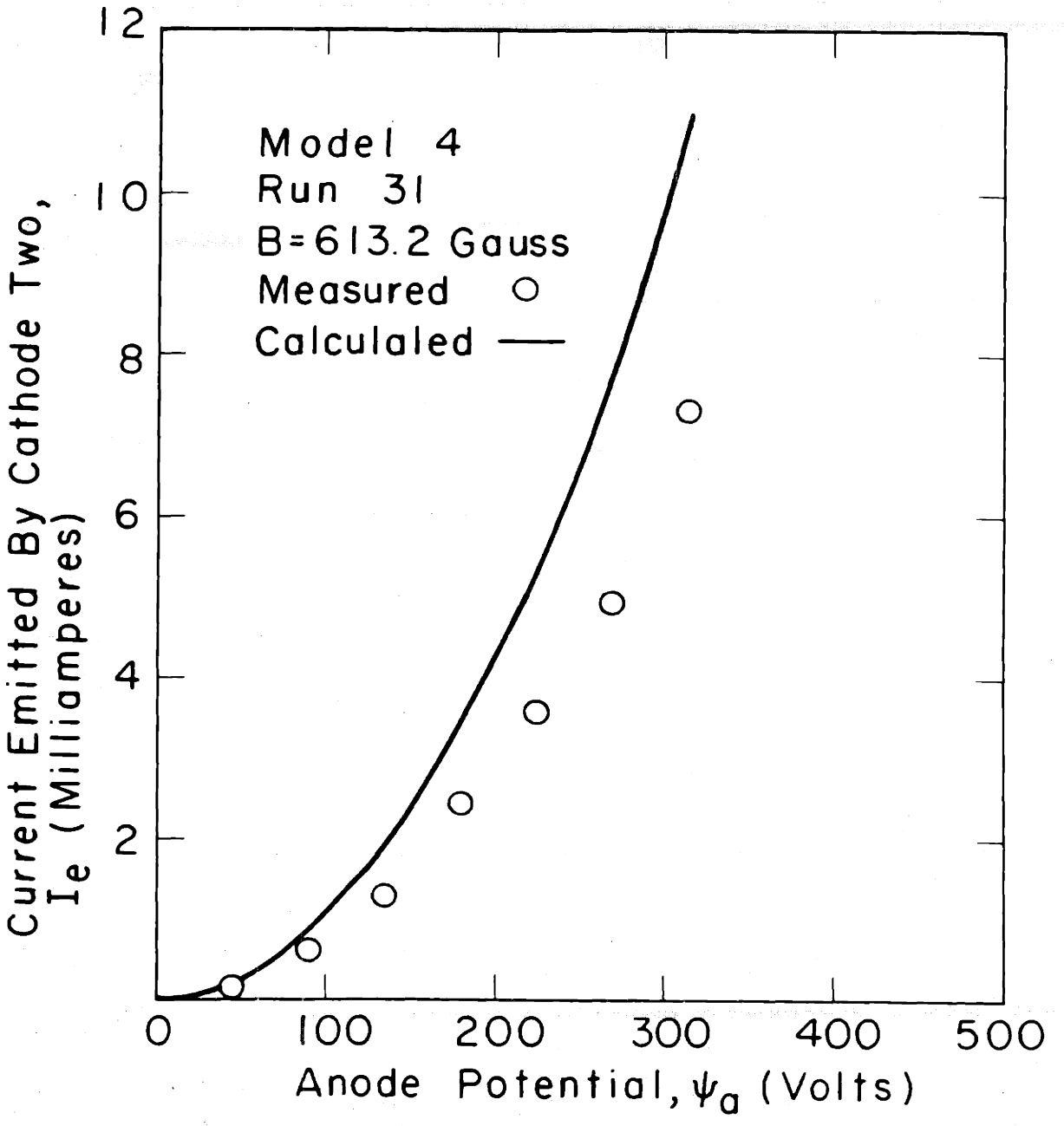
Model 4
Run 31
B=613.2 Gauss
Measured
Calculaled
Current Emitted By Cathode Two, I_e (Milliamperes)
Anode Potential, ψ_a (Volts)
0
100
200
300
400
500
2
4
6
8
10
12

Fig.61

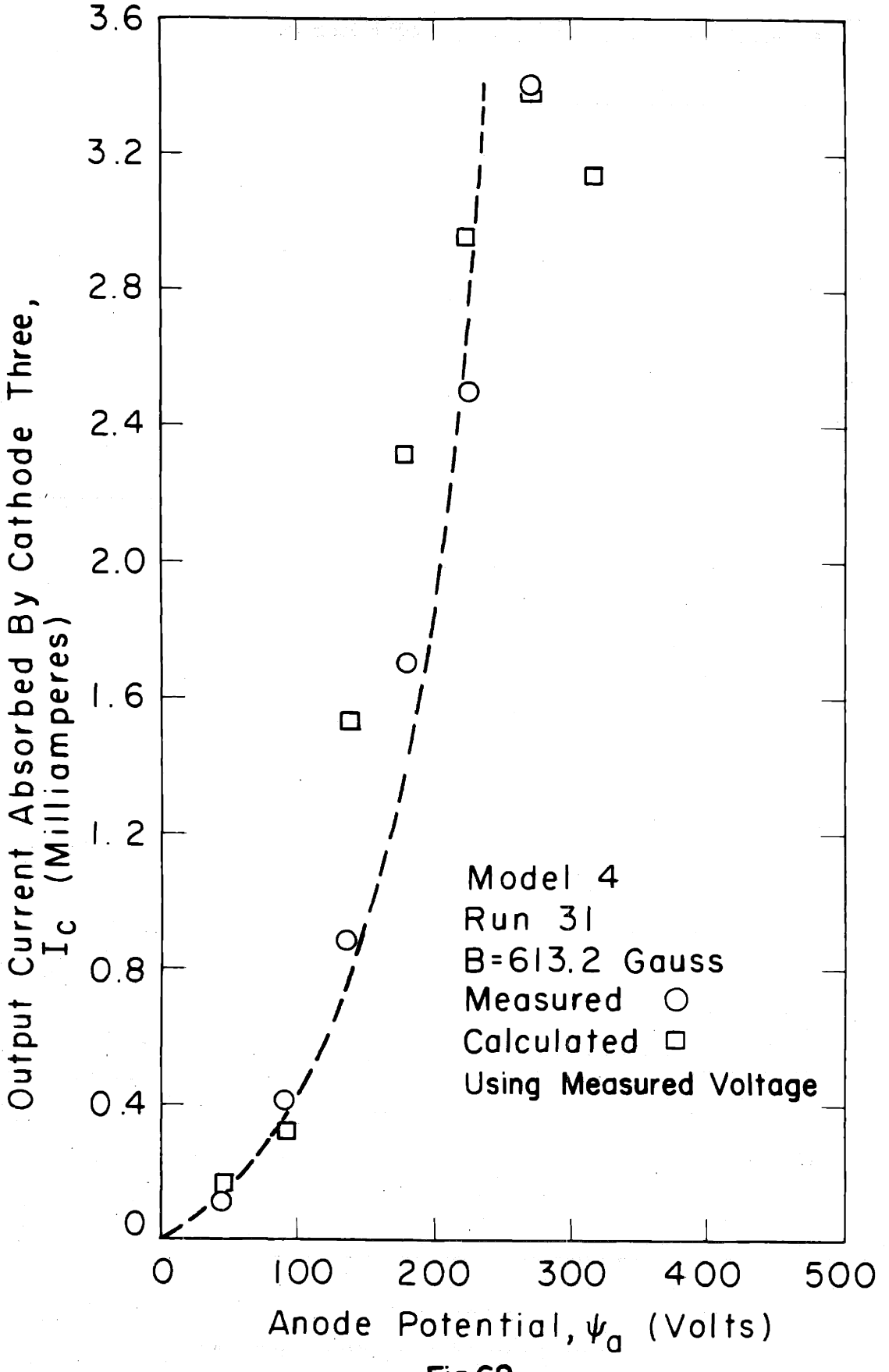
Output Current Absorbed By Cathode Three, I_c (Milliamperes)
3.6
3.2
2.8
2.4
2.0
1.6
1.2
0.8
0.4
0
0
100
200
300
400
500
Anode Potential, ψ_a (Volts)
Model 4
Run 31
B=613.2 Gauss
Measured ○
Calculated □
Using Measured Voltage

Fig.62

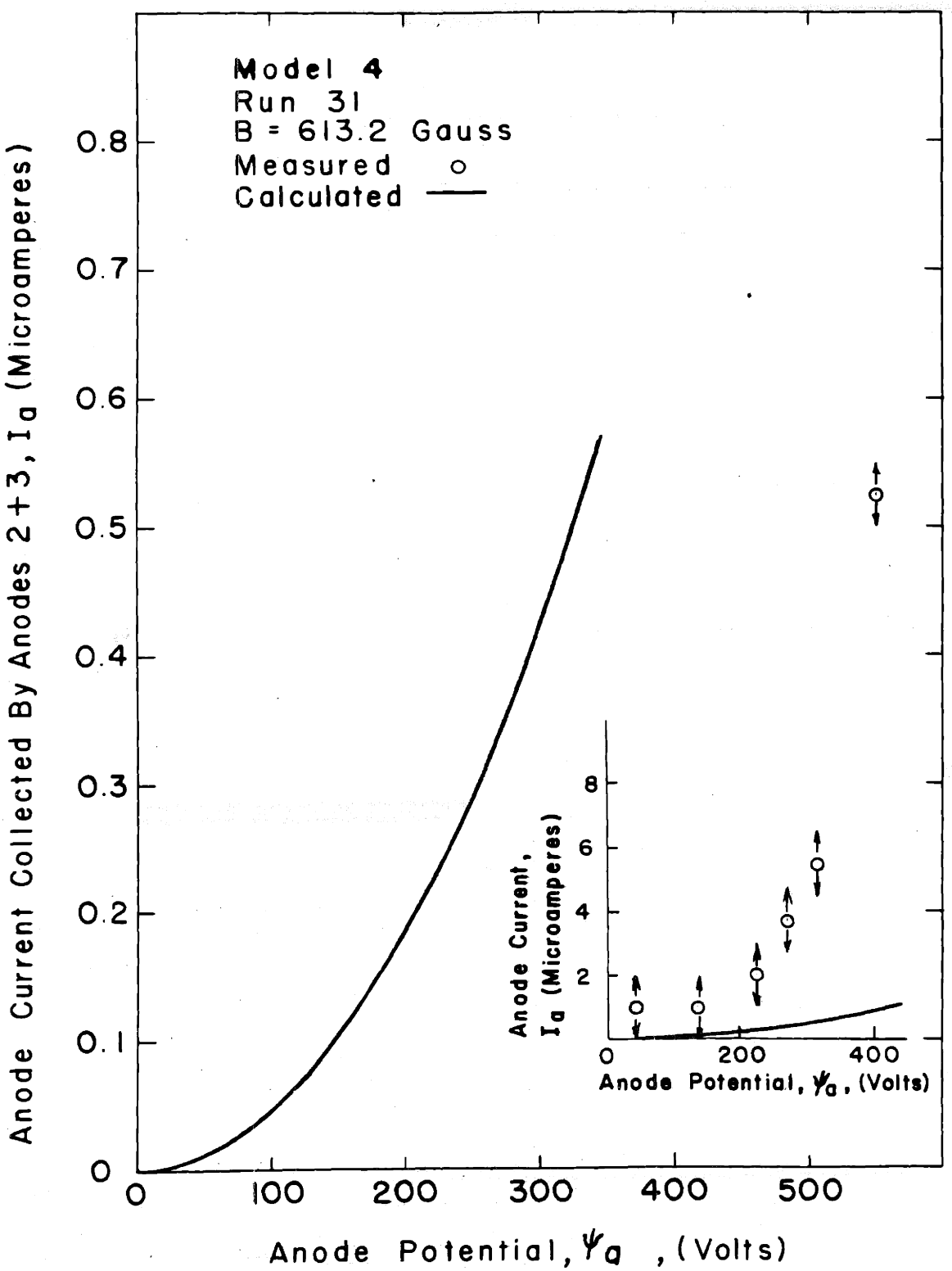
Model 4
Run 31
B = 613.2 Gauss
Measured o
Calculated —
Anode Current Collected By Anodes 2+3, Ia (Microamperes)
0
0.1
0.2
0.3
0.4
0.5
0.6
0.7
0.8
0
100
200
300
400
500
Anode Potential, ψa , (Volts)
Anode Current, Ia (Microamperes)
2
4
6
8
0
200
400
Anode Potential, ψa, (Volts)

Fig.63

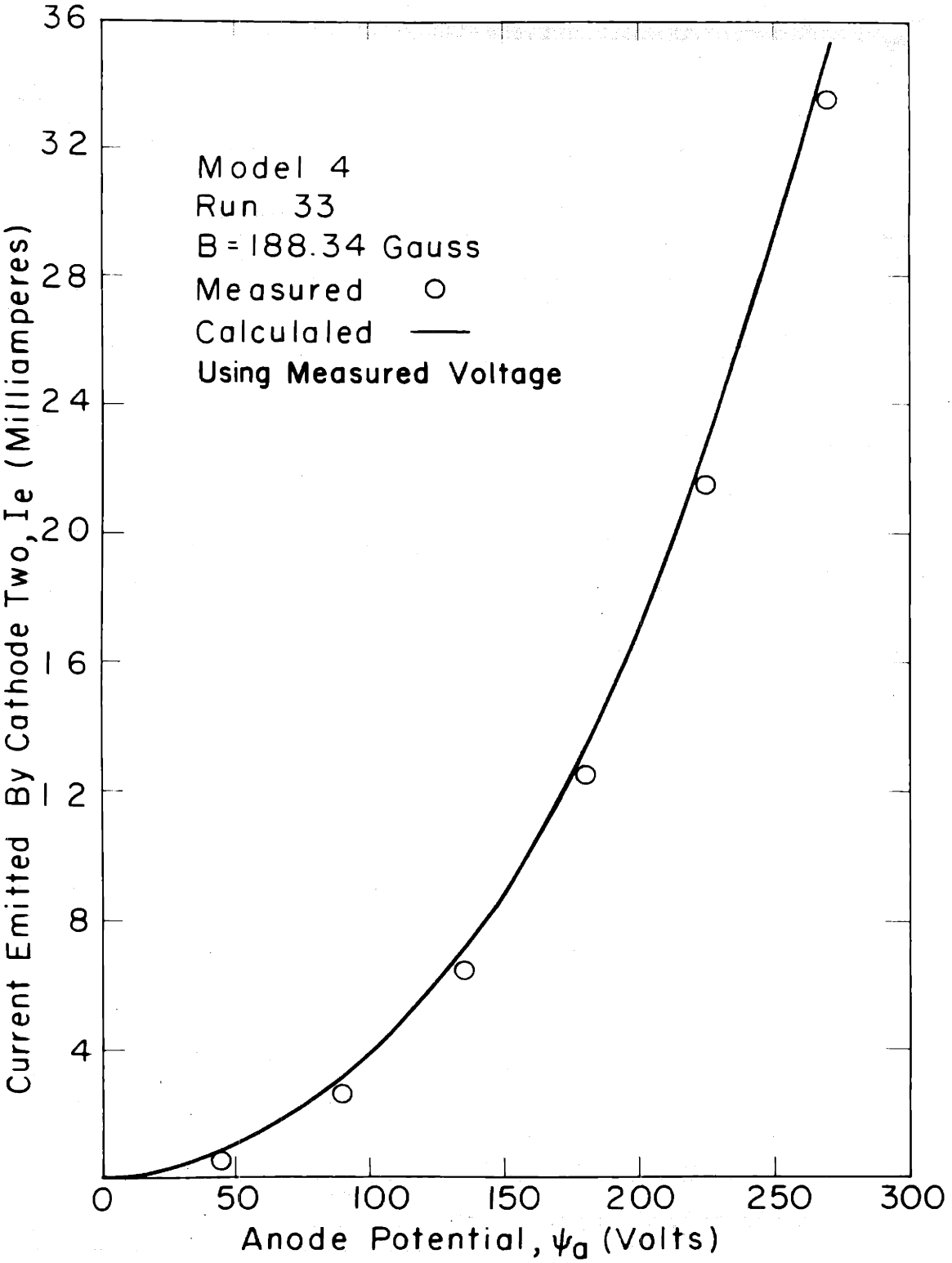
Model 4
Run 33
B = 188.34 Gauss
Measured O
Calculaled —
Using Measured Voltage
Current Emitted By Cathode Two, Ie (Milliamperes)
Anode Potential, ψa (Volts)
0
4
8
12
16
20
24
28
32
36
50
100
150
200
250
300

Fig.64

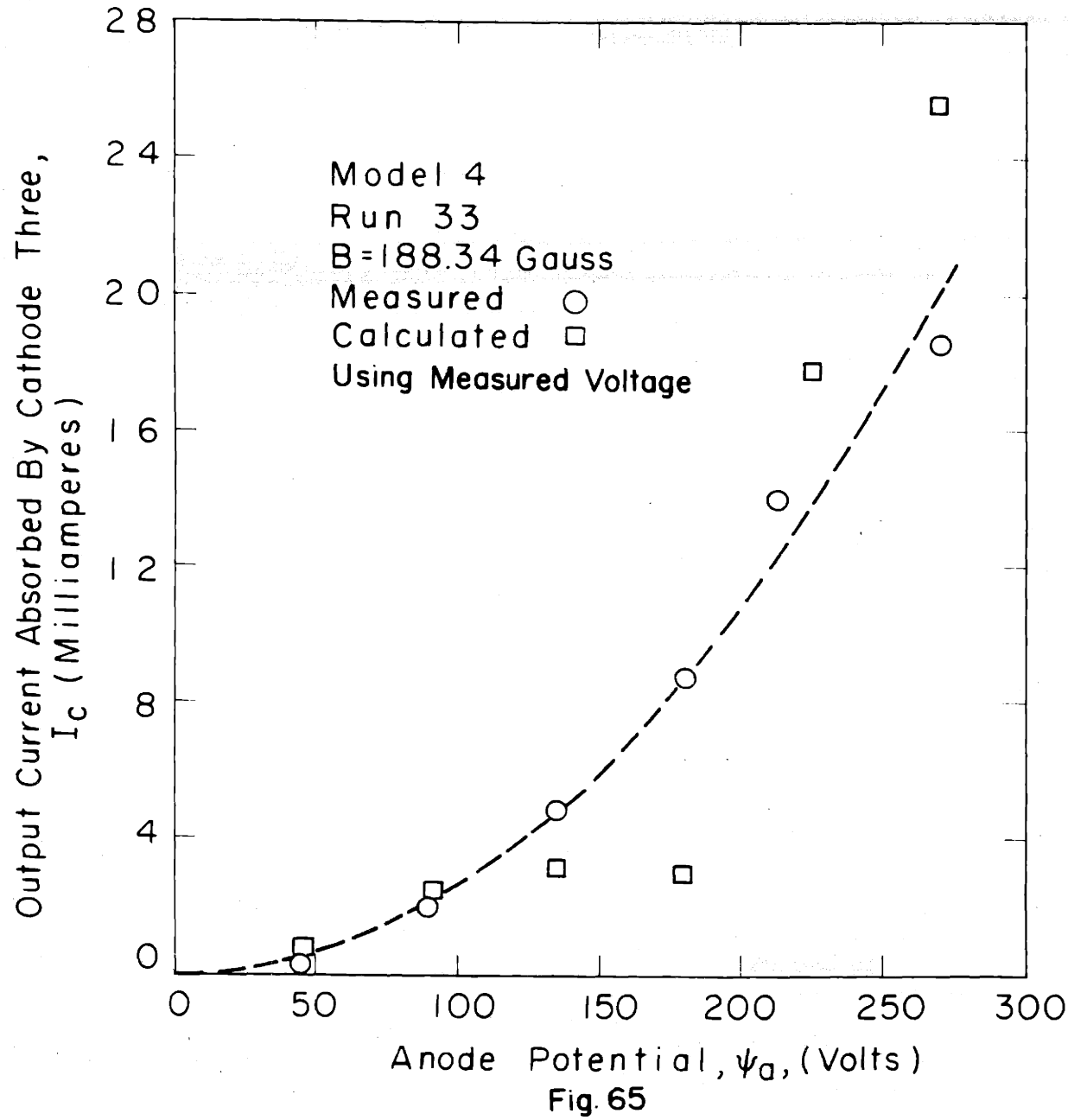
Model 4
Run 33
B=188.34 Gauss
Measured ○
Calculated □
Using Measured Voltage
Output Current Absorbed By Cathode Three, I_c (Milliamperes)
Anode Potential, ψ_a, (Volts)
0
4
8
12
16
20
24
28
0
50
100
150
200
250
300

Fig. 65

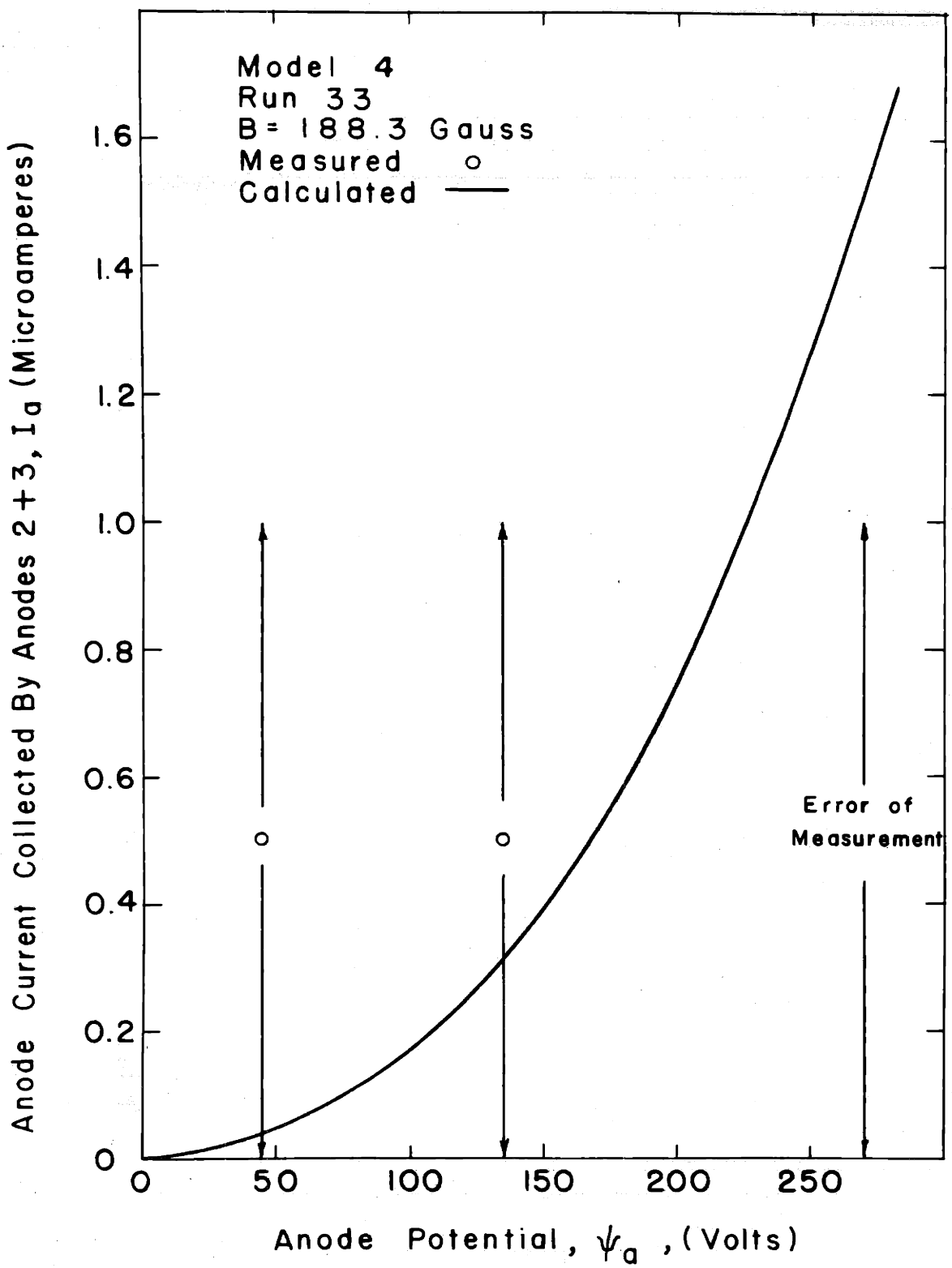
Model 4
Run 33
B = 188.3 Gauss
Measured o
Calculated —
Error of Measurement
Anode Current Collected By Anodes 2+3, Ia (Microamperes)
Anode Potential, ψa, (Volts)
0
0.2
0.4
0.6
0.8
1.0
1.2
1.4
1.6
0
50
100
150
200
250

Fig. 66

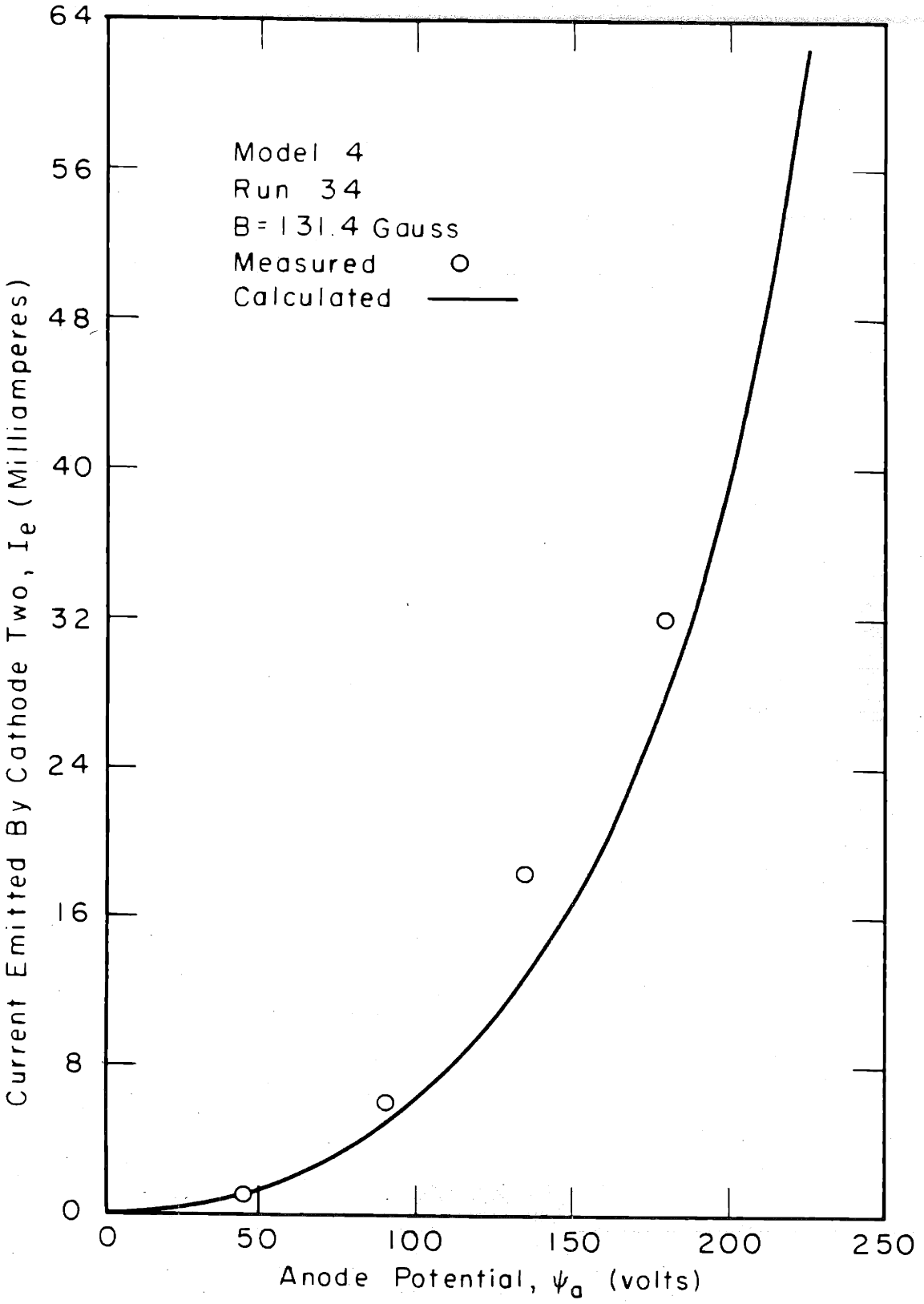
Model 4
Run 34
B = 131.4 Gauss
Measured
Calculated
Current Emitted By Cathode Two, I_e (Milliamperes)
Anode Potential, ψ_a (volts)
0
8
16
24
32
40
48
56
64
0
50
100
150
200
250

Fig. 67

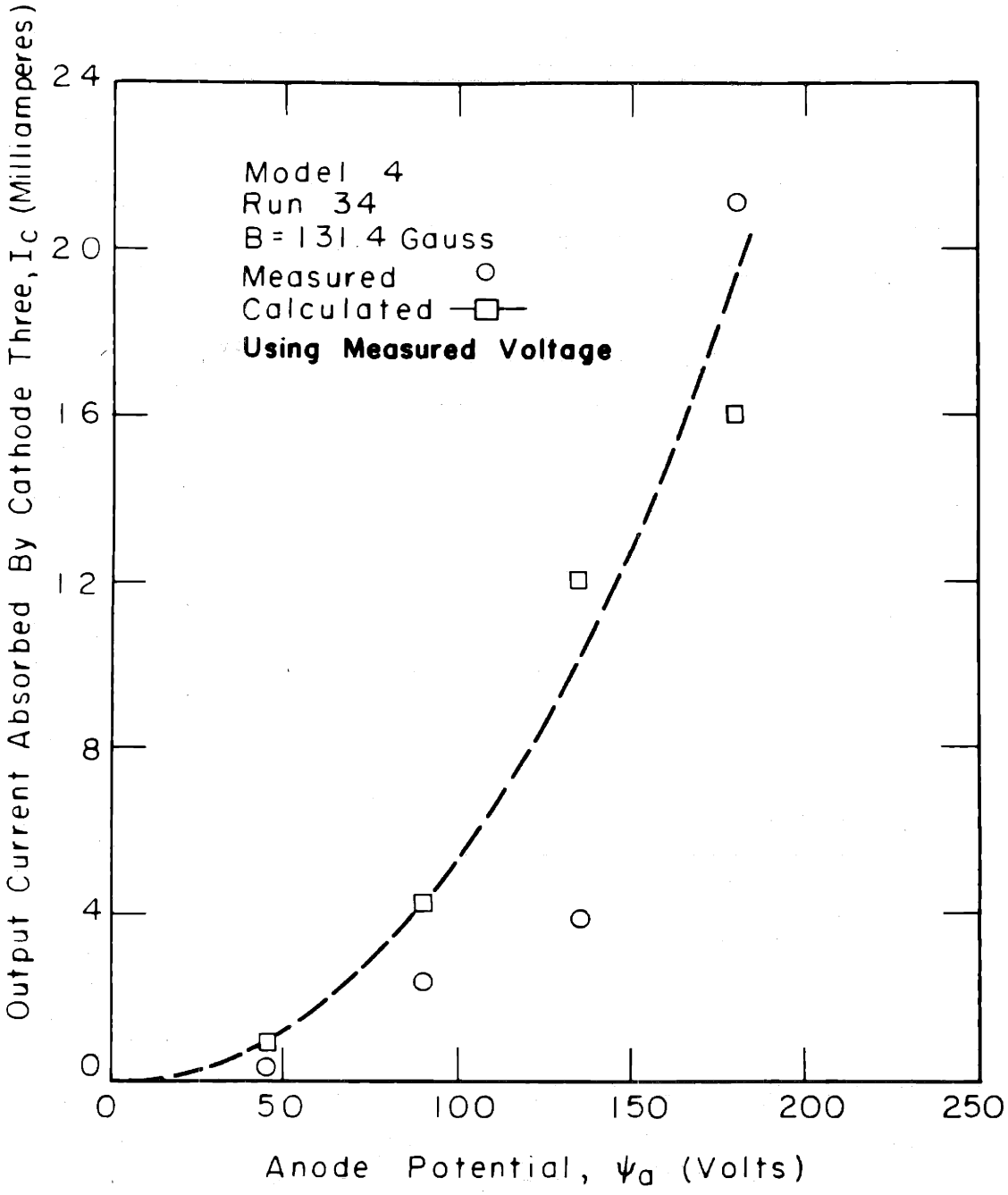
Model 4
Run 34
B = 131.4 Gauss
Measured
Calculated
Using Measured Voltage
Output Current Absorbed By Cathode Three, I_c (Milliamperes)
0
4
8
12
16
20
24
0
50
100
150
200
250
Anode Potential, ψ_a (Volts)

Fig. 68

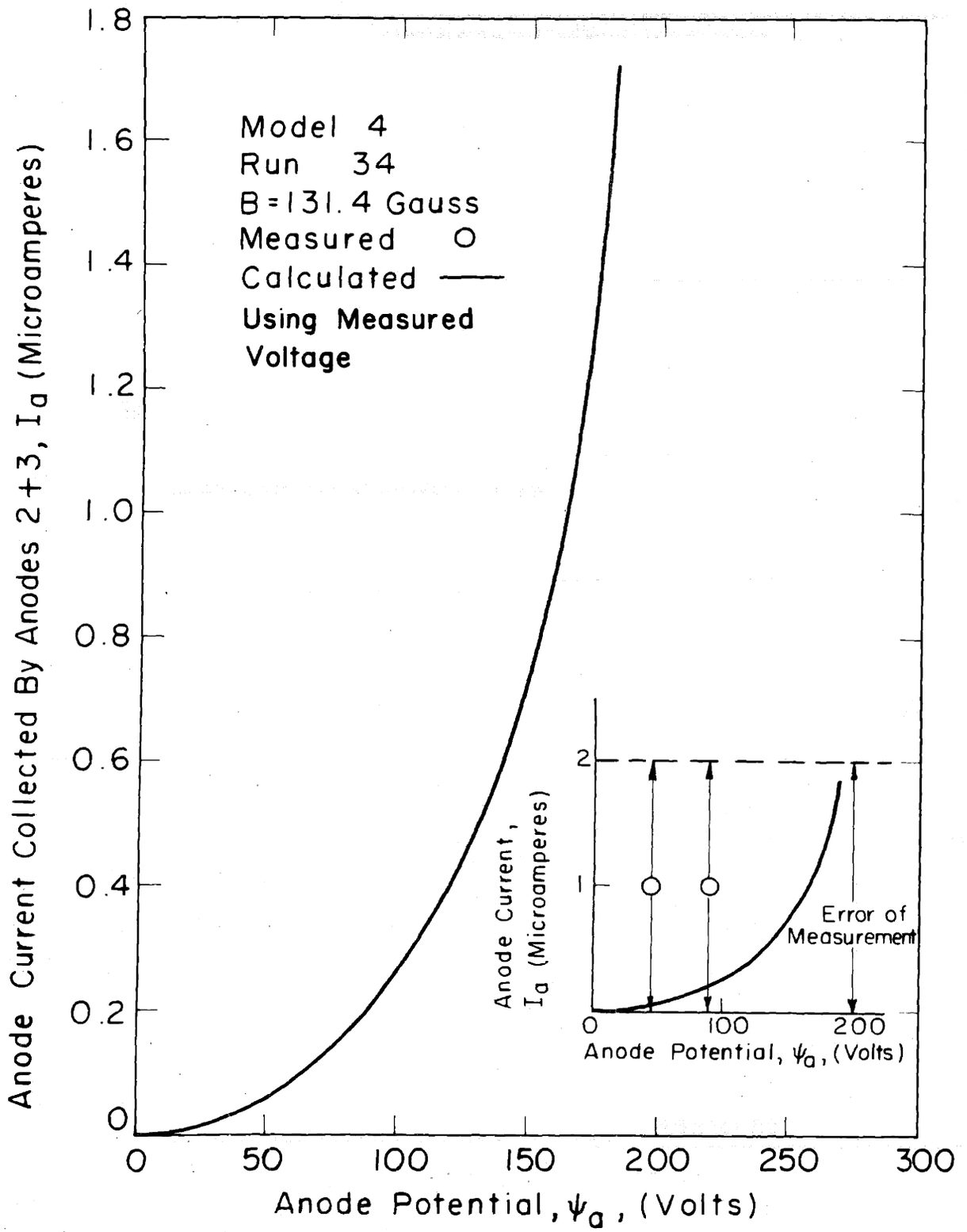
Model 4
Run 34
B = 131.4 Gauss
Measured O
Calculated —
Using Measured
Voltage
Anode Current Collected By Anodes 2+3, I_a (Microamperes)
Anode Potential, ψ_a, (Volts)
0
0.2
0.4
0.6
0.8
1.0
1.2
1.4
1.6
1.8
0
50
100
150
200
250
300
Anode Current, I_a (Microamperes)
Error of Measurement
Anode Potential, ψ_a, (Volts)
1
2
100
200

Fig. 69

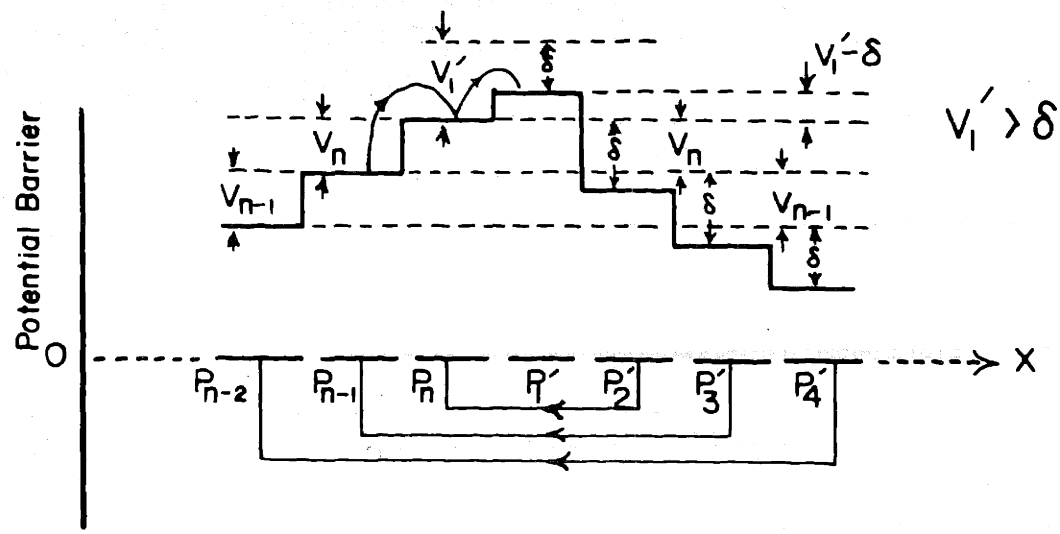
Potential Barrier
0
X
V_1'
$V_1'-\delta$
$V_1' > \delta$
V_n
V_{n-1}
δ
P_{n-2}
P_{n-1}
P_n
P_1'
P_2'
P_3'
P_4'

Fig. 71

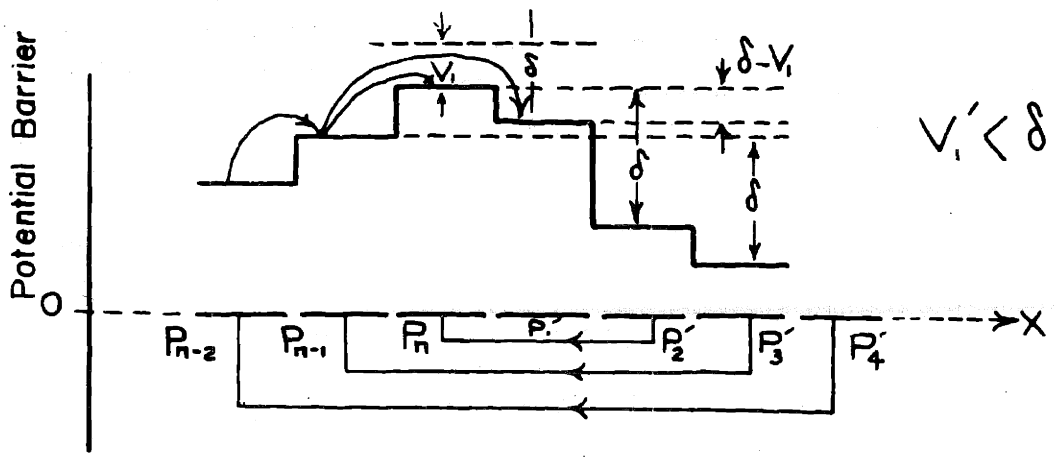
Potential Barrier
0
X
V_1
δ
$\delta-V_1$
$V_1' < \delta$
P_{n-2}
P_{n-1}
P_n
P_1'
P_2'
P_3'
P_4'

Fig. 72

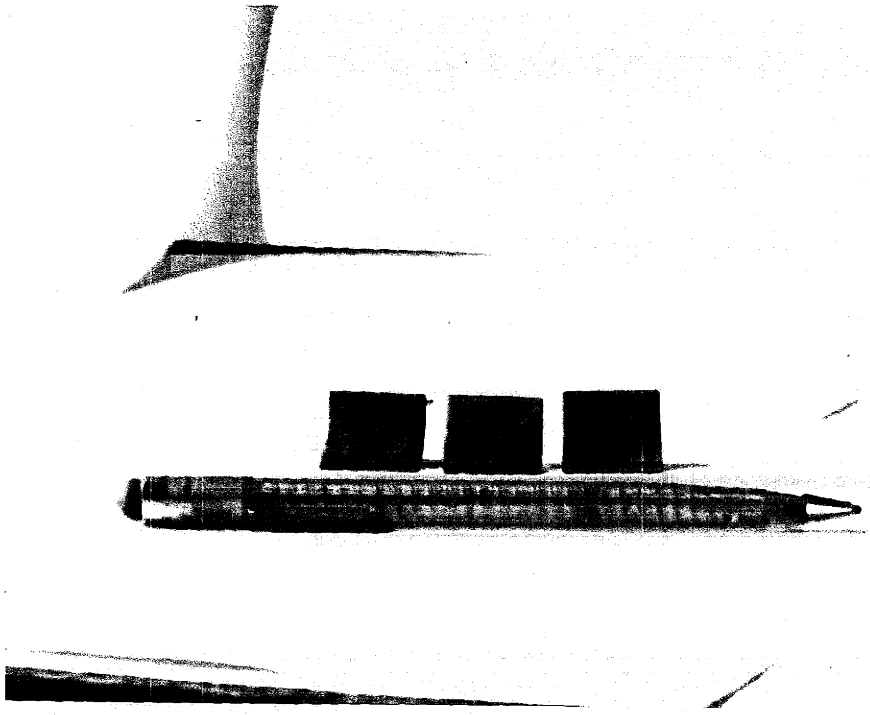

FIGURE 70 - ANODES MODEL 5 AFTER SHORTENING

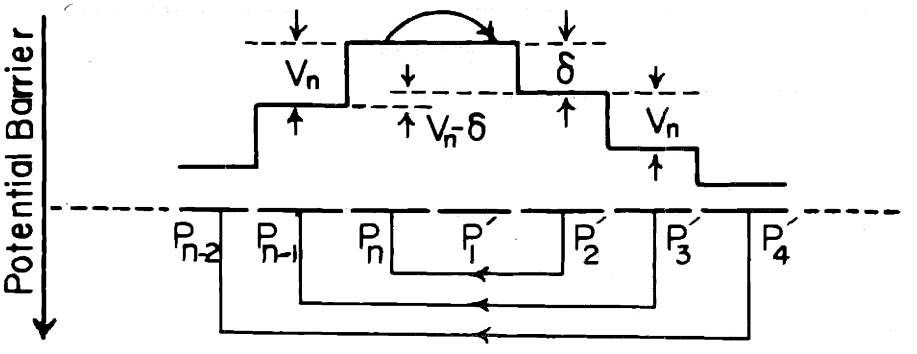

Figure 73

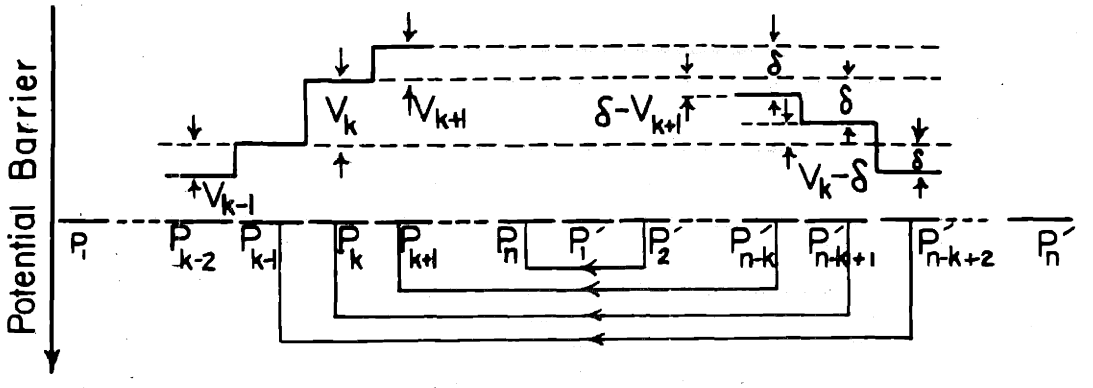

Figure 74

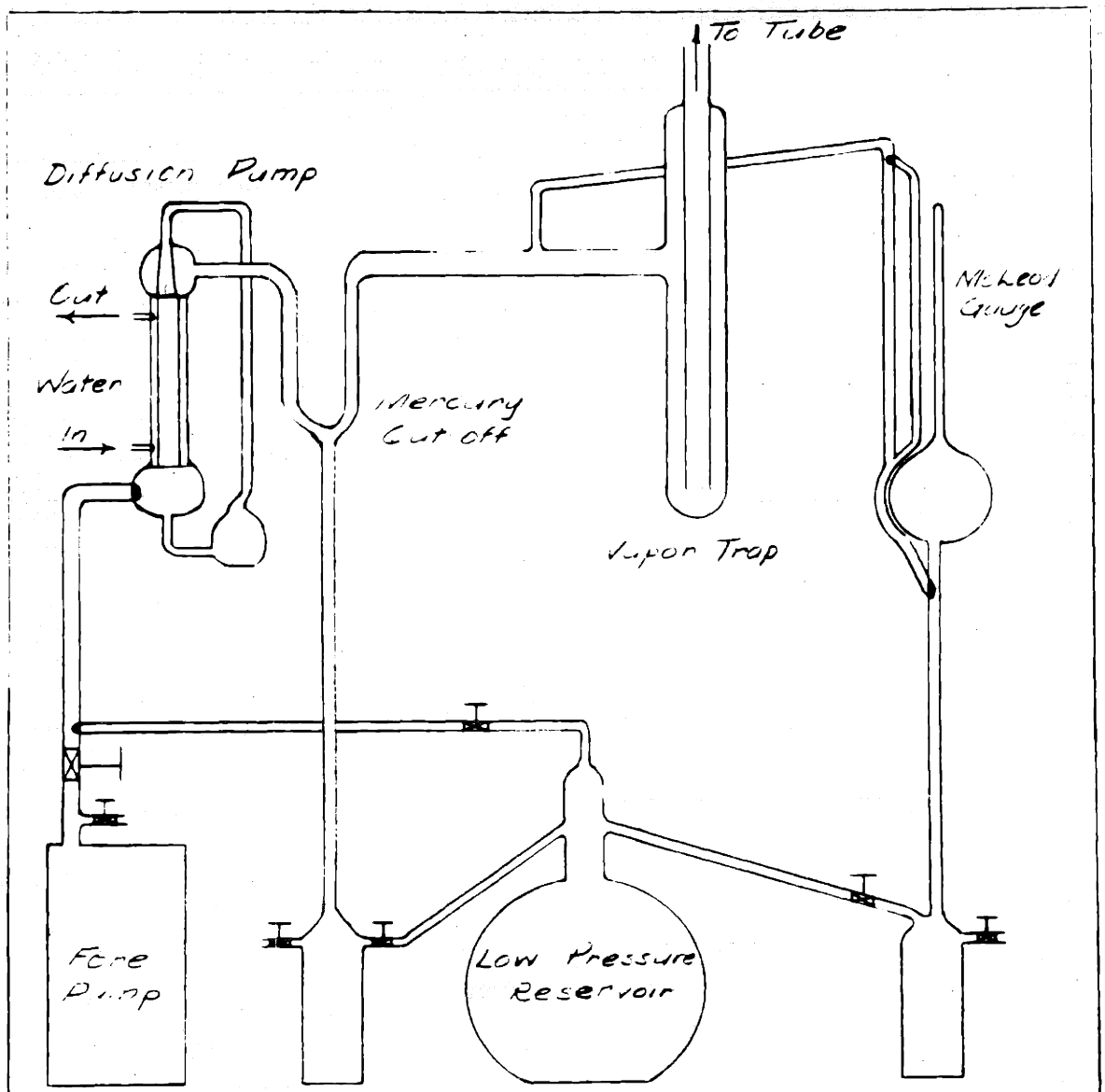

Fig. 76, Schematic Representation of Vacuum System

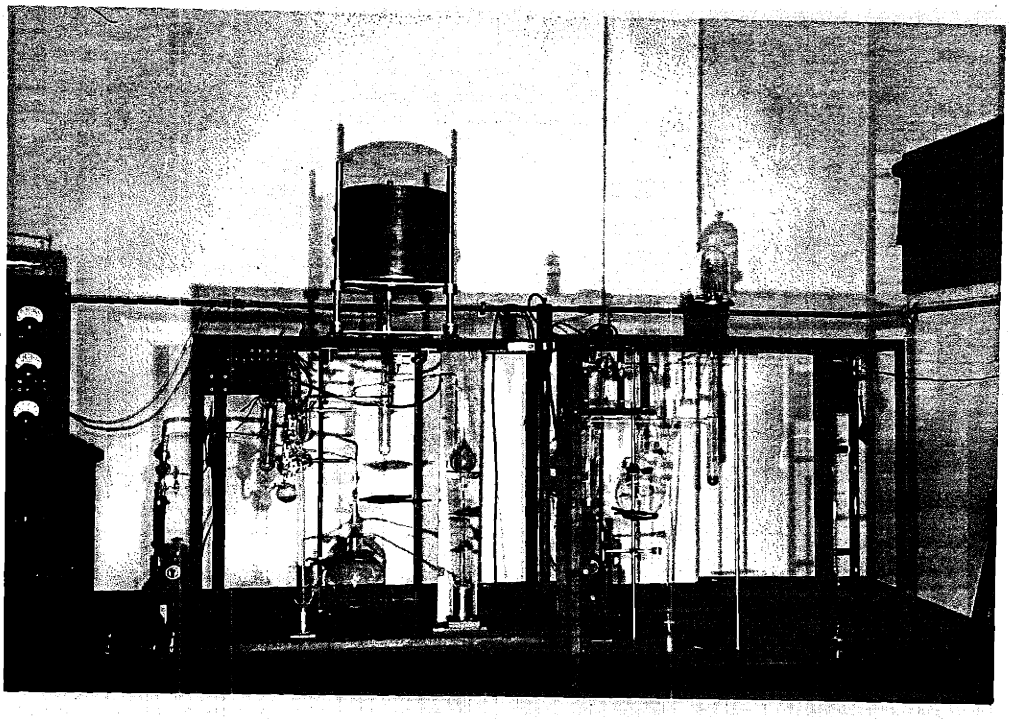

FIGURE 77 - VACUUM SYSTEM

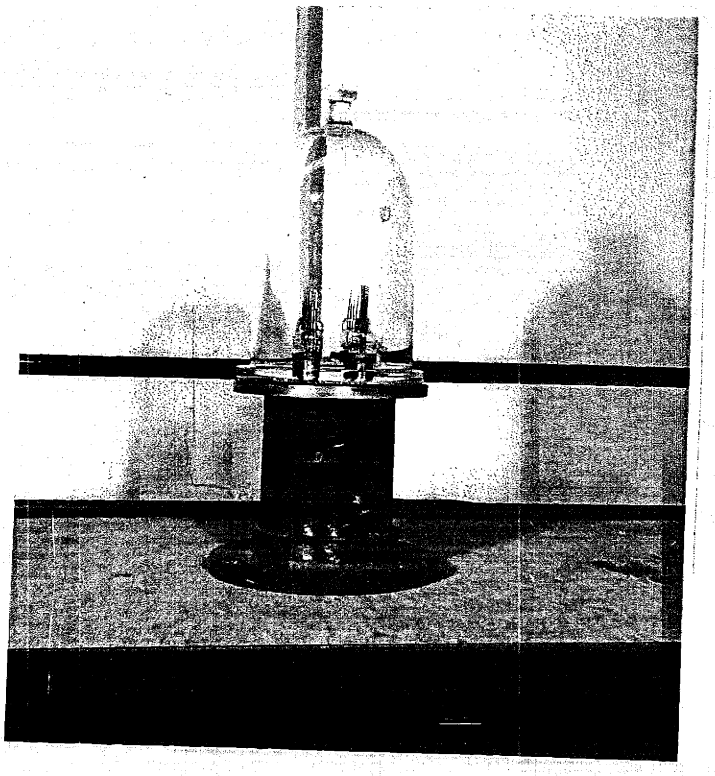

FIGURE 78 - BELL JAR

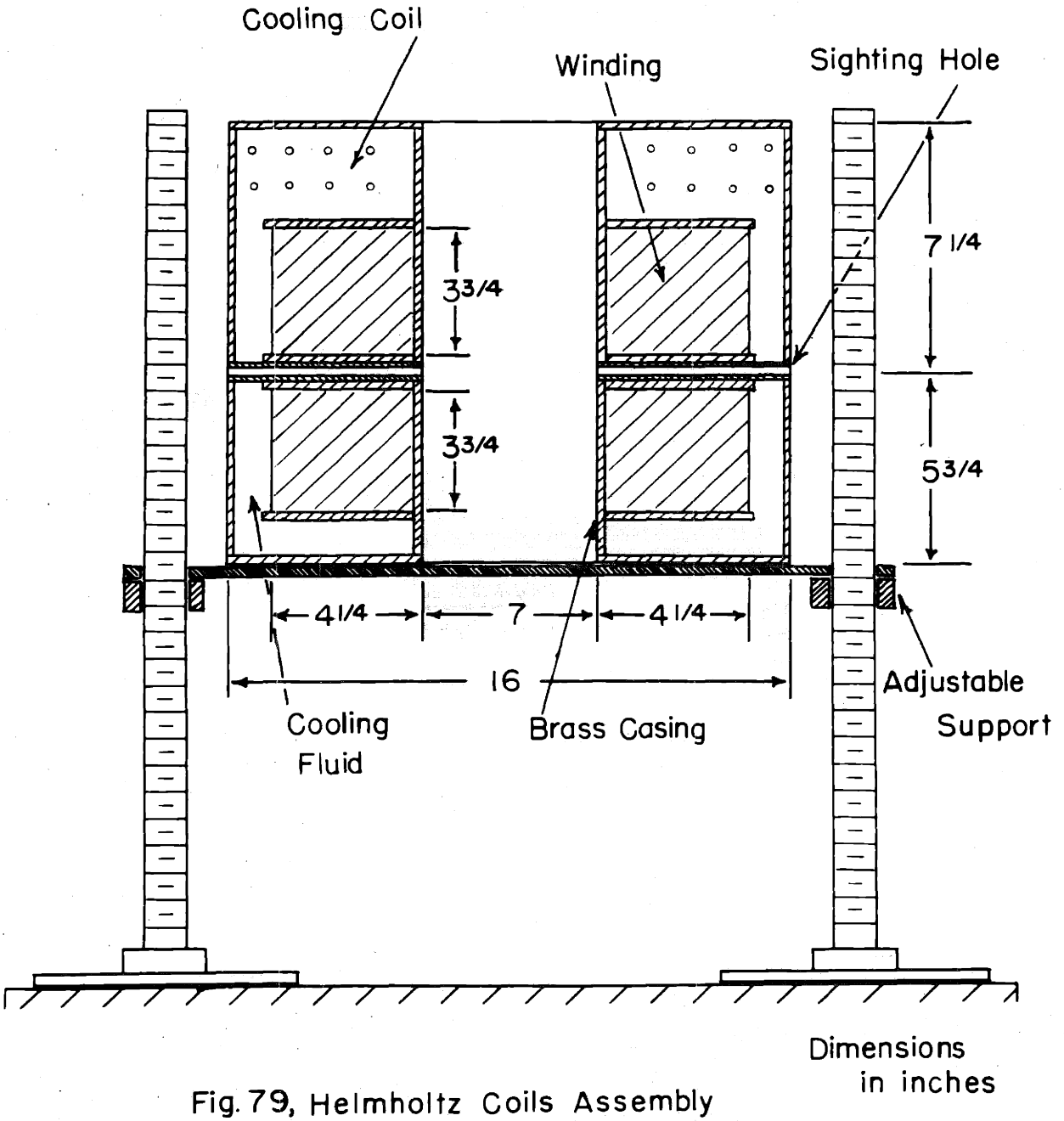

Fig. 79, Helmholtz Coils Assembly

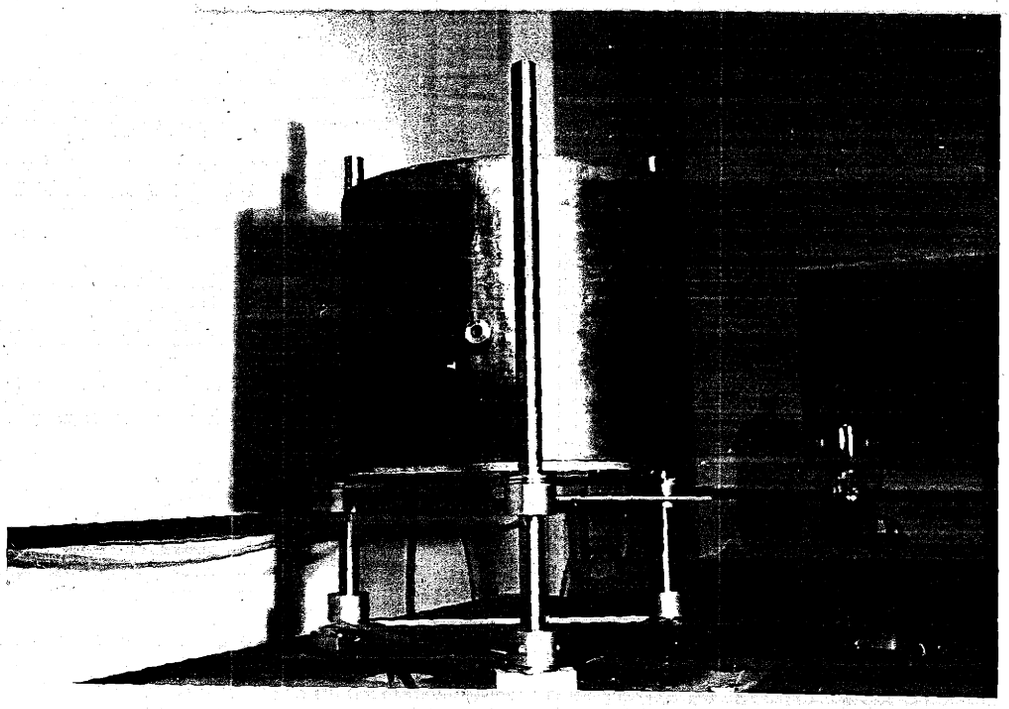

FIGURE 80 - HELMHOLTZ COIL ASSEMBLY (MAGNET)

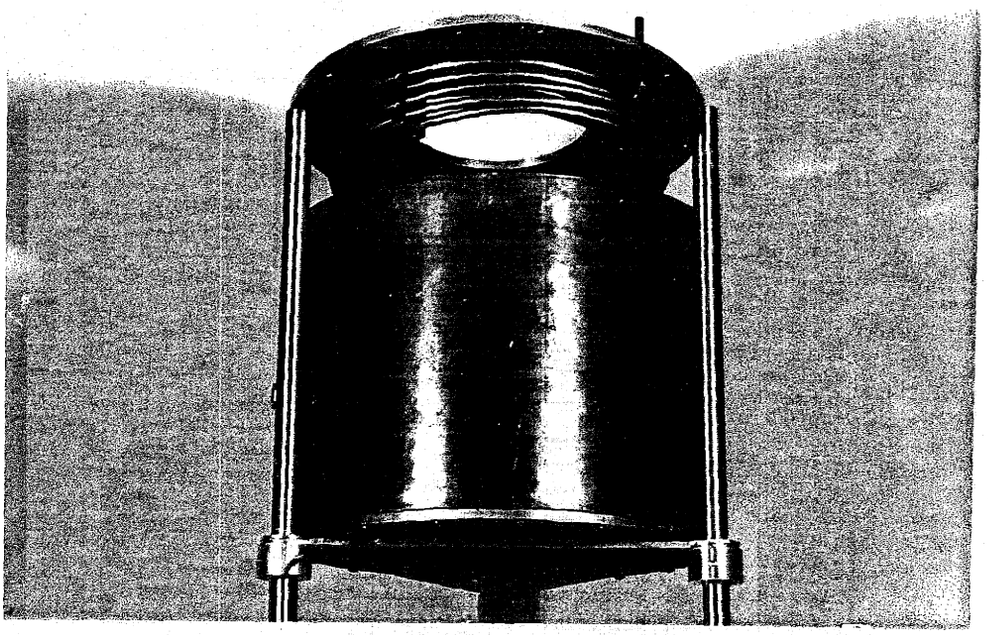

FIGURE 81 - COOLING COIL FOR MAGNET